

Mode and Ridge Estimation in Euclidean and Directional Product Spaces: A Mean Shift Approach

Yikun Zhang
Yen-Chi Chen

Department of Statistics
University of Washington
Seattle, WA 98195, USA

YIKUN@UW.EDU
YENCHIC@UW.EDU

Abstract

The set of local modes and the ridge lines estimated from a dataset are important summary characteristics of the data-generating distribution. In this work, we consider estimating the local modes and ridges from point cloud data in a product space with two or more Euclidean/directional metric spaces. Specifically, we generalize the well-known (subspace constrained) mean shift algorithm to the product space setting and illuminate some pitfalls in such generalization. We derive the algorithmic convergence of the proposed method, provide practical guidelines on the implementation, and demonstrate its effectiveness on both simulated and real datasets.

Keywords: Mean shift algorithm, ridge estimation, optimization on manifolds

1. Introduction

The rapid development of artificial intelligence in the past several decades has been accompanied by the increasing amount of large-scale data with complicated structures. As it may be computationally intractable to conduct direct analyses on such data, practitioners generally resort to some low-dimensional representations of the original data that preserve as much information as possible. There are numerous methods available in the literature; see [Izenman \(2012\)](#); [Fefferman et al. \(2016\)](#) and the references therein. Among various characterizations of the low-dimensional data representation, we focus on the local modes and density ridges (also known as principal curves/surfaces in [Ozertem and Erdogmus 2011](#)) of the data-generating distribution because of two reasons. Statistically, the local modes and density ridges are able to capture the intrinsic low-dimensional structure of the data and can be consistently estimated by kernel density estimator (KDE) ([Romano, 1988](#); [Mokkadem and Pelletier, 2003](#); [Genovese et al., 2014](#)). Practically, the mean shift algorithm ([Fukunaga and Hostetler, 1975](#); [Cheng, 1995](#); [Comaniciu and Meer, 2002](#)) and its subspace constrained variant ([Ozertem and Erdogmus, 2011](#)) are available for identifying the estimated local modes and density ridges of KDE in Euclidean spaces.

However, we may encounter the case where the original data do not lie on a flat Euclidean space but some nonlinear manifolds, such as a q -dimensional sphere. For instance, the dihedral angles in protein structures are periodic and can be viewed as observations on a unit circle ($q = 1$) ([Zimmermann and Hansmann, 2006](#)). Moreover, some point cloud data may consist of components coming from different metric spaces. In a broader sense, such data are known as spatio-temporal data, where the spatial part can be either Euclidean



(a) Simulated points on Ω_2 .

(b) Simulated points on $\Omega_1 \times \Omega_1$.

Figure 1: Simulated dataset $\{(\theta_i, \phi_i)\}_{i=1}^{1000}$ on Ω_2 and $\Omega_1 \times \Omega_1$. Each observation (θ_i, ϕ_i) is sampled uniformly from $[2p_1\pi, 2(p_1 + 1)\pi) \times \{2p_2\pi\}$ for some integers p_1, p_2 .

or directional while the temporal part is continual or periodic (Hall et al., 2006). Data of this type also arise in astronomy, where the location of an astronomical object is generally recorded as a three-element tuple, (right ascension, declination, redshift) (Dawson et al., 2016; Brown et al., 2018). The first two elements encode its position on the celestial sphere ($q = 2$) and the redshift value reflects its distance to Earth. Under these complicated forms of data, the standard KDE and mean shift algorithm are no longer applicable.

In this paper, we explore the idea of estimating local modes and ridges of a (density) function supported on a (Cartesian) product space $\mathcal{S}_1 \times \mathcal{S}_2$ through KDE and (subspace constrained) mean shift algorithms, where $\mathcal{S}_1, \mathcal{S}_2$ are either a Euclidean/linear space \mathbb{R}^D or directional space

$$\Omega_q = \{\mathbf{x} \in \mathbb{R}^{q+1} : \|\mathbf{x}\|_2 = 1\}$$

with $\|\cdot\|_2$ being the usual \mathcal{L}_2 norm, respectively. We only discuss the case where the product space has two (topological) factors. One can generalize our methodology to a product space with finitely many factors with little effort. Although the mode-seeking and ridge-finding problems have been studied separately in \mathbb{R}^D and Ω_q (Chacón, 2020; Genovese et al., 2014; Zhang and Chen, 2021c), their extensions to $\mathcal{S}_1 \times \mathcal{S}_2$ are innovative, especially when any factor space \mathcal{S}_j is directional for $j = 1, 2$. In this case, $\mathcal{S}_1 \times \mathcal{S}_2$ is topologically different from \mathbb{R}^D or Ω_q . Consider, for example, a dataset $\{(\theta_i, \phi_i)\}_{i=1}^n$ with θ_i and ϕ_i being periodic, respectively. Each observation can be viewed as a point on the sphere Ω_2 , where (θ_i, ϕ_i) represents the longitude and latitude, or a point on the torus $\Omega_1 \times \Omega_1$. The supports Ω_2 and $\Omega_1 \times \Omega_1$ of the same dataset are topological different; see Figure 1.

Main Results. • For the mode-seeking problem, we derive two versions of the mean shift algorithm with coordinate-adaptive bandwidths on $\mathcal{S}_1 \times \mathcal{S}_2$ and establish their (linear) convergence results; see Section 3.

• While formulating the mean shift algorithm on $\mathcal{S}_1 \times \mathcal{S}_2$ is natural, its subspace constrained

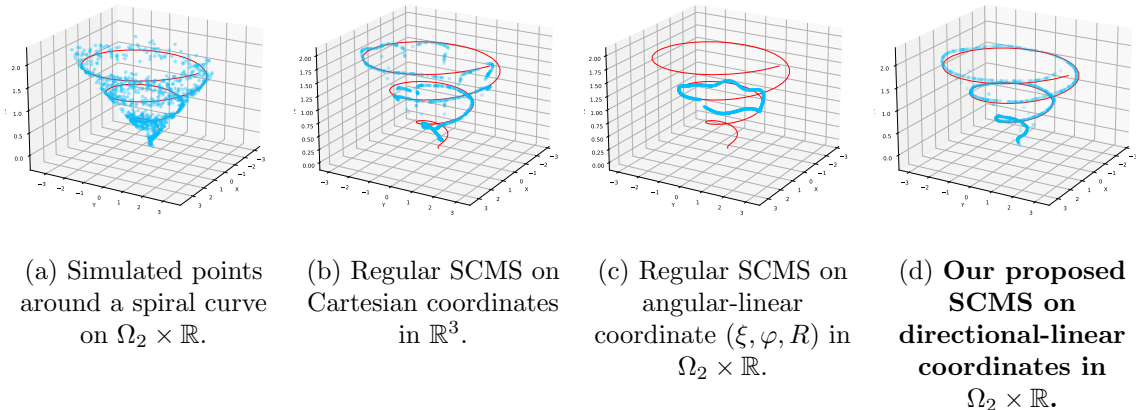


Figure 2: Estimated ridges obtained by various SCMS algorithms on the spiral curve data. In each panel, the red curve is the hidden manifold structure while the blue dots are final convergent points of SCMS algorithms.

extension is nontrivial and requires cautions. We propose our subspace constrained mean shift (SCMS) algorithm on $\mathcal{S}_1 \times \mathcal{S}_2$ and prove its (linear) convergence. More importantly, a both theoretically and empirically valid guideline for tuning the step size parameter in the algorithm is provided as well; see Section 4.

- We demonstrate the effectiveness of our proposed mean shift and SCMS algorithms through both simulation studies and real-world applications; see Figure 2 with more details in Section 5 and Appendix A. The code for reproducing the experiments and figures in this paper can be found at <https://github.com/zhangyk8/ProdSCMS>.

Related Work. Kernel density estimator (KDE) has been applied to countless scientific fields with miscellaneous forms of data. Some comprehensive reviews of KDE include Silverman (1986); Scott (2015); Chen (2017). One generalization of the standard KDE that is closely related to our work is to adapt KDE to directional-linear (DirLin) and directional-directional (DirDir) data (Marzio et al., 2011; García-Portugués et al., 2013, 2015). These authors leveraged the directional KDE proposed by Hall et al. (1987); Bai et al. (1988) and the product kernel technique to not only estimate the density but also carry out independence and goodness-of-fit tests. We will extend their KDE to mode-seeking and ridge-finding problems.

The mean shift algorithm has also been adapted to directional (Oba et al., 2005; Kafai et al., 2010; Zhang and Chen, 2021b) or more general manifold data (Subbarao and Meer, 2006, 2009; Cetingul and Vidal, 2009) since its inception at the end of last century; see Carreira-Perpiñán (2015) for a full review. Besides providing an efficient avenue to obtain local modes of KDE, the mean shift algorithm can be modified to a subspace constrained version in order to identify the density ridges (Genovese et al., 2014; Chen et al., 2014). The algorithmic convergence properties of the subspace constrained mean shift (SCMS) algorithm and its extensions were studied in Ghassabeh et al. (2013); Qiao and Polonik (2021).

Setup and Notation. We assume that our interested data consist of independent and identically distributed (i.i.d.) observations $\{\mathbf{Z}_i\}_{i=1}^n = \{(\mathbf{X}_i, \mathbf{Y}_i)\}_{i=1}^n$ sampled from a distribution on $\mathcal{S}_1 \times \mathcal{S}_2$ with density f , where

$$\int_{\mathcal{S}_1 \times \mathcal{S}_2} f(\mathbf{x}, \mathbf{y}) \omega_1(d\mathbf{x}) \omega_2(d\mathbf{y}) = 1$$

for Lebesgue measures ω_1, ω_2 on $\mathcal{S}_1, \mathcal{S}_2$, and $\mathcal{S}_j = \Omega_{D_j}$ or \mathbb{R}^{D_j} for $j = 1, 2$. Whenever $\mathcal{S}_j = \mathbb{R}^{D_j}$, we also assume that the projection of f on \mathcal{S}_j has a compact support. Note that D_j is the intrinsic/manifold dimension of \mathcal{S}_j , and more importantly, the ambient space of \mathcal{S}_j is $\mathbb{R}^{D_j+1 \mathbb{1}_{\{\mathcal{S}_j = \Omega_{D_j}\}}}$ for $j = 1, 2$, where the indicator $\mathbb{1}_{\{\mathcal{S}_j = \Omega_{D_j}\}}$ accommodates the directional data space Ω_{D_j} with its ambient space as \mathbb{R}^{D_j+1} . Under some differentiability assumption, the *total* gradient and Hessian of f in the ambient space of $\mathcal{S}_1 \times \mathcal{S}_2$ are defined as:

$$\nabla f = \begin{pmatrix} \nabla_{\mathbf{x}} f \\ \nabla_{\mathbf{y}} f \end{pmatrix}, \quad \nabla^2 f = \begin{pmatrix} \nabla_{\mathbf{x}}^2 f & \nabla_{\mathbf{y}} \nabla_{\mathbf{x}} f \\ \nabla_{\mathbf{x}} \nabla_{\mathbf{y}} f & \nabla_{\mathbf{y}}^2 f \end{pmatrix}, \quad (1)$$

where $\nabla_{\mathbf{x}} f(\mathbf{z}) = \left(\frac{\partial f(\mathbf{z})}{\partial x_1}, \dots, \frac{\partial f(\mathbf{z})}{\partial x_D} \right)^T$ with $\mathbf{z} = (\mathbf{x}, \mathbf{y}) \in \mathcal{S}_1 \times \mathcal{S}_2$ denotes the total gradient within the (smallest) ambient Euclidean space \mathbb{R}^D containing \mathcal{S}_1 , and the same applies to $\nabla_{\mathbf{y}} f(\mathbf{z})$. That is, $D = D_1 + 1$ when $\mathcal{S}_1 = \Omega_{D_1}$ (directional space) while $D = D_1$ when $\mathcal{S}_1 = \mathbb{R}^{D_1}$ (Euclidean space).

We use the big-O notation $h(x) = O(g(x))$ or $h(x) \lesssim g(x)$ if the absolute value of $h(x)$ is upper bounded by a positive constant multiple of $g(x)$ for all sufficiently large x . In contrast, $h(x) = o(g(x))$ when $\lim_{x \rightarrow \infty} \frac{|h(x)|}{g(x)} = 0$. For random vectors, the notation $o_P(1)$ is short for a sequence of random vectors that converges to zero in probability. The expression $O_P(1)$ denotes a sequence that is bounded in probability; see Section 2.2 of [Vaart \(1998\)](#) for details.

2. Background

This section reviews the construction of KDE in a Euclidean/directional product space $\mathcal{S}_1 \times \mathcal{S}_2$ and derives the Riemannian gradient and Hessian in this space.

2.1 Kernel Density Estimator on $\mathcal{S}_1 \times \mathcal{S}_2$

As the data $\{\mathbf{Z}_i\}_{i=1}^n = \{(\mathbf{X}_i, \mathbf{Y}_i)\}_{i=1}^n$ lie on a product space $\mathcal{S}_1 \times \mathcal{S}_2$, it is natural to estimate the underlying density f via the KDE with a product kernel in [Hall et al. \(2006\)](#); [García-Portugués et al. \(2013, 2015\)](#) as:

$$\hat{f}_{\mathbf{h}}(\mathbf{x}, \mathbf{y}) = \frac{1}{n} \sum_{i=1}^n K_1 \left(\frac{\mathbf{x} - \mathbf{X}_i}{h_1} \right) K_2 \left(\frac{\mathbf{y} - \mathbf{Y}_i}{h_2} \right), \quad (2)$$

where for each $j = 1, 2$, $K_j : \mathcal{S}_j \rightarrow \mathbb{R}$ is a kernel function, and each element of $\mathbf{h} = (h_1, h_2)$ is a bandwidth parameter. Depending on the geometry of \mathcal{S}_j , the radially symmetric kernel

function K_j takes the form:

$$K_j(\mathbf{u}) = C_{k_j, D_j}(h_j) \cdot k_j\left(\|\mathbf{u}\|_2^2\right) = \begin{cases} \frac{C_{k, D_j}}{h_j^{D_j}} \cdot k\left(\frac{\|\mathbf{u}\|_2^2}{2}\right) & \text{if } \mathcal{S}_j = \mathbb{R}^{D_j}, \\ C_{L, D_j}(h_j) \cdot L\left(\frac{\|\mathbf{u}\|_2^2}{2}\right) & \text{if } \mathcal{S}_j = \Omega_{D_j}, \end{cases} \quad (3)$$

for $j = 1, 2$, where k and L are the profiles of linear and directional kernels, respectively. One salient difference between linear and directional kernels in (3) is whether their normalizing constants can be separated out from the bandwidth parameters. While it is intuitive to see that the normalizing constant has asymptotic rate $O\left(1/h_j^{D_j}\right)$ under the linear kernel, it is less obvious to obtain the similar rate in the directional kernel as (García-Portugués, 2013):

$$C_{L, D_j}(h_j)^{-1} = \int_{\Omega_{D_j}} L\left(\frac{1 - \mathbf{x}^T \mathbf{y}}{h_j^2}\right) \omega_j(d\mathbf{y}) = O\left(h_j^{D_j}\right).$$

A common choice of both linear and directional kernel profiles is $k(s) = L(s) = e^{-s/2}$, where the resulting linear kernel is called Gaussian kernel and the directional kernel is named as von Mises kernel. The name of von Mises kernel originates from the classical von Mises-Fisher (vMF) distribution (Mardia and Jupp, 2000) on Ω_q with the density

$$f_{\text{vMF}}(\mathbf{x}; \boldsymbol{\mu}, \kappa) = C_q(\kappa) \cdot \exp\left(\kappa \boldsymbol{\mu}^T \mathbf{x}\right) \quad \text{with} \quad C_q(\kappa) = \frac{\kappa^{\frac{q-1}{2}}}{(2\pi)^{\frac{q+1}{2}} \mathcal{I}_{\frac{q-1}{2}}(\kappa)},$$

where $\boldsymbol{\mu} \in \Omega_q$ is the directional mean of the vMF distribution, $\kappa \geq 0$ is the concentration parameter, and $\mathcal{I}_\nu(\kappa)$ is the modified Bessel function of the first kind of order ν .

With applications of Gaussian and/or von Mises kernels to K_1 and K_2 , the KDE (2) reduces to the following concise form as:

$$\hat{f}_{\mathbf{h}}(\mathbf{z}) = \frac{C(\mathbf{H})}{n} \sum_{i=1}^n \exp\left(-\frac{(\mathbf{z} - \mathbf{Z}_i)^T \mathbf{H}^{-1} (\mathbf{z} - \mathbf{Z}_i)}{2}\right), \quad (4)$$

where $\mathbf{z} = (\mathbf{x}, \mathbf{y}) \in \mathcal{S}_1 \times \mathcal{S}_2$,

$$\mathbf{H} = \text{Diag}\left(h_1^2 \mathbf{I}_{D_1+1_{\{\mathcal{S}_1=\Omega_{D_1}\}}}, h_2^2 \mathbf{I}_{D_2+1_{\{\mathcal{S}_2=\Omega_{D_2}\}}}\right)$$

is a (block) diagonal bandwidth matrix, \mathbf{I}_D is the identity matrix in $\mathbb{R}^{D \times D}$, and $C(\mathbf{h}) \equiv \prod_{j=1}^2 C_{k_j, D_j}(h_j)$ is the normalizing constant inherited from (2). Our subsequent theory is also adaptive to a general (unconstrained) positive definite bandwidth matrix \mathbf{H} , though it is preferable to have a diagonal bandwidth matrix (i.e., independent smoothing parameters; Wand and Jones 1993). Moreover, whenever $\mathcal{S}_j = \Omega_{D_j}$, it is more appropriate to apply a single bandwidth parameter h_j to each coordinate on Ω_{D_j} given its isotropic geometry. Later, in Sections 3 and 4, while showing the possibility to derive the (subspace constrained) mean shift algorithms under general kernels, we will focus on implementing the algorithms with Gaussian and/or von Mises kernels in practice given their favorable properties.

2.2 Gradient and Hessian System on $\mathcal{S}_1 \times \mathcal{S}_2$

Since each factor of the product space $\mathcal{S}_1 \times \mathcal{S}_2$ can be a nonlinear manifold Ω_q , we study the Riemannian gradient and Hessian of a (density) function f defined in the tangent spaces of $\mathcal{S}_1 \times \mathcal{S}_2$ and their relations to the total gradient and Hessian in the ambient (Euclidean) space. Assume that the (density) function f is at least twice continuously differentiable within an open neighborhood in the ambient space containing $\mathcal{S}_1 \times \mathcal{S}_2$; see the complete assumptions in Appendix B.1.

• **(Riemannian Gradient)** The definition of Riemannian gradient is built on top of the differential of f at $z = (\mathbf{x}, \mathbf{y}) \in \mathcal{S}_1 \times \mathcal{S}_2$, which is a linear map $df_z : T_z \equiv T_{\mathbf{x}}(\mathcal{S}_1) \times T_{\mathbf{y}}(\mathcal{S}_2) \rightarrow \mathbb{R}$ given by

$$df_z(\mathbf{v}) = \nabla_{\mathbf{x}} f(\mathbf{x}, \mathbf{y})^T \mathbf{v}_{\mathbf{x}} + \nabla_{\mathbf{y}} f(\mathbf{x}, \mathbf{y})^T \mathbf{v}_{\mathbf{y}} \quad (5)$$

for any $\mathbf{v} = (\mathbf{v}_{\mathbf{x}}, \mathbf{v}_{\mathbf{y}}) \in T_z \equiv T_{\mathbf{x}}(\mathcal{S}_1) \times T_{\mathbf{y}}(\mathcal{S}_2)$. Correspondingly, the *Riemannian gradient* $\text{grad } f(z)$ is a vector field in the tangent space T_z defined as:

$$df_z(\mathbf{v}) = \langle \text{grad } f(z), (\mathbf{v}_{\mathbf{x}}, \mathbf{v}_{\mathbf{y}}) \rangle = \text{grad } f(z)^T \mathbf{v} \quad (6)$$

where the inner product $\langle \cdot, \cdot \rangle$ is inherited from the usual one in the ambient Euclidean space. Combining (5) and (6), we obtain a vector form of $\text{grad } f(\mathbf{x}, \mathbf{y})$:

$$\begin{aligned} \text{grad } f(z) &= \mathcal{P}_z \nabla f(z) \quad \text{with} \quad \mathcal{P}_z = \begin{pmatrix} \mathcal{P}_1 & \mathbf{0} \\ \mathbf{0} & \mathcal{P}_2 \end{pmatrix} \\ \text{and} \quad \begin{cases} \mathcal{P}_1 = \mathbf{I}_{D_1+1} - \mathbf{x}\mathbf{x}^T \cdot \mathbb{1}_{\{\mathcal{S}_1=\Omega_{D_1}\}} \\ \mathcal{P}_2 = \mathbf{I}_{D_2+1} - \mathbf{y}\mathbf{y}^T \cdot \mathbb{1}_{\{\mathcal{S}_2=\Omega_{D_2}\}} \end{cases} \end{aligned} \quad (7)$$

Here, \mathcal{P}_z is the projection matrix onto the tangent space T_z and \mathbf{I}_D is an identity matrix in $\mathbb{R}^{D \times D}$. That is, the projection matrix \mathcal{P}_z will be the identity matrix (has no effect) if $\mathcal{S}_1 \times \mathcal{S}_2$ is Euclidean and will have a projection effect if any of $\mathcal{S}_j, j = 1, 2$ is directional.

• **(Riemannian Hessian)** The *Riemannian Hessian* of f is a symmetric linear map $\mathcal{H}f(z)$ of the tangent space $T_z \equiv T_{\mathbf{x}}(\mathcal{S}_1) \times T_{\mathbf{y}}(\mathcal{S}_2)$ into itself defined by

$$\mathcal{H}f(z)[\mathbf{v}] = \bar{\nabla}_{\mathbf{v}} \text{grad } f(z), \quad (8)$$

for any tangent vector $\mathbf{v} = (\mathbf{v}_{\mathbf{x}}, \mathbf{v}_{\mathbf{y}}) \in T_z$, where $\bar{\nabla}_{\mathbf{v}}$ is the Riemannian connection on $\mathcal{S}_1 \times \mathcal{S}_2$; see Section 5.5 in Absil et al. (2009). As the domain $\mathcal{S}_1 \times \mathcal{S}_2$ can be viewed as a (nonlinear) submanifold in its ambient Euclidean space, Proposition 5.3.2 in Absil et al. (2009) suggests that the Riemannian Hessian $\mathcal{H}f(z)$ in (8) can be written as

$$\begin{aligned} \mathcal{H}f(z)[\mathbf{v}] &= \mathcal{P}_z \left(\nabla_{\mathbf{x}} \text{grad } f(z), \nabla_{\mathbf{y}} \text{grad } f(z) \right) [\mathbf{v}] \\ &= \mathcal{P}_z \left[\nabla^2 f(z) - \text{Diag}(\mathcal{A}_1, \mathcal{A}_2) \right] [\mathbf{v}] \\ \text{with} \quad \begin{cases} \mathcal{A}_1 = \mathbf{x}^T \nabla f(z) \mathbf{I}_{D_1+1} \cdot \mathbb{1}_{\{\mathcal{S}_1=\Omega_{D_1}\}} \\ \mathcal{A}_2 = \mathbf{y}^T \nabla f(z) \mathbf{I}_{D_2+1} \cdot \mathbb{1}_{\{\mathcal{S}_2=\Omega_{D_2}\}} \end{cases} \end{aligned} \quad (9)$$

where $\text{Diag}(\mathcal{A}_1, \mathcal{A}_2)$ is a (block) diagonal matrix, and we plug in the formula (7) of $\text{grad} f(\mathbf{z})$ in the second equality. \mathcal{A}_j can be viewed as the ‘corrections’ when the space \mathcal{S}_j is directional for $j = 1, 2$. When the space \mathcal{S}_j is Euclidean, \mathcal{A}_j will be a $\mathbf{0}$ matrix. Using $\mathbf{v} \in T_{\mathbf{z}}$ and the symmetric property of $\mathcal{H}f(\mathbf{z})$, we can express the operator $\mathcal{H}f(\mathbf{z})$ as a matrix

$$\mathcal{H}f(\mathbf{z}) = \mathcal{P}_{\mathbf{z}} \left[\nabla^2 f(\mathbf{z}) - \text{Diag}(\mathcal{A}_1, \mathcal{A}_2) \right] \mathcal{P}_{\mathbf{z}}. \quad (10)$$

Notice that both $\text{grad} f(\mathbf{z})$ and $\mathcal{H}f(\mathbf{z})$ reduce to the total gradient $\nabla f(\mathbf{z})$ and Hessian $\nabla^2 f(\mathbf{z})$ when $\mathcal{S}_1, \mathcal{S}_2$ are Euclidean/linear spaces.

3. Mean Shift Algorithm on $\mathcal{S}_1 \times \mathcal{S}_2$

• **Mode Estimation on $\mathcal{S}_1 \times \mathcal{S}_2$.** The Riemannian gradient $\text{grad} f(\mathbf{z})$ and Hessian $\mathcal{H}f(\mathbf{z})$ in Section 2.2 induce the set of local modes \mathcal{M} of f on the product space $\mathcal{S}_1 \times \mathcal{S}_2$ as:

$$\mathcal{M} = \{ \mathbf{z} \in \mathcal{S}_1 \times \mathcal{S}_2 : \text{grad} f(\mathbf{z}) = \mathbf{0}, \lambda_1(\mathbf{z}) < 0 \}, \quad (11)$$

where $\lambda_1(\mathbf{z})$ is the largest eigenvalue of $\mathcal{H}f(\mathbf{z})$ within the tangent space $T_{\mathbf{z}}$. Given the KDE $\hat{f}_{\mathbf{h}}$ in (2), a plug-in estimator of \mathcal{M} is given by

$$\widehat{\mathcal{M}} = \left\{ \mathbf{z} \in \mathcal{S}_1 \times \mathcal{S}_2 : \text{grad} \hat{f}_{\mathbf{h}}(\mathbf{z}) = \mathbf{0}, \widehat{\lambda}_1(\mathbf{z}) < 0 \right\}. \quad (12)$$

Under some regularity conditions on kernel functions and f , $\widehat{\mathcal{M}}$ is a consistent estimator of \mathcal{M} ; see Appendix B.2 for a detailed discussion.

• **Derivations of the Mean Shift Algorithm on $\mathcal{S}_1 \times \mathcal{S}_2$.** We assume that the linear and directional kernel profiles k and L in (3) are continuously differentiable. Given the quadratic nature of K_1, K_2 in (2), the total gradient of $\hat{f}_{\mathbf{h}}(\mathbf{z})$ becomes

$$\nabla \hat{f}_{\mathbf{h}}(\mathbf{z}) = \begin{pmatrix} \nabla_{\mathbf{x}} \hat{f}_{\mathbf{h}}(\mathbf{z}) \\ \nabla_{\mathbf{y}} \hat{f}_{\mathbf{h}}(\mathbf{z}) \end{pmatrix} = \begin{pmatrix} G_{\mathbf{x}} \left[\frac{\sum_{i=1}^n \mathbf{X}_i k'_1 \left(\left\| \frac{\mathbf{x} - \mathbf{X}_i}{h_1} \right\|_2 \right) K_2 \left(\frac{\mathbf{y} - \mathbf{Y}_i}{h_2} \right)}{\sum_{i=1}^n k'_1 \left(\left\| \frac{\mathbf{x} - \mathbf{X}_i}{h_1} \right\|_2 \right) K_2 \left(\frac{\mathbf{y} - \mathbf{Y}_i}{h_2} \right)} - \mathbf{x} \right] \\ G_{\mathbf{y}} \left[\frac{\sum_{i=1}^n \mathbf{Y}_i K_1 \left(\frac{\mathbf{x} - \mathbf{X}_i}{h_1} \right) k'_2 \left(\left\| \frac{\mathbf{y} - \mathbf{Y}_i}{h_2} \right\|_2 \right)}{\sum_{i=1}^n K_1 \left(\frac{\mathbf{x} - \mathbf{X}_i}{h_1} \right) k'_2 \left(\left\| \frac{\mathbf{y} - \mathbf{Y}_i}{h_2} \right\|_2 \right)} - \mathbf{y} \right] \end{pmatrix}, \quad (13)$$

where, with $C(\mathbf{h}) \equiv \prod_{j=1}^2 C_{k_j, D_j}(h_j)$, both factors

$$\begin{aligned} G_{\mathbf{x}} &= -\frac{2C(\mathbf{h})}{nh_1^2} \sum_{i=1}^n k'_1 \left(\left\| \frac{\mathbf{x} - \mathbf{X}_i}{h_1} \right\|_2 \right) K_2 \left(\frac{\mathbf{y} - \mathbf{Y}_i}{h_2} \right), \\ G_{\mathbf{y}} &= -\frac{2C(\mathbf{h})}{nh_2^2} \sum_{i=1}^n K_1 \left(\frac{\mathbf{x} - \mathbf{X}_i}{h_1} \right) k'_2 \left(\left\| \frac{\mathbf{y} - \mathbf{Y}_i}{h_2} \right\|_2 \right) \end{aligned} \quad (14)$$

are non-negative and $\mathbf{z} = (\mathbf{x}, \mathbf{y}) \in \mathcal{S}_1 \times \mathcal{S}_2$. Thus, the mean shift vector $\Xi(\mathbf{z})$ in $\mathcal{S}_1 \times \mathcal{S}_2$ is defined as:

$$\Xi(\mathbf{z}) = \begin{pmatrix} \Xi_{\mathbf{x}}(\mathbf{x}, \mathbf{y}) \\ \Xi_{\mathbf{y}}(\mathbf{x}, \mathbf{y}) \end{pmatrix} = \begin{pmatrix} \frac{\sum_{i=1}^n \mathbf{X}_i k'_1 \left(\left\| \frac{\mathbf{x} - \mathbf{X}_i}{h_1} \right\|_2^2 \right) K_2 \left(\frac{\mathbf{y} - \mathbf{Y}_i}{h_2} \right)}{\sum_{i=1}^n k'_1 \left(\left\| \frac{\mathbf{x} - \mathbf{X}_i}{h_1} \right\|_2^2 \right) K_2 \left(\frac{\mathbf{y} - \mathbf{Y}_i}{h_2} \right)} - \mathbf{x} \\ \frac{\sum_{i=1}^n \mathbf{Y}_i K_1 \left(\frac{\mathbf{x} - \mathbf{X}_i}{h_1} \right) k'_2 \left(\left\| \frac{\mathbf{y} - \mathbf{Y}_i}{h_2} \right\|_2^2 \right)}{\sum_{i=1}^n K_1 \left(\frac{\mathbf{x} - \mathbf{X}_i}{h_1} \right) k'_2 \left(\left\| \frac{\mathbf{y} - \mathbf{Y}_i}{h_2} \right\|_2^2 \right)} - \mathbf{y} \end{pmatrix}. \quad (15)$$

Unlike the standard mean shift vector in a Euclidean space (Comaniciu and Meer, 2002), $\Xi(\mathbf{z})$ does not align with the total gradient estimator $\nabla \hat{f}_{\mathbf{h}}(\mathbf{z})$ because $G_{\mathbf{x}} \neq G_{\mathbf{y}}$ in general.

Although $\Xi(\mathbf{z})$ is not proportional to $\nabla \hat{f}_{\mathbf{h}}(\mathbf{z})$, they share the same solution within $T_{\mathbf{z}}$! Namely, the collection of solutions of $\mathcal{P}_{\mathbf{z}} \Xi(\mathbf{z}) = \mathbf{0}$ is an equivalent quantity of the set of (estimated) local modes $\widehat{\mathcal{M}}$ as:

$$\widehat{\mathcal{M}}^{(T)} = \{\mathbf{z} \in \mathcal{S}_1 \times \mathcal{S}_2 : \mathcal{P}_{\mathbf{z}} \cdot \Xi(\mathbf{z}) = \mathbf{0}\} \equiv \widehat{\mathcal{M}}.$$

This is because from (13), the mean shift vector $\Xi(\mathbf{z})$ in (15) is indeed estimating a transformed total gradient $\tilde{D}(\mathbf{z})^{-1} \nabla \hat{f}_{\mathbf{h}}(\mathbf{z})$ with

$$\tilde{D}(\mathbf{z}) = \text{Diag} \left(G_{\mathbf{x}} \mathbf{I}_{D_1+1} \{\mathcal{S}_1 = \Omega_{D_1}\}, G_{\mathbf{y}} \mathbf{I}_{D_2+1} \{\mathcal{S}_2 = \Omega_{D_2}\} \right). \quad (16)$$

As $\tilde{D}(\mathbf{z})$ will be nonsingular under any strictly decreasing kernel, such as Gaussian and von Mises kernels, the projection of $\tilde{D}(\mathbf{z})^{-1} \nabla \hat{f}_{\mathbf{h}}(\mathbf{z}) = \Xi(\mathbf{z})$ onto the tangent space is zero if and only if the Riemannian gradient estimator $\mathbf{grad} \hat{f}_{\mathbf{h}}(\mathbf{z})$ is zero. Therefore, it is still valid to use $\Xi(\mathbf{z})$ to find the local modes of $\hat{f}_{\mathbf{h}}(\mathbf{z})$. Here, we introduce two different versions of the mean shift algorithm on $\mathcal{S}_1 \times \mathcal{S}_2$ based on $\Xi(\mathbf{z})$ and prove their (linear) convergence in Theorems 1 and 2.

Version A (Simultaneous Mean Shift). This version updates all the components $\mathbf{z}^{(t)} = (\mathbf{x}^{(t)}, \mathbf{y}^{(t)}) \in \mathcal{S}_1 \times \mathcal{S}_2$ simultaneously, in which for $t = 0, 1, \dots$,

$$\left(\mathbf{z}^{(t+1)} \right)^T \leftarrow \Xi(\mathbf{z}^{(t)}) + \left(\mathbf{z}^{(t)} \right)^T = \begin{pmatrix} \frac{\sum_{i=1}^n \mathbf{X}_i k'_1 \left(\left\| \frac{\mathbf{x}^{(t)} - \mathbf{X}_i}{h_1} \right\|_2^2 \right) K_2 \left(\frac{\mathbf{y}^{(t)} - \mathbf{Y}_i}{h_2} \right)}{\sum_{i=1}^n k'_1 \left(\left\| \frac{\mathbf{x}^{(t)} - \mathbf{X}_i}{h_1} \right\|_2^2 \right) K_2 \left(\frac{\mathbf{y}^{(t)} - \mathbf{Y}_i}{h_2} \right)} \\ \frac{\sum_{i=1}^n \mathbf{Y}_i K_1 \left(\frac{\mathbf{x}^{(t)} - \mathbf{X}_i}{h_1} \right) k'_2 \left(\left\| \frac{\mathbf{y}^{(t)} - \mathbf{Y}_i}{h_2} \right\|_2^2 \right)}{\sum_{i=1}^n K_1 \left(\frac{\mathbf{x}^{(t)} - \mathbf{X}_i}{h_1} \right) k'_2 \left(\left\| \frac{\mathbf{y}^{(t)} - \mathbf{Y}_i}{h_2} \right\|_2^2 \right)} \end{pmatrix} \quad (17)$$

with extra standardizations $\mathbf{x}^{(t+1)} \leftarrow \frac{\mathbf{x}^{(t+1)}}{\left\| \mathbf{x}^{(t+1)} \right\|_2}$ and/or $\mathbf{y}^{(t+1)} \leftarrow \frac{\mathbf{y}^{(t+1)}}{\left\| \mathbf{y}^{(t+1)} \right\|_2}$ if \mathcal{S}_1 and/or \mathcal{S}_2 are directional. It organically combines the Euclidean and directional mean shift algorithms into the iteration formula (17).

Version B (Componentwise Mean Shift). This version updates the sequence $\{\mathbf{z}^{(t)}\}_{t=0}^{\infty} = \{(\mathbf{x}^{(t)}, \mathbf{y}^{(t)})\}_{t=0}^{\infty}$ in a two-step manner as:

$$\begin{aligned} \mathbf{x}^{(t+1)} &\leftarrow \Xi_{\mathbf{x}}(\mathbf{x}^{(t)}, \mathbf{y}^{(t)}) + \mathbf{x}^{(t)} & \text{with} & \quad \mathbf{x}^{(t+1)} \leftarrow \frac{\mathbf{x}^{(t+1)}}{\|\mathbf{x}^{(t+1)}\|_2^2} & \text{if } \mathcal{S}_1 = \Omega_{D_1}, \\ \mathbf{y}^{(t+1)} &\leftarrow \Xi_{\mathbf{y}}(\mathbf{x}^{(t+1)}, \mathbf{y}^{(t)}) + \mathbf{y}^{(t)} & \text{with} & \quad \mathbf{y}^{(t+1)} \leftarrow \frac{\mathbf{y}^{(t+1)}}{\|\mathbf{y}^{(t+1)}\|_2^2} & \text{if } \mathcal{S}_2 = \Omega_{D_2} \end{aligned} \quad (18)$$

for $t = 0, 1, \dots$. The formula updates the two components $\mathbf{x}^{(t)}$ and $\mathbf{y}^{(t)}$ alternatively by first holding $\mathbf{y}^{(t)}$, updating $\mathbf{x}^{(t)}$, and then switching their roles. Such updating procedures borrows the spirit of the well-known coordinate ascent/descent algorithm (Wright, 2015).

One can easily specialize the above two versions to the mean shift algorithms with von Mises and/or Gaussian kernels. We thus omit the details. Under some mild conditions on kernel profiles, we establish the ascending and convergent properties of the mean shift algorithm on $\mathcal{S}_1 \times \mathcal{S}_2$, whose proofs are in Appendix D.

Theorem 1. Denote the sequence defined by the mean shift algorithm by $\{\mathbf{z}^{(t)}\}_{t=0}^{\infty} = \{(\mathbf{x}^{(t)}, \mathbf{y}^{(t)})\} \subset \mathcal{S}_1 \times \mathcal{S}_2$. Assume that

- **(C1)** The kernel profiles k_1, k_2 (either linear k or directional L) are strictly decreasing and differentiable on $[0, \infty)$ with $k_1(0), k_2(0) < \infty$.

- **(Weak Condition)** Both k_1 and k_2 are convex.

- **(Strong Condition)** The entire product kernel profile $K(r, s) = k_1(r) \cdot k_2(s)$ is convex.

(a) Under **(C1)** and **Weak Condition**, the sequence of density estimates $\{\hat{f}_{\mathbf{h}}(\mathbf{z}^{(t)})\}_{t=0}^{\infty}$ yielded by Version B is non-decreasing and thus converges.

(b) Under **(C1)** and **Strong Condition**, the sequence of density estimates $\{\hat{f}_{\mathbf{h}}(\mathbf{z}^{(t)})\}_{t=0}^{\infty}$ yielded by either Version A or B is non-decreasing and thus converges.

(c) Under the assumptions in (a) or (b), we have that $\lim_{t \rightarrow \infty} \|\mathbf{z}^{(t+1)} - \mathbf{z}^{(t)}\|_2 = 0$.

(d) Assume the conditions in (a) or (b). If the local modes of $\hat{f}_{\mathbf{h}}$ are isolated, $\{\mathbf{z}^{(t)}\}_{t=0}^{\infty}$ converges to a local mode of $\hat{f}_{\mathbf{h}}$ when it is initialized within its small neighborhood.

When the entire product kernel profile $K(r, s) = k_1(r) \cdot k_2(s)$ is convex, its components k_1 and k_2 will be convex as well. In other words, the strong condition in Theorem 1 implies the weak condition, whereas the converse is not true in general. It is easy to verify that under the Gaussian and/or von Mises kernel profiles $k(s) = L(s) = e^{-s}$, the conditions in (a,b,c) are satisfied. Finally, the isolation of local modes of $\hat{f}_{\mathbf{h}}$ is implied by some regularity conditions on the original (density) function f under the uniform consistency of $\hat{f}_{\mathbf{h}}$; see Theorem 7 in Appendix B.

The result in (d) of Theorem 1 is known as local convergence. For global convergence (from almost everywhere on $\mathcal{S}_1 \times \mathcal{S}_2$) of our mean shift algorithm, one feasible way is to formulate it as a (generalized) EM algorithm (Carreira-Perpiñán, 2007; Zhang and Chen, 2021a) and leverage the convergence theory of EM algorithm (Wu, 1983; McLachlan and Krishnan, 2008).

Finally, we establish the following linear convergence of our proposed mean shift algorithms (17) and (18) under the gradient ascent framework on $\mathcal{S}_1 \times \mathcal{S}_2$ with their intrinsic step sizes depending on the bandwidths h_1, h_2 ; see Appendix C for details.

Theorem 2. *Assume that the conditions of Theorem 7 in Appendix B.2 hold. Given the sequence $\{\mathbf{z}^{(t)}\}_{t=0}^{\infty}$ defined by our mean shift algorithm (17) or (18), there exist constants $\tilde{r}_1 > 0, \Upsilon_1 \in (0, 1)$ such that*

$$d_g(\mathbf{z}^{(t)}, \widehat{\mathbf{m}}) \leq \Upsilon_1^t \cdot d_g(\mathbf{z}^{(0)}, \widehat{\mathbf{m}}),$$

and with probability at least $1 - \delta$ under any $\delta \in (0, 1)$,

$$d_g(\mathbf{z}^{(t)}, \mathbf{m}) \leq \Upsilon_1^t \cdot d_g(\mathbf{z}^{(0)}, \mathbf{m}) + O(h^2) + O_P \left(\sqrt{\frac{|\log h|}{nh^{D_T}}} \right)$$

when $\mathbf{z}^{(0)} \in \{\mathbf{z} \in \mathcal{S}_1 \times \mathcal{S}_2 : d_g(\mathbf{z}, \mathbf{m}) \leq \tilde{r}_1\}$ with $\mathbf{m} \in \mathcal{M}$ and $\max(\mathbf{h}) = \max\{h_1, h_2\} \lesssim h$ is sufficiently small, where $D_T = D_1 + D_2$ is the intrinsic dimension and $d_g(\cdot, \cdot)$ is the geodesic distance on $\mathcal{S}_1 \times \mathcal{S}_2$.

4. SCMS Algorithm on $\mathcal{S}_1 \times \mathcal{S}_2$

• **Ridge Estimation on $\mathcal{S}_1 \times \mathcal{S}_2$.** Given the Riemannian gradient $\text{grad } f(\mathbf{z})$ and Hessian $\mathcal{H}f(\mathbf{z})$ on $\mathcal{S}_1 \times \mathcal{S}_2$, we generalize the definitions of order- d Euclidean (Eberly, 1996; Genovese et al., 2014) and directional (Zhang and Chen, 2021c) (density) ridges to the product space as:

$$\mathcal{R}_d = \{\mathbf{z} \in \mathcal{S}_1 \times \mathcal{S}_2 : V_d(\mathbf{z})V_d(\mathbf{z})^T \nabla f(\mathbf{z}) = \mathbf{0}, \lambda_{d+1}(\mathbf{z}) < 0\}, \quad (19)$$

where $\mathbf{z} = (\mathbf{x}, \mathbf{y})$, $\lambda_1(\mathbf{z}) \geq \dots \geq \lambda_{D_T}(\mathbf{z})$ are eigenvalues of $\mathcal{H}f(\mathbf{z})$ within the tangent space, $D_T = D_1 + D_2$ is the intrinsic dimension of $\mathcal{S}_1 \times \mathcal{S}_2$, and $V_d(\mathbf{z}) = (\mathbf{v}_{d+1}(\mathbf{z}), \dots, \mathbf{v}_{D_T}(\mathbf{z}))$ with its columns as unit eigenvectors associated with the $(D_T - d)$ smallest eigenvalues within the tangent space $T_{\mathbf{z}}$. Whenever $\mathcal{S}_1 = \Omega_{D_1}$, $(\mathbf{x}, \mathbf{0})$ is a unit eigenvector of $\mathcal{H}f(\mathbf{z})$ associated with eigenvalue 0 and orthogonal to $T_{\mathbf{z}}$. The same applies to $(\mathbf{0}, \mathbf{y})$ when $\mathcal{S}_2 = \Omega_{D_2}$.

Similar to the mode estimation in Section 3, our KDE $\widehat{f}_{\mathbf{h}}$ in (2) provides a natural estimator of \mathcal{R}_d as:

$$\widehat{\mathcal{R}}_d = \{\mathbf{z} \in \mathcal{S}_1 \times \mathcal{S}_2 : \widehat{V}_d(\mathbf{z})\widehat{V}_d(\mathbf{z})^T \nabla \widehat{f}_{\mathbf{h}}(\mathbf{z}) = \mathbf{0}, \widehat{\lambda}_{d+1}(\mathbf{z}) < 0\}, \quad (20)$$

where $\widehat{V}_d(\mathbf{z})$ and $\widehat{\lambda}_{d+1}(\mathbf{z})$ are counterparts of $V_d(\mathbf{z})$ and $\lambda_{d+1}(\mathbf{z})$ defined by $\mathcal{H}\widehat{f}_{\mathbf{h}}(\mathbf{z})$. Under some regularity conditions, $\widehat{\mathcal{R}}_d$ is also a consistent estimator of \mathcal{R}_d ; see Appendix B.3 for a detailed discussion.

• **SCMS Algorithm on $\mathcal{S}_1 \times \mathcal{S}_2$: Pitfall and Solution.** To identify the estimated density ridges $\widehat{\mathcal{R}}_d$ in practice, the SCMS algorithm is one of the most effective off-the-shelf methods for this task. However, generalizing the mean shift algorithm in Section 3 with the standard technique in Ozertem and Erdogmus (2011); Ghassabeh et al. (2013) will lead to incorrect estimated ridges.

Pitfall. Naively, one may mimic the standard SCMS iteration and update the sequence $\{\mathbf{z}^{(t)}\}_{t=0}^{\infty} \subset \mathcal{S}_1 \times \mathcal{S}_2$ based on the mean shift vector (15) as:

$$\mathbf{z}^{(t+1)} \leftarrow \mathbf{z}^{(t)} + \widehat{V}_d(\mathbf{z}^{(t)})\widehat{V}_d(\mathbf{z}^{(t)})^T \Xi(\mathbf{z}^{(t)}) \quad (21)$$

with some additional standardization whenever \mathcal{S}_1 and/or \mathcal{S}_2 are directional for $t = 0, 1, \dots$. However, this naive SCMS iteration on $\mathcal{S}_1 \times \mathcal{S}_2$ will instead converge to a transformed estimated ridge $\widehat{\mathcal{R}}_d^{(T)}$ as:

$$\widehat{\mathcal{R}}_d^{(T)} = \{z \in \mathcal{S}_1 \times \mathcal{S}_2 : \widehat{V}_d(z)\widehat{V}_d(z)^T \widetilde{D}(z)^{-1} \nabla \widehat{f}_h(z) = \mathbf{0}, \widehat{\lambda}_{d+1}(z) < 0\}, \quad (22)$$

where $\widetilde{D}(z)$ is defined in (16). The key reason is that the mean shift vector (15) does not align with the total gradient estimator (13) but is instead equal to the transformed gradient $\widetilde{D}(z)^{-1} \nabla \widehat{f}_h(z)$. When the factors G_x, G_y in $\widetilde{D}(z)$ are not equal, $\widehat{\mathcal{R}}_d \neq \widehat{\mathcal{R}}_d^{(T)}$.

Asymptotically, $\widehat{\mathcal{R}}_d^{(T)}$ is approaching the quantity

$$\mathcal{R}_d^{(T)} = \{z \in \mathcal{S}_1 \times \mathcal{S}_2 : V_d(z)V_d(z)^T \mathbf{H}\widetilde{F}(z)^{-1} \nabla f(z) = \mathbf{0}, \lambda_{d+1}(z) < 0\},$$

when $h_1, h_2 \lesssim h$ are small and the sample size n is large because of the following proposition. As $\mathcal{R}_d^{(T)} \neq \mathcal{R}_d$, the naive SCMS algorithm will lead to an inconsistent estimator of the true ridge \mathcal{R}_d .

Proposition 3. *Assume conditions (A1-2). Then,*

$$\left[\mathbf{H}\widetilde{D}(z) \right]^{-1} \text{grad } \widehat{f}_h(z) - \widetilde{F}(z)^{-1} \text{grad } f(z) = O(h^2) + O_P \left(\sqrt{\frac{1}{nh^{D_1+D_2+2}}} \right)$$

for any fixed $z \in \mathcal{S}_1 \times \mathcal{S}_2$ with $h_1, h_2 \lesssim h \rightarrow 0$ and $nh^{D_1+D_2+2} \rightarrow \infty$, where $\widetilde{F}(z)$ is a nonrandom function depending on $f(z)$ and kernels; see Appendix D.

Solution. Some simple algebra from (4) show that $\mathbf{H}^{-1}\Xi(z) = \frac{\nabla \widehat{f}_h(z)}{\widehat{f}_h(z)}$ under Gaussian and/or von Mises kernels. Based on this insight, we propose our SCMS algorithm on $\mathcal{S}_1 \times \mathcal{S}_2$ with iterative steps as:

$$z^{(t+1)} \leftarrow z^{(t)} + \eta \cdot \widehat{V}_d(z^{(t)})\widehat{V}_d(z^{(t)})^T \mathbf{H}^{-1}\Xi(z^{(t)}) \quad (23)$$

with some additional standardization whenever \mathcal{S}_1 and/or \mathcal{S}_2 are directional for $t = 0, 1, \dots$, where $\eta > 0$ is the step size. Different from the naive SCMS algorithm (21), there is an extra tuning parameter, step size η , that influences the performance of our proposed SCMS algorithm, and we discuss in Appendix C.3 that it is inappropriate to take η as a constant, says, $\eta = 1$. As a guideline, we suggest taking the step size to be adaptive to bandwidth parameters as:

$$\eta = \min\{\max(\mathbf{h}) \cdot \min(\mathbf{h}), 1\} = \min\{h_1 h_2, 1\}. \quad (24)$$

so that when $h_1, h_2 \lesssim h$ are small, η mimics the asymptotic rate $O(h^2)$ of adaptive step sizes in Euclidean/directional (subspace constrained) mean shift algorithms (Cheng, 1995; Arias-Castro et al., 2016; Zhang and Chen, 2021c). The upper bound 1 is introduced to prevent η from being too large. Unlike the mean shift algorithm in Section 3, we do not formulate the componentwise SCMS algorithm because the eigenspace projector $\widehat{V}_d(z)\widehat{V}_d(z)^T$ needs recomputing in each sub-step of its iteration. Given the time complexity $O((D_1 + D_2)^3)$ of the spectral decomposition on $\mathcal{H}\widehat{f}_h(z)$, the componentwise SCMS algorithm falls short in computational efficiency compared to (23).

Under (24), we have the following (linear) convergence results for our proposed SCMS algorithm on $\mathcal{S}_1 \times \mathcal{S}_2$. We also provide simulation studies in Appendix C.3 to demonstrate the effectiveness of (24).

Theorem 4. *Assume that all the assumptions in Theorem 8 and condition (A4) in Appendix C.4 hold. Given the sequence $\{\mathbf{z}^{(t)}\}_{t=0}^{\infty}$ defined by our SCMS algorithm (23) with step size η dominated by $\max(\mathbf{h})$, there exist constants $\tilde{A}, \tilde{r}_2 > 0$ and $\Upsilon_2 \in (0, 1)$ such that with probability at least $1 - \delta$ for any $\delta \in (0, 1)$,*

$$\max \left\{ d_g(\mathbf{z}^{(t)}, \hat{\mathcal{R}}_d), d_g(\mathbf{z}^{(t)}, \mathcal{R}_d) \right\} \leq \tilde{A} \cdot \Upsilon_2^t$$

when $\mathbf{z}^{(0)} \in \mathcal{R}_d \oplus \tilde{r}_2 = \{\mathbf{z} \in \mathcal{S}_1 \times \mathcal{S}_2 : d_g(\mathbf{z}, \mathcal{R}_d) \leq \tilde{r}_2\}$ and $\max(\mathbf{h})$ is sufficiently small.

The key step of proving Theorem 4 is to show that our proposed SCMS algorithm (23) fits well into the general subspace constrained gradient ascent framework with an intrinsic step size related to the bandwidths h_1, h_2 ; see Appendix C for details. Theorem 4 indicates that our proposed rule of thumb for the step size η guarantees the (linear) convergence of the algorithm when the bandwidths h_1, h_2 are small. Therefore, the time complexity of our proposed SCMS algorithm (23) applied to the entire dataset with size n on $\mathcal{S}_1 \times \mathcal{S}_2$ is $O(n \times (D_1 + D_2)^3 \times \log(1/\epsilon))$ for reaching an ϵ -error.

5. Experiments

In this section, we unfold our experiments on both simulated and real-world datasets, in which the presentations come from two aspects: mode-seeking and ridge-finding problems with directional-linear and directional-directional data. Unless specified otherwise, the initial set of mesh points in each experiment is chosen as the original dataset, and the tolerance level for stopping the algorithm is 10^{-7} . Moreover, we implement our proposed SCMS algorithm under the logarithm of KDE given its faster convergence speed (Ghassabeh et al., 2013) and statistical stability of resulting ridges (Genovese et al., 2014).

• **Simulation 1: Mode-Seeking on $\Omega_1 \times \mathbb{R}$.** We simulate 1000 points of a vMF-Gaussian mixture model modified from García-Portugués et al. (2013) as:

$$\frac{2}{5} \text{vMF}((1, 0), 3) \mathcal{N}\left(0, \frac{1}{4}\right) + \frac{1}{5} \text{vMF}((0, 1), 10) \mathcal{N}(1, 1) + \frac{2}{5} \text{vMF}((-1, 0), 3) \mathcal{N}(2, 1).$$

The directional bandwidth $h_1 \approx 0.454$ and linear bandwidth $h_2 \approx 0.314$ are selected via the rule of thumb described in Appendix A.1. We also remove the data points whose density values are lower than 5% quantiles of density estimates on the entire simulated dataset before applying the mean shift algorithm (17) or (18) in order to avoid spurious local modes. Panels (a-b) of Figure 3 present the estimated local modes

$$(0.998, 0.064, 0.066), (0, 1, 1.20), (-1, 0, 1.84) \in \Omega_1 \times \mathbb{R}$$

yielded by our mean shift algorithm on the simulated directional-linear data, which are close to the true mode under some precision level. In addition, the local modes obtained by simultaneous (17) and componentwise (18) mean shift algorithms are essentially the same

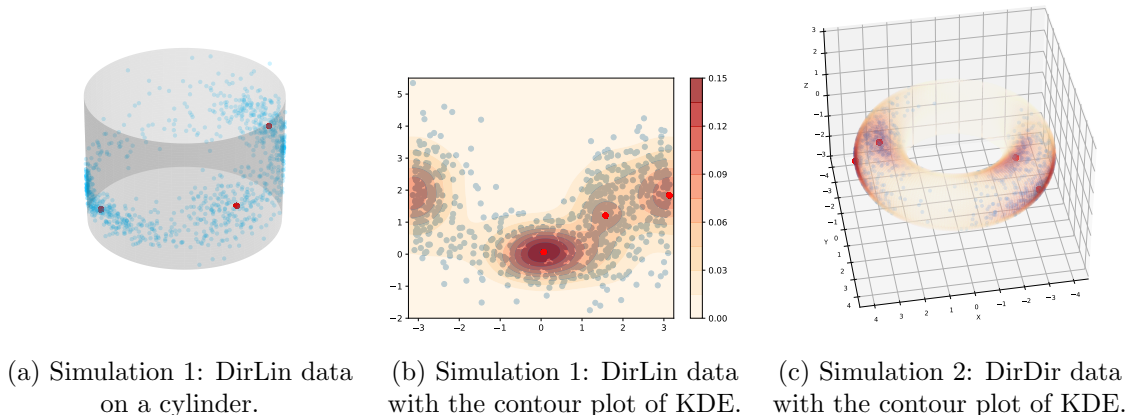


Figure 3: Local modes obtained by our mean shift algorithm on the simulated DirLin and DirDir data. In each panel, the red dots are estimated local modes while the blue dots are simulated points.

under von Mises and Gaussian kernels, while the simultaneous version excels in terms of time efficiency.

• **Simulation 2: Mode-Seeking on $\Omega_1 \times \Omega_1$.** We sample 1000 points from an independent product of two vMF mixture densities as:

$$\left[\frac{1}{2} \text{vMF}((1, 0), 5) + \frac{1}{4} \text{vMF}((0, 1), 5) \right] \times \left[\frac{1}{2} \text{vMF}((1, 0), 7) + \frac{1}{4} \text{vMF}((1/\sqrt{2}, -1/\sqrt{2}), 7) \right],$$

where the four true local modes are $(0, 0)$, $(0, 3\pi/4)$, $(\pi/2, 0)$, and $(\pi/2, 3\pi/4)$ under the angular coordinate system. We apply our mean shift algorithm on this simulated data with bandwidths $h_1 \approx 0.218$, $h_2 \approx 0.339$ selected via the rule of thumb in Appendix A. As shown in Panel (c) of Figure 3 on a torus, the estimated local modes $(-0.01, -0.05)$, $(0.01, 2.37)$, $(1.52, 0.04)$, $(1.70, 2.38)$ are not only consistent to the contour of KDE (2) but also close to the true local modes.

• **Simulation 3: Ridge-Finding on $\Omega_2 \times \mathbb{R}$.** The simulation studies on ridge estimation with our proposed SCMS algorithm (23) on DirLin and DirDir data are delineated in Appendix C.3 when we investigate the effects of varying the step size η . To compare our proposed method with the regular/Euclidean SCMS algorithm, we describe another simulated example on $\Omega_2 \times \mathbb{R}$. Consider a spiral curve

$$\begin{aligned} \mathcal{C} &= \{ (t \cos(\pi/6) \cos(5t), t \cos(\pi/6) \sin(5t), t \sin(\pi/6)) : \\ &\quad 0 \leq t \leq 4 \} \\ &\equiv \{ (\xi, \phi, R) = ((900t/\pi)^\circ, 30^\circ, t) : 0 \leq t \leq 4 \}, \end{aligned}$$

where we convert the first two radian coordinates into their degree measures in the second angular-linear representation of \mathcal{C} . We sample 1000 observations on the spiral curve with additive Gaussian noises $\mathcal{N}(0, 0.2^2)$ to their angular-linear coordinates; see Panel (a)

of Figure 2. One may think of (ξ, ϕ, R) as (right ascension, declination, redshift) under the astronomical survey coordinate system. Hence, each simulated observation has three different coordinates: (i) Cartesian in $\mathbb{R}^3 : (x_i, y_i, z_i)$; (ii) angular-linear on $\Omega_2 \times \mathbb{R} : (\xi_i, \phi_i, R_i)$; (iii) directional-linear on $\Omega_2 \times \mathbb{R} : (\mathbf{X}_i, R_i)$; where, for $i = 1, \dots, 1000$, $(x_i, y_i, z_i) = (R_i \cos \phi_i \cos \xi_i, R_i \cos \phi_i \sin \xi_i, R_i \sin \phi_i)$ and $\mathbf{X}_i = (\cos \phi_i \cos \xi_i, \cos \phi_i \sin \xi_i, \sin \phi_i)$. We apply the regular SCMS algorithm to $\{(x_i, y_i, z_i)\}_{i=1}^{1000}$ and $\{(\xi_i, \phi_i, R_i)\}_{i=1}^{1000}$ as well as our proposed SCMS algorithm to $\{(\mathbf{X}_i, R_i)\}_{i=1}^{1000}$ under the same simulated dataset. As shown in Figure 2, the regular SCMS algorithm fails to approximate the underlying curve with its yielded ridges while on the contrary, our proposed SCMS algorithm converges to estimated ridges near the true structure. Quantitatively, our proposed SCMS algorithm also outperforms the regular one in terms of the manifold-recovering error measure in \mathbb{R}^3 defined in Appendix A.2 as:

$$d_H(\widehat{\mathcal{R}}_1, \mathcal{C}) \approx \begin{cases} 0.199 & \text{for Panel (b) of Figure 2,} \\ 0.546 & \text{for Panel (c) of Figure 2,} \\ 0.058 & \text{for Panel (d) of Figure 2.} \end{cases}$$

Other additional simulated examples and real-world applications of our proposed SCMS algorithm can be found in Appendix A.

6. Conclusion and Future Work

In this paper, we generalized the (subspace constrained) mean shift algorithms to a Euclidean/directional product space, established their (linear) convergence properties, and provided empirical guidelines for using the algorithms in practice. The effectiveness of our proposed methods was also tested on both DirLin and DirDir datasets. In the future, we may consider extending the mean shift and SCMS algorithms to a product space with an infinite number of factors, such as some functional spaces. In this direction, the kernelized mean shift algorithm (Anand et al., 2013) might be a good starting point. Another future direction is to study mode-seeking and ridge-finding problems on a product space whose factors are more general topological spaces, such as some sophisticated (Riemannian) manifolds (Zhang et al., 2021).

Acknowledgments

YC is supported by NSF DMS 1952781, NSF DMS 2112907, and NIH U24 AG072122.

Funding for the Sloan Digital Sky Survey IV has been provided by the Alfred P. Sloan Foundation, the U.S. Department of Energy Office of Science, and the Participating Institutions. SDSS-IV acknowledges support and resources from the Center for High Performance Computing at the University of Utah. The SDSS website is www.sdss.org.

SDSS-IV is managed by the Astrophysical Research Consortium for the Participating Institutions of the SDSS Collaboration including the Brazilian Participation Group, the Carnegie Institution for Science, Carnegie Mellon University, Center for Astrophysics — Harvard & Smithsonian, the Chilean Participation Group, the French Participation

Group, Instituto de Astrofísica de Canarias, The Johns Hopkins University, Kavli Institute for the Physics and Mathematics of the Universe (IPMU) / University of Tokyo, the Korean Participation Group, Lawrence Berkeley National Laboratory, Leibniz Institut für Astrophysik Potsdam (AIP), Max-Planck-Institut für Astronomie (MPIA Heidelberg), Max-Planck-Institut für Astrophysik (MPA Garching), Max-Planck-Institut für Extraterrestrische Physik (MPE), National Astronomical Observatories of China, New Mexico State University, New York University, University of Notre Dame, Observatório Nacional / MCTI, The Ohio State University, Pennsylvania State University, Shanghai Astronomical Observatory, United Kingdom Participation Group, Universidad Nacional Autónoma de México, University of Arizona, University of Colorado Boulder, University of Oxford, University of Portsmouth, University of Utah, University of Virginia, University of Washington, University of Wisconsin, Vanderbilt University, and Yale University.

References

- P.-A. Absil, R. Mahony, and R. Sepulchre. *Optimization algorithms on matrix manifolds*. Princeton University Press, 2009.
- R. Ahumada, C. A. Prieto, A. Almeida, F. Anders, S. F. Anderson, B. H. Andrews, B. Anguiano, R. Arcodia, E. Armengaud, M. Aubert, et al. The 16th data release of the sloan digital sky surveys: first release from the apogee-2 southern survey and full release of eboss spectra. *The Astrophysical Journal Supplement Series*, 249(1):3, 2020.
- Y. Aliyari Ghassabeh. A sufficient condition for the convergence of the mean shift algorithm with gaussian kernel. *Journal of Multivariate Analysis*, 135:1 – 10, 2015.
- S. Anand, S. Mittal, O. Tuzel, and P. Meer. Semi-supervised kernel mean shift clustering. *IEEE transactions on pattern analysis and machine intelligence*, 36(6):1201–1215, 2013.
- E. Arias-Castro, D. Mason, and B. Pelletier. On the estimation of the gradient lines of a density and the consistency of the mean-shift algorithm. *Journal of Machine Learning Research*, 17(43):1–28, 2016. URL <http://jmlr.org/papers/v17/ariascastro16a.html>.
- Z. Bai, C. Rao, and L. Zhao. Kernel estimators of density function of directional data. *Journal of Multivariate Analysis*, 27(1):24 – 39, 1988.
- A. Banerjee, I. S. Dhillon, J. Ghosh, and S. Sra. Clustering on the unit hypersphere using von mises-fisher distributions. *Journal of Machine Learning Research*, 6:1345–1382, 2005.
- A. Brown, A. Vallenari, T. Prusti, J. De Bruijne, C. Babusiaux, C. Bailer-Jones, M. Biermann, D. W. Evans, L. Eyer, F. Jansen, et al. Gaia data release 2-summary of the contents and survey properties. *Astronomy & astrophysics*, 616:A1, 2018.
- M. Á. Carreira-Perpiñán. Gaussian mean-shift is an em algorithm. *IEEE Transactions on Pattern Analysis and Machine Intelligence*, 29(5):767–776, 2007.
- M. Á. Carreira-Perpiñán. A review of mean-shift algorithms for clustering. *arXiv preprint arXiv:1503.00687*, 2015.

- M. Cautun, R. Van De Weygaert, B. J. Jones, and C. S. Frenk. Evolution of the cosmic web. *Monthly Notices of the Royal Astronomical Society*, 441(4):2923–2973, 2014.
- H. E. Cetingul and R. Vidal. Intrinsic mean shift for clustering on stiefel and grassmann manifolds. In *2009 IEEE Conference on Computer Vision and Pattern Recognition*, pages 1896–1902. IEEE, 2009.
- E. J. Chacón, T. Duong, and P. M. Wand. Asymptotics for general multivariate kernel density derivative estimators. *Statistica Sinica*, 21:807, 2011.
- J. E. Chacón. The modal age of statistics. *International Statistical Review*, 88(1):122–141, 2020.
- J. E. Chacón and T. Duong. Data-driven density derivative estimation, with applications to nonparametric clustering and bump hunting. *Electronic Journal of Statistics*, 7:499–532, 2013.
- J. E. Chacón and P. Monfort. A comparison of bandwidth selectors for mean shift clustering. *arXiv preprint arXiv:1310.7855*, 2013.
- Y.-C. Chen. A tutorial on kernel density estimation and recent advances. *Biostatistics & Epidemiology*, 1(1):161–187, 2017.
- Y.-C. Chen, C. R. Genovese, and L. Wasserman. Generalized mode and ridge estimation. *arXiv preprint arXiv:1406.1803*, 2014. URL <https://arxiv.org/abs/1406.1803>.
- Y.-C. Chen, C. R. Genovese, and L. Wasserman. Asymptotic theory for density ridges. *Annals of Statistics*, 43(5):1896–1928, 10 2015.
- Y.-C. Chen, C. R. Genovese, and L. Wasserman. A comprehensive approach to mode clustering. *Electronic Journal of Statistics*, 10(1):210–241, 2016. URL <https://doi.org/10.1214/15-EJS1102>.
- Y. Cheng. Mean shift, mode seeking, and clustering. *IEEE Transactions on Pattern Analysis and Machine Intelligence*, 17(8):790–799, 1995.
- J. Clampitt, H. Miyatake, B. Jain, and M. Takada. Detection of stacked filament lensing between sdss luminous red galaxies. *Monthly Notices of the Royal Astronomical Society*, 457(3):2391–2400, 2016.
- D. Comaniciu and P. Meer. Mean shift: a robust approach toward feature space analysis. *IEEE Transactions on Pattern Analysis and Machine Intelligence*, 24(5):603–619, 2002.
- K. S. Dawson, J.-P. Kneib, W. J. Percival, S. Alam, F. D. Albareti, S. F. Anderson, E. Armengaud, É. Aubourg, S. Bailey, J. E. Bautista, et al. The sdss-iv extended baryon oscillation spectroscopic survey: overview and early data. *The Astronomical Journal*, 151(2):44, 2016.
- V. De Lapparent, M. J. Geller, and J. P. Huchra. A slice of the universe. *The astrophysical journal*, 302:L1–L5, 1986.

- M. do Carmo. *Differential Geometry of Curves and Surfaces: Revised and Updated Second Edition*. Dover Books on Mathematics. Dover Publications, 2016.
- M. P. Do Carmo. *Riemannian geometry*. Springer Science & Business Media, 2013.
- D. Eberly. *Ridges in Image and Data Analysis*. Computational Imaging and Vision. Springer Netherlands, 1996.
- U. Einmahl and D. M. Mason. Uniform in bandwidth consistency of kernel-type function estimators. *Annals of Statistics*, 33(3):1380–1403, 06 2005.
- C. Fefferman, S. Mitter, and H. Narayanan. Testing the manifold hypothesis. *Journal of the American Mathematical Society*, 29(4):983–1049, 2016.
- K. Fukunaga and L. Hostetler. The estimation of the gradient of a density function, with applications in pattern recognition. *IEEE Transactions on Information Theory*, 21(1):32–40, 1975.
- E. García-Portugués. Exact risk improvement of bandwidth selectors for kernel density estimation with directional data. *Electronic Journal of Statistics*, 7:1655–1685, 2013.
- E. García-Portugués, R. M. Crujeiras, and W. González-Manteiga. Kernel density estimation for directional-linear data. *Journal of Multivariate Analysis*, 121:152 – 175, 2013.
- E. García-Portugués, R. M. Crujeiras, and W. González-Manteiga. Central limit theorems for directional and linear random variables with applications. *Statistica Sinica*, pages 1207–1229, 2015.
- C. R. Genovese, M. Perone-Pacifico, I. Verdinelli, and L. Wasserman. Nonparametric ridge estimation. *Annals of Statistics*, 42(4):1511–1545, 08 2014.
- Y. A. Ghassabeh, T. Linder, and G. Takahara. On some convergence properties of the subspace constrained mean shift. *Pattern Recognition*, 46:3140–3147, 2013.
- E. Giné and A. Guillou. Rates of strong uniform consistency for multivariate kernel density estimators. *Annales de l’Institut Henri Poincaré (B) Probability and Statistics*, 38(6):907 – 921, 2002.
- P. Hall, G. S. Watson, and J. Cabrara. Kernel density estimation with spherical data. *Biometrika*, 74(4):751–762, 12 1987. ISSN 0006-3444. URL <https://doi.org/10.1093/biomet/74.4.751>.
- P. Hall, H.-G. Müller, and P.-S. Wu. Real-time density and mode estimation with application to time-dynamic mode tracking. *Journal of Computational and Graphical Statistics*, 15(1):82–100, 2006.
- D. W. Hogg. Distance measures in cosmology. *arXiv preprint astro-ph/9905116*, 1999.
- A. J. Izenman. Introduction to manifold learning. *Wiley Interdisciplinary Reviews: Computational Statistics*, 4(5):439–446, 2012.

- M. Kafai, Y. Miao, and K. Okada. Directional mean shift and its application for topology classification of local 3d structures. In *2010 IEEE Computer Society Conference on Computer Vision and Pattern Recognition-Workshops*, pages 170–177. IEEE, 2010.
- J. Klemelä. Estimation of densities and derivatives of densities with directional data. *Journal of Multivariate Analysis*, 73(1):18 – 40, 2000.
- J. M. Lee. *Riemannian manifolds: an introduction to curvature*, volume 176. Springer Science & Business Media, 2006.
- X. Li, Z. Hu, and F. Wu. A note on the convergence of the mean shift. *Pattern Recognition*, 40(6):1756 – 1762, 2007.
- V. Marchitelli, P. Harabaglia, C. Troise, and G. De Natale. On the correlation between solar activity and large earthquakes worldwide. *Scientific reports*, 10(1):1–10, 2020.
- K. Mardia and P. Jupp. *Directional Statistics*. Wiley Series in Probability and Statistics. Wiley, 2000.
- J. S. Marron and D. Ruppert. Transformations to reduce boundary bias in kernel density estimation. *Journal of the Royal Statistical Society: Series B (Methodological)*, 56(4): 653–671, 1994.
- M. D. Marzio, A. Panzera, and C. C. Taylor. Kernel density estimation on the torus. *Journal of Statistical Planning and Inference*, 141(6):2156 – 2173, 2011.
- G. J. McLachlan and T. Krishnan. *The EM algorithm and extensions*. Wiley series in probability and statistics. Wiley, 2. ed edition, 2008.
- A. Mokkadem and M. Pelletier. The law of the iterated logarithm for the multivariate kernel mode estimator. *ESAIM: Probability and statistics*, 7:1–21, 2003.
- P. Moritz, R. Nishihara, S. Wang, A. Tumanov, R. Liaw, E. Liang, M. Elibol, Z. Yang, W. Paul, M. I. Jordan, et al. Ray: A distributed framework for emerging {AI} applications. In *13th {USENIX} Symposium on Operating Systems Design and Implementation ({OSDI} 18)*, pages 561–577, 2018.
- S. Oba, K. Kato, and S. Ishii. Multi-scale clustering for gene expression profiling data. In *Fifth IEEE Symposium on Bioinformatics and Bioengineering (BIBE'05)*, pages 210–217, Oct 2005.
- U. Ozertem and D. Erdogmus. Locally defined principal curves and surfaces. *Journal of Machine Learning Research*, 12(34):1249–1286, 2011.
- X. Pennec. Intrinsic statistics on riemannian manifolds: Basic tools for geometric measurements. *Journal of Mathematical Imaging and Vision*, 25(1):127–154, 2006.
- W. Qiao and W. Polonik. Algorithms for ridge estimation with convergence guarantees. *arXiv preprint arXiv:2104.12314*, 2021.

- J. P. Romano. On weak convergence and optimality of kernel density estimates of the mode. *The Annals of Statistics*, pages 629–647, 1988.
- D. Ruppert and D. B. Cline. Bias reduction in kernel density estimation by smoothed empirical transformations. *The Annals of Statistics*, pages 185–210, 1994.
- A. Schuster. On lunar and solar periodicities of earthquakes. *Proceedings of the Royal Society of London*, 61(369-377):455–465, 1897.
- D. Scott. *Multivariate Density Estimation: Theory, Practice, and Visualization*. Wiley Series in Probability and Statistics. Wiley, 2015.
- B. W. Silverman. *Density Estimation for Statistics and Data Analysis*. Chapman & Hall, London, 1986.
- V. Springel, C. S. Frenk, and S. D. White. The large-scale structure of the universe. *nature*, 440(7088):1137–1144, 2006.
- R. Subbarao and P. Meer. Nonlinear mean shift for clustering over analytic manifolds. In *2006 IEEE Computer Society Conference on Computer Vision and Pattern Recognition (CVPR'06)*, volume 1, pages 1168–1175. IEEE, 2006.
- R. Subbarao and P. Meer. Nonlinear mean shift over riemannian manifolds. *International journal of computer vision*, 84(1):1, 2009.
- M. Tavares, A. Azevedo, et al. Influences of solar cycles on earthquakes. *Natural Science*, 3(06):436, 2011.
- E. Tempel, R. Stoica, V. J. Martinez, L. Liivamägi, G. Castellan, and E. Saar. Detecting filamentary pattern in the cosmic web: a catalogue of filaments for the sdss. *Monthly Notices of the Royal Astronomical Society*, 438(4):3465–3482, 2014.
- A. W. v. d. Vaart. *Asymptotic statistics*. Cambridge series on statistical and probabilistic mathematics. Cambridge University Press, 1998.
- M. P. Wand and M. C. Jones. Comparison of smoothing parameterizations in bivariate kernel density estimation. *Journal of the American Statistical Association*, 88(422):520–528, 1993.
- M. P. Wand and M. C. Jones. *Kernel smoothing*. CRC press, 1994.
- L. Wasserman. *All of Nonparametric Statistics (Springer Texts in Statistics)*. Springer-Verlag, Berlin, Heidelberg, 2006.
- D. M. Wilkinson, C. Maraston, D. Goddard, D. Thomas, and T. Parikh. Firefly (fitting iteratively for likelihood analysis): a full spectral fitting code. *Monthly Notices of the Royal Astronomical Society*, 472(4):4297–4326, 2017.
- S. J. Wright. Coordinate descent algorithms. *Mathematical Programming*, 151(1):3–34, 2015.

- C. J. Wu. On the convergence properties of the em algorithm. *The Annals of statistics*, pages 95–103, 1983.
- H. Zhang and S. Sra. First-order methods for geodesically convex optimization. In *Conference on Learning Theory*, pages 1617–1638. PMLR, 2016.
- S. Zhang, A. Moscovich, and A. Singer. Product manifold learning. In *International Conference on Artificial Intelligence and Statistics*, pages 3241–3249. PMLR, 2021.
- Y. Zhang and Y.-C. Chen. The em perspective of directional mean shift algorithm. *arXiv preprint arXiv:2101.10058*, 2021a. URL <https://arxiv.org/abs/2101.10058>.
- Y. Zhang and Y.-C. Chen. Kernel smoothing, mean shift, and their learning theory with directional data. *Journal of Machine Learning Research*, 22(154):1–92, 2021b. URL <http://jmlr.org/papers/v22/20-1194.html>.
- Y. Zhang and Y.-C. Chen. Linear convergence of the subspace constrained mean shift algorithm: From euclidean to directional data. *arXiv preprint arXiv:2104.14977*, 2021c. URL <https://arxiv.org/abs/2104.14977>.
- Y. Zhang, X. Yang, A. Faltenbacher, V. Springel, W. Lin, and H. Wang. The spin and orientation of dark matter halos within cosmic filaments. *The Astrophysical Journal*, 706(1):747, 2009.
- Y. Zhang, X. Yang, H. Wang, L. Wang, H. Mo, and F. C. Van den Bosch. Alignments of galaxies within cosmic filaments from sdss dr7. *The Astrophysical Journal*, 779(2):160, 2013.
- L. Zhao and C. Wu. Central limit theorem for integrated squared error of kernel estimators of spherical density. *Sci. China Ser. A Math.*, 44(4):474–483, 2001.
- O. Zimmermann and U. H. Hansmann. Support vector machines for prediction of dihedral angle regions. *Bioinformatics*, 22(24):3009–3015, 2006.

Appendices

The Appendices contain some auxiliary results and proofs of theorems in the main paper. Here is an outline of the Appendices.

- **Appendix A: Additional Experimental Details and Results.** We include additional experiments and provide some implementation details about our experiments.
- **Appendix B: Statistical Consistency.** We describe our assumptions and the statistical convergence rates of KDE in $\mathcal{S}_1 \times \mathcal{S}_2$ as well as the associated mode and ridge estimators.
- **Appendix C: Linear Convergence of the Mean Shift and SCMS Algorithms on $\mathcal{S}_1 \times \mathcal{S}_2$.** We formulate the (subspace constrained) gradient ascent framework on a general product manifold. Further, we argue how the proposed mean shift and SCMS algorithms fit into this framework and consequently, obtain their linear convergence properties. In addition, we present some empirical evidence from simulation studies that our suggested rule of thumb for the step size parameter η in the proposed SCMS algorithm is effective.
- **Appendix D: Proofs of Theorem 1 and Proposition 3.** We provide the proofs of Theorem 1 and Proposition 3.

A. Additional Experimental Details and Results

In this section, we describe complementary details of our experiments in the main paper and present some additional experimental results.

A.1 Bandwidth Selection

As studying the choices of bandwidth parameters for the directional and linear data is not the main focus of this paper, we leverage some existing rule-of-thumb bandwidth selectors in the literature. Without loss of generality, we assume that the dataset $\{\mathbf{Z}_i\}_{i=1}^n = \{(\mathbf{X}_i, \mathbf{Y}_i)\}_{i=1}^n \subset \Omega_{D_1} \times \mathbb{R}^{D_2}$ is directional-linear. For the bandwidth parameter in the directional part $\{\mathbf{X}_i\}_{i=1}^n$ on Ω_{D_1} , we utilize the rule of thumb in Proposition 2 of [García-Portugués \(2013\)](#), where the estimated concentration parameter is given by (4.4) in [Banerjee et al. \(2005\)](#). That is,

$$h_{\text{ROT}} = \left[\frac{4\pi^{\frac{1}{2}} \mathcal{I}_{\frac{D_1-1}{2}}(\hat{\kappa})^2}{\hat{\kappa}^{\frac{D_1+1}{2}} \left[2D_1 \cdot \mathcal{I}_{\frac{D_1+1}{2}}(2\hat{\kappa}) + (D_1+2)\hat{\kappa} \cdot \mathcal{I}_{\frac{D_1+3}{2}}(2\hat{\kappa}) \right] n} \right]^{\frac{1}{D_1+4}} \quad (25)$$

with $\hat{\kappa} = \frac{\bar{R}(D_1+1-\bar{R})}{1-\bar{R}^2}$,

where $\bar{R} = \frac{\|\sum_{i=1}^n \mathbf{X}_i\|_2}{n}$ given the directional dataset $\{\mathbf{X}_i\}_{i=1}^n \subset \Omega_{D_1} \subset \mathbb{R}^{D_1+1}$ and $\mathcal{I}_\alpha(\kappa)$ is the modified Bessel function of the first kind of order κ . For the bandwidth parameter in

the linear part $\{\mathbf{Y}_i\}_{i=1}^n$ on \mathbb{R}^{D_2} , we adopt the normal reference rule from Equation (17) in Chen et al. (2016) as:

$$h_{\text{NR}} = \bar{S}_n \times \left(\frac{4}{D_2 + 4} \right)^{\frac{1}{D_2+6}} n^{-\frac{1}{D_2+6}} \quad \text{with} \quad \bar{S}_n = \frac{1}{D_2} \sum_{j=1}^{D_2} S_{n,j}, \quad (26)$$

where $S_{n,j}$ is the sample standard deviation along the j -th coordinates of $\{\mathbf{Y}_i\}_{i=1}^n$.

A.2 Manifold-Recovering Error Measure

Given some noisy observations from a hidden manifold structure \mathcal{C} , such as the spiral curve in the Simulation 3 of Section 5 in the main paper, a manifold learning method can learn a collection of discrete data points or a set of solutions to a system of equations that approximate \mathcal{C} . For our proposed SCMS algorithm, this set of data points is represented by a discrete sample from the estimated ridge $\hat{\mathcal{R}}_d$. To quantify the estimation error of $\hat{\mathcal{R}}_d$ in recovering the true manifold structure \mathcal{C} , one cannot simply rely on the (average) distances of points on $\hat{\mathcal{R}}_d$ to \mathcal{C} as:

$$\frac{1}{|\hat{\mathcal{R}}_d|} \sum_{\mathbf{z} \in \hat{\mathcal{R}}_d} d(\mathbf{z}, \mathcal{C}),$$

where $|\hat{\mathcal{R}}_d|$ is the cardinality of (a discrete sample from) $\hat{\mathcal{R}}_d$ and $d(\mathbf{z}, \mathcal{C})$ is the distance measure defined in the (ambient) metric space containing $\hat{\mathcal{R}}_d$ and \mathcal{C} . This is because the estimated ridge $\hat{\mathcal{R}}_d$ (or any other estimated manifold structures) may only approximate a small portion of the true manifold \mathcal{C} even with uniform (but noisy) observations from \mathcal{C} ; see, for instance, Panel (c) of Figure 2 in the main paper or Panel (c) of Figure 4. Hence, we borrow the idea from the definition of Hausdorff distances and define our manifold-recovering error measure as:

$$d_H(\hat{\mathcal{R}}_d, \mathcal{C}) = \frac{1}{2} \left[\frac{1}{|\hat{\mathcal{R}}_d|} \sum_{\mathbf{z} \in \hat{\mathcal{R}}_d} d(\mathbf{z}, \mathcal{C}) + \frac{1}{|\mathcal{D}^c|} \sum_{\mathbf{z} \in \mathcal{D}^c} d(\mathbf{z}, \hat{\mathcal{R}}_d) \right], \quad (27)$$

where \mathcal{D}^c is a set of uniformly sampling points from the true manifold structure \mathcal{C} . This error measure averages over the approximation error and coverage of \mathcal{C} with the estimated ridge/manifold.

A.3 Simulation Study: Surface-Recovering on $\Omega_2 \times \mathbb{R}$

In the main paper (Simulation 3 of Section 5), we have shown the effectiveness of using our proposed SCMS algorithm to recover the underlying spiral curve from its noisy observations. As the previous experiments of our proposed (subspace constrained) mean shift algorithm focus exclusively on locating the local modes and ridges with intrinsic/manifold dimension 1, we now present an example of recovering a hidden surface with our proposed SCMS algorithm and compare the result with the regular SCMS algorithm.

Consider a simulated dataset with 2000 points $\{\mathbf{X}_i\}_{i=1}^{2000}$ on the circle of latitude 45° on the unit sphere Ω_2 with additive Gaussian noises $\mathcal{N}(0, 0.1^2)$ to their Cartesian coordinates in \mathbb{R}^3 . To ensure that the noisy simulated data points $\{\mathbf{X}_i\}_{i=1}^{2000}$ are on Ω_2 , we standardize them

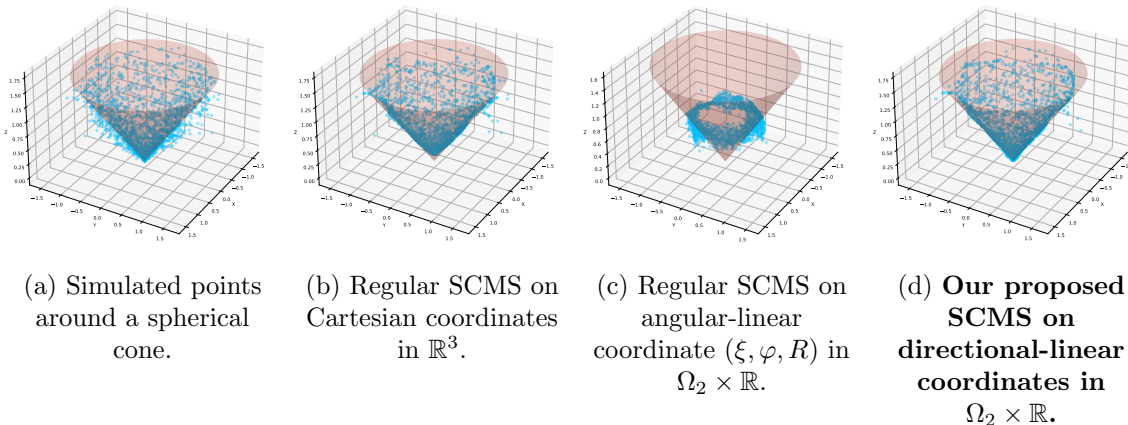


Figure 4: Estimated ridges obtained by various SCMS algorithms on the spherical cone data. In each panel, the red surface is the hidden manifold structure while the blue dots are final convergent points of SCMS algorithms.

back to Ω_2 via $\mathbf{X}_i = \frac{\mathbf{X}_i}{\|\mathbf{X}_i\|_2}$. In addition, we sample 2000 observations $\{R_i\}_{i=1}^{2000}$ uniformly from the interval $[0, 2]$. The entire simulated directional-linear dataset thus consists of observations $\{(\mathbf{X}_i, R_i)\}_{i=1}^{2000}$. In other words, for any data point (\mathbf{X}_i, R_i) , we view \mathbf{X}_i as its position on a sphere while R_i as the radius of the sphere for $i = 1, \dots, 2000$. More importantly, the true manifold structure can be regarded as a spherical cone \mathcal{C} with its apex angle as $\frac{\pi}{2}$; see Panel (a) of Figure 4. As in simulation 3 of Section 5 in the main paper, the directional-linear dataset $\{(\mathbf{X}_i, R_i)\}_{i=1}^{2000}$ has alternative representations as:

$$\begin{aligned} \text{Cartesian in } \mathbb{R}^3 &: (x_i, y_i, z_i), \\ \text{Angular-linear on } \Omega_2 \times \mathbb{R} &: (\xi_i, \phi_i, R_i), \end{aligned}$$

where (ξ_i, ϕ_i) is the angular representation of \mathbf{X}_i in degree measure and

$$(x_i, y_i, z_i) = (R_i \cos \phi_i \cos \xi_i, R_i \cos \phi_i \sin \xi_i, R_i \sin \phi_i)$$

for $i = 1, \dots, 2000$. We apply the regular SCMS algorithm to the data representations $\{(x_i, y_i, z_i)\}_{i=1}^{1000}$ and $\{(\xi_i, \phi_i, R_i)\}_{i=1}^{1000}$ as well as our proposed SCMS algorithm to $\{(\mathbf{X}_i, R_i)\}_{i=1}^{1000}$ under the same simulated dataset so as to estimate density ridges (or principal surfaces) with dimension 2. As shown in Figure 4, the regular SCMS algorithm fails to approximate the true spherical cone with its yielded ridge under the angular-linear coordinate system; see Panel (c) of Figure 4. Moreover, although the regular SCMS algorithm produces an estimated ridge capturing most parts of the true spherical cone under the Cartesian coordinate system, it fails to recover the surface near the apex; see Panel (b) of Figure 4. In contrast, our proposed SCMS algorithm converges to an estimated ridge near the true structure. Quantitatively, our proposed SCMS algorithm also outperforms the regular one

in terms of the manifold-recovering error measure (27) in \mathbb{R}^3 as:

$$d_H(\widehat{\mathcal{R}}_1, \mathcal{C}) \approx \begin{cases} 0.049 & \text{for Panel (b) of Figure 4,} \\ 0.255 & \text{for Panel (c) of Figure 4,} \\ 0.034 & \text{for Panel (d) of Figure 4.} \end{cases}$$

A.4 Real-World Application I: Local Mode Estimation on Earthquake Data

It is well-known in seismology (Schuster, 1897; Tavares et al., 2011; Marchitelli et al., 2020) that the solar and lunar periodicities and their related activities influence the occurrence of earthquakes. Here, as a preliminary application of our proposed mean shift algorithm in product spaces, we intend to jointly identify the times and places that earthquakes happen more intensively. With this goal in mind, we analyze the earthquakes worldwide with at least 2.5 magnitudes in a three-month period from 2021-07-01 00:00:00 UTC to 2021-09-30 23:59:59 UTC on the Earthquake Catalog (<https://earthquake.usgs.gov/earthquakes/search/>) of the United States Geological Survey. This dataset contains 7602 earthquakes in total. We convert their longitudes and latitudes to data points $\{\mathbf{X}_i\}_{i=1}^{7602}$ on the unit sphere Ω_2 and denote the striking time of each earthquake by its timestamp t_i . Therefore, the final dataset $\{(\mathbf{X}_i, t_i)\}_{i=1}^{7602} \subset \Omega_2 \times \mathbb{R}$ is directional-linear (or spatio-temporal). Analogous to our preceding simulation studies, we select the bandwidth parameters h_1, h_2 for directional and linear components through the rule of thumb (25) and normal reference rule (26), yielding that $h_1 \approx 0.225$ and $h_2 \approx 359081.318$. The initial set of points for the (simultaneous) mean shift algorithm is chosen as the original dataset. We implement the algorithm on the directional-linear product space $\Omega_2 \times \mathbb{R}$ via parallel programming under the Ray environment (Moritz et al., 2018) with stopping criteria as $\left\| \left(\mathbf{X}_i^{(t+1)}, t_i^{(t+1)} \right) - \left(\mathbf{X}_i^{(t)}, t_i^{(t)} \right) \right\|_2 \leq 10^{-7}$ or reaching the maximum iteration time 5000. Those non-convergent points after 5000 mean shift iterations will be removed from the output set of estimated local modes.

In Figure 5, we show the estimated local modes on the earthquake data yielded by our mean shift algorithm on $\Omega_2 \times \mathbb{R}$. As we project the modes onto the directional (location) space and linear (time) space in Panels (a,b) respectively, the resulting modes appear in more locations than the local modes of the marginal estimated density due to the multi-modal nature of the directional-linear density on $\Omega_2 \times \mathbb{R}$. Nevertheless, our proposed mean shift algorithm is still able to capture places where earthquakes are known to happen more intensively, such as the West Coast of the United States and Indonesia in Panel (a) of Figure 5. Moreover, we notice that earthquakes tend to strike more frequently in the first half of each month than the second half in Panel (b) of Figure 5. It will be interesting to study more about whether this phenomenon is related to the solar or lunar activities in the future. Further, one may also consider converting the striking times of earthquake data to the corresponding time points in solar or lunar calendar and apply our proposed mean shift algorithm to seeking out the earthquake modes. We believe that the yielded local modes should have better interpretations in solar or lunar cycle.

A.5 Real-World Application II: Cosmic Filament Detection

Previous observational and simulation studies have been suggesting that on megaparsec scales, matter in the Universe is not uniformly distributed but rather forms a complicated

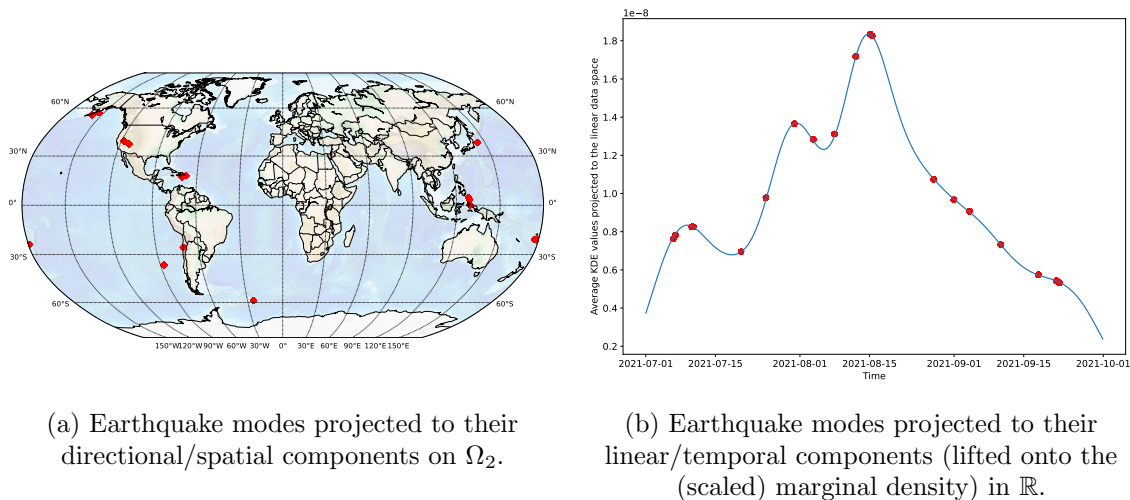
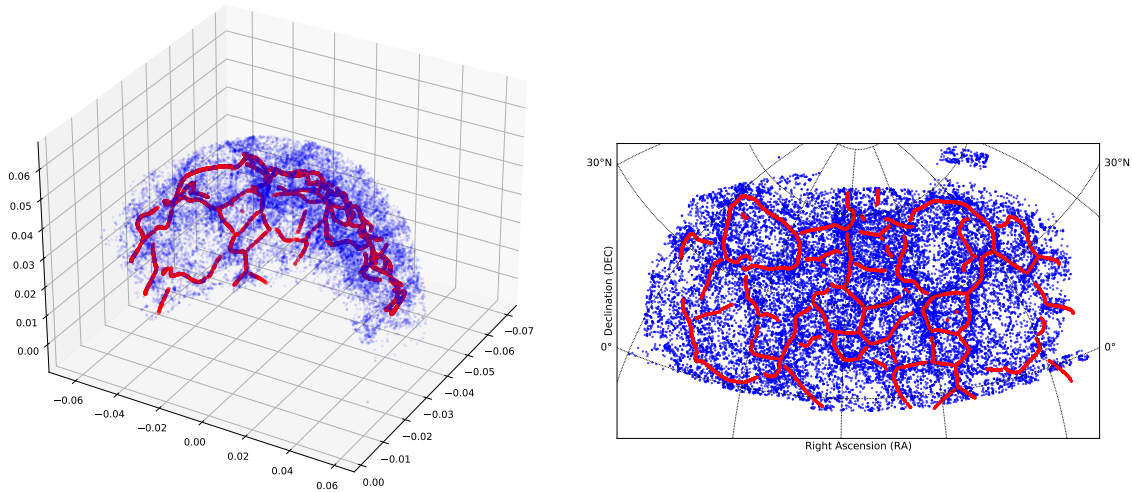


Figure 5: Local modes obtained by our mean shift algorithm on the earthquake data. In each panel, the red dots are estimated earthquake modes. The (earthquake) density estimates in (b) is obtained by averaging the directional-linear KDE over the directional/spatial space and projecting the values onto the linear/temporal space. In other words, the density plot in (b) is the estimated (scaled) marginal density with respect to time t .

large-scale network structure called the cosmic web (De Lapparent et al., 1986; Springel et al., 2006; Cautun et al., 2014). Among the several salient characteristics of the cosmic web, filaments are of great research interest to astrophysicists, because they contain information about the nature of dark matter (Zhang et al., 2009) and are correlated with the stellar properties of nearby galaxies (Zhang et al., 2013; Clampitt et al., 2016). Here, we demonstrate the possibility of leveraging our proposed SCMS algorithm to detect cosmic filaments from astronomical survey data from a novel angle.

For an illustrative purpose, we focus on a small portion of galaxies in the Data Release 16 (DR16) (Ahumada et al., 2020) of the Sloan Digital Sky Survey (SDSS-IV) with redshift value $0.05 \leq z < 0.07$. As the original spectroscopic file contains too many noisy samples, we obtain the galaxy data from the output of FIREFLY value-added catalog (Wilkinson et al., 2017) through the link (https://data.sdss.org/sas/dr16/eboss/spectro/firefly/v1_1_1/sdss_eboss_firefly-dr16.fits). The description of each column of the data file is on the website (https://data.sdss.org/datamodel/files/EBOSS_FIREFLY/FIREFLY_VER/sdss_eboss_firefly-DR16.html). We only consider the objects classified as galaxies with reliable and positive definite redshift values ($\text{CLASS_NOQSO} = \text{'galaxy'}$ and $\text{Z_NOQSO} > \text{Z_ERR_NOQSO} > 0$). Each galaxy in the dataset has its coordinate as (ξ_i, ϕ_i, z_i) , where ξ_i is its right ascension (RA), ϕ_i is its declination (DEC), and z_i is its redshift value (Z_NOQSO). We focus on the North Galactic Cap region ($100 < \text{RA} < 270$ and $-5 < \text{DEC} < 70$), in which the total number of galaxies with redshift value $0.05 \leq z < 0.07$ are 97435. Moreover, we only keep 80% of the galaxy observations with higher estimated density values so the final number of galaxies is $n = 77948$.



(a) Observed galaxies and detected filaments under the Cartesian coordinate system in \mathbb{R}^3 .

(b) Observed galaxies and detected filaments projected onto the (RA, DEC) space on Ω_2 .

Figure 6: Visualization of (a subset of) galaxies (blue dots) and detected filament points (red dots) by our proposed SCMS algorithm. For the purpose of visualization, we randomly sample 30000 galaxies from the original (subset of) galaxy data and plot them in Panels (a) and (b).

Traditionally, people apply the regular SCMS or other filament detection algorithms in a 3D Cartesian space, where each galaxy has a Cartesian coordinate (X_i, Y_i, Z_i) as

$$X_i = g(z_i) \cos \xi_i \cos \phi_i, \quad Y_i = g(z_i) \sin \xi_i \cos \phi_i, \quad Z_i = g(z_i) \sin \phi_i,$$

with $g(\cdot)$ being a distance transforming function; see [Tempel et al. \(2014\)](#) for details. As it might be difficult to choose an appropriate distance transforming function ([Hogg, 1999](#)), we consider recovering the filamentary structure in the original directional-linear space with our proposed SCMS algorithm under the galaxy data $\{(\mathbf{X}_i, z_i)\}_{i=1}^n \subset \Omega_2 \times \mathbb{R}$, where \mathbf{X}_i is the Cartesian coordinate of (ξ_i, ϕ_i) for $i = 1, \dots, n$. The bandwidth parameters, however, are selected via the rule of thumb (25) and normal reference rule (26) on a larger portion of observed galaxies on the North Galactic Cap with redshift value $0 \leq z < 2$, which leads to $h_1 \approx 0.0376$ for the directional part and $h_2 \approx 0.0187$ for the linear component. Computing the bandwidth parameters on a larger galaxy sample helps stabilize the detected filament structure. As in the above mode-seeking problem on earthquake data, we implement our proposed SCMS algorithm via parallel programming under the Ray environment ([Moritz et al., 2018](#)) with tolerance level 10^{-7} and maximum iteration time 5000. Again, those non-convergent points after 5000 SCMS iterations will be removed from the final set of estimated cosmic filaments.

Figure 6 presents the observed galaxies and detected cosmic filament points in 3D Cartesian and 2D (RA, DEC) spaces. It is noticeable that the filament structures obtained by

our proposed SCMS algorithm trace the regions with dense galaxies. In the future, we are interested in applying our method to the entire SDSS-IV galaxy data and study the correlations between detected filaments and the stellar properties of observed galaxies.

B. Statistical Consistency

This section is devoted to the discussion of consistency results for KDE $\widehat{f}_{\mathbf{h}}$ in (2) of the main paper (and its derivatives), its induced mode estimator $\widehat{\mathcal{M}}$, and ridge estimator $\widehat{\mathcal{R}}_d$ on $\mathcal{S}_1 \times \mathcal{S}_2$.

We reserve the notation $D^{[\tau]}f = f^{(\tau)}$ for the $|\tau|$ -th order partial derivative operator with the coordinate chart of $\mathcal{S}_1 \times \mathcal{S}_2$, where $[\tau] = (\tau_1, \dots, \tau_{D_T})$ is a multi-index and $D_T = D_1 + D_2$ is the sum of intrinsic dimensions of \mathcal{S}_1 and \mathcal{S}_2 . For $\ell = 0, 1, \dots$, we define the functional norms

$$\|f\|_{\infty}^{(\ell)} = \max_{\tau:|\tau|=\ell} \sup_{\mathbf{z} \in \mathcal{S}_1 \times \mathcal{S}_2} |f^{(\tau)}(\mathbf{z})|.$$

Notice that these functional norms are defined via the derivatives of f within the tangent space $T_{\mathbf{x}}(\mathcal{S}_1) \times T_{\mathbf{y}}(\mathcal{S}_2)$. In addition, we define $\|f\|_{\infty, \ell}^* = \max_{i=0, \dots, \ell} \|f\|_{\infty}^{(i)}$. For any matrix $A \in \mathbb{R}^{m \times n}$, its maximum norm is defined as $\|A\|_{\max} = \max_{i,j} A_{ij}$ with A_{ij} being the (i, j) entry of A .

B.1 Assumptions and Consistency of KDE

Whenever \mathcal{S}_1 and/or \mathcal{S}_2 are directional, we extend the (density) function f from $\mathcal{S}_1 \times \mathcal{S}_2$ to its ambient space $\mathcal{S} \setminus N_A$ as

$$\begin{cases} f(\mathbf{x}, \cdot) \equiv f\left(\frac{\mathbf{x}}{\|\mathbf{x}\|_2}, \cdot\right) & \text{if } \mathcal{S}_1 = \Omega_{D_1}, \\ f(\cdot, \mathbf{y}) \equiv f\left(\cdot, \frac{\mathbf{y}}{\|\mathbf{y}\|_2}\right) & \text{if } \mathcal{S}_2 = \Omega_{D_2}, \end{cases} \quad (28)$$

where $\mathcal{S} = \mathbb{R}^{D_1+1}_{\{\mathcal{S}_1=\Omega_{D_1}\}} \times \mathbb{R}^{D_2+1}_{\{\mathcal{S}_2=\Omega_{D_2}\}}$ and

$$N_A = \left\{ (\mathbf{x}, \mathbf{y}) \in \mathcal{S} : \left(\mathbf{x} \cdot \mathbb{1}_{\{\mathcal{S}_1=\Omega_{D_1}\}}, \mathbf{y} \cdot \mathbb{1}_{\{\mathcal{S}_2=\Omega_{D_2}\}} \right) = \mathbf{0} \right\}.$$

The indicators $\mathbb{1}_{\{\mathbf{x} \in \Omega_{D_j}\}}$ with $j = 1, 2$ are introduced to accommodate the directional data space Ω_{D_j} , whose ambient space is \mathbb{R}^{D_j+1} for $j = 1, 2$. Such extension is common when one needs to deal with directional densities (García-Portugués, 2013; García-Portugués et al., 2013, 2015; Zhang and Chen, 2021b,c). Besides assuming that the projection of f on \mathcal{S}_j has a compact support when $\mathcal{S}_j = \mathbb{R}^{D_j}$ is Euclidean for $j = 1, 2$, we impose the following conditions on f as well as the linear and directional kernel profiles k and L :

- **(A1)** Under the above extension of the (density) function f on $\mathcal{S}_1 \times \mathcal{S}_2$, we assume that the total gradient $\nabla f(\mathbf{z})$, total Hessian $\nabla^2 f(\mathbf{z})$, and third-order derivative tensor $\nabla^3 f(\mathbf{z})$ exists and are continuous in $\mathcal{S} \setminus N_A$. Moreover, they are assumed to be square integrable on $\mathcal{S}_1 \times \mathcal{S}_2$. Finally, f is assumed to have bounded fourth-order derivatives on $\mathcal{S}_1 \times \mathcal{S}_2$.

- **(A2)** Given the KDE \widehat{f}_h defined in (2) and (3) in the main paper, we assume that its kernel profiles $k_1, k_2 : [0, \infty) \rightarrow [0, \infty)$ are non-increasing and at least three times continuously differentiable with bounded fourth-order partial derivatives. We also assume that the resulting kernel functions satisfy

$$\int_{\mathbb{R}^{D_j}} \|\mathbf{x}\|_2^2 K_j^{(\tau)}(\mathbf{x}) d\mathbf{x} < \infty, \quad \int_{\mathbb{R}^{D_j}} \left[K_j^{(\tau)}(\mathbf{x}) \right]^2 d\mathbf{x} < \infty$$

for any multi-index with $|\tau| \leq 3$ when K_j has a linear kernel profile for $j = 1, 2$, and

$$0 < \int_0^\infty |L^{(\ell)}(r)| r^{\frac{D_j}{2}-1} dr < \infty$$

for all $D_j \geq 1$ and $\ell = 1, 2, 3$ when K_j has a directional kernel profile L for $j = 1, 2$.

- **(A3)** Let

$$\mathcal{K} = \left\{ (\mathbf{u}, \mathbf{v}) \mapsto K_1^{(\tau_1)} \left(\frac{\mathbf{x} - \mathbf{u}}{h_1} \right) K_2^{(\tau_2)} \left(\frac{\mathbf{y} - \mathbf{v}}{h_2} \right) : \right. \\ \left. \mathbf{x}, \mathbf{u} \in \mathcal{S}_1, \mathbf{y}, \mathbf{v} \in \mathcal{S}_2, |\tau_1|, |\tau_2| = 0, 1, 2, 3, h_1, h_2 > 0 \right\}.$$

We assume that \mathcal{K} is a bounded VC (subgraph) class of measurable functions on $\mathcal{S}_1 \times \mathcal{S}_2$; that is, there exists constants $A, v > 0$ such that for any $0 < \epsilon < 1$,

$$\sup_Q N(\mathcal{K}, \mathcal{L}_2(Q), \epsilon \|F\|_{\mathcal{L}_2(Q)}) \leq \left(\frac{A}{\epsilon} \right)^v,$$

where $N(T, d_T, \epsilon)$ is the ϵ -covering number of the pseudometric space (T, d_T) , Q is any probability measure with the same support as P on $\mathcal{S}_1 \times \mathcal{S}_2$, and F is an envelope function of \mathcal{K} . The constants A and v are usually called the VC characteristics of \mathcal{K} , and the norm $\|F\|_{L_2(Q)}$ is defined as $\left[\int_{\mathcal{S}_1 \times \mathcal{S}_2} |F(\mathbf{x})|^2 dQ(\mathbf{x}) \right]^{\frac{1}{2}}$.

Conditions (A1) and (A2) are standard assumptions for establishing the (pointwise) consistency results for KDE and its derivatives in directional and/or linear product spaces; see Wand and Jones (1994); Wasserman (2006) for linear/Euclidean KDE and Hall et al. (1987); Klemelä (2000); Zhao and Wu (2001) for directional KDE. The VC-typed assumption (A3) is a well-known regularity condition developed by Giné and Guillou (2002); Einmahl and Mason (2005) for the uniform consistency of KDE and its derivatives.

The techniques in Hall et al. (1987); Chacón et al. (2011); García-Portugués et al. (2013, 2015); Zhang and Chen (2021b) can be adopted to establish the following pointwise rates of convergence for KDE \widehat{f}_h and its derivatives.

Lemma 5. *Assume conditions (A1-2). Then,*

$$\nabla_{T_z}^\ell \widehat{f}_h(\mathbf{z}) - \nabla_{T_z}^\ell f(\mathbf{z}) = O(h^2) + O_P \left(\sqrt{\frac{1}{nh^{D_1+D_2+2\ell}}} \right)$$

as $\max(\mathbf{h}) = \max\{h_1, h_2\} \lesssim h \rightarrow 0$ and $nh^{D_1+D_2+2\ell} \rightarrow \infty$ for any integer ℓ , where $\mathbf{z} = (\mathbf{x}, \mathbf{y}) \in \mathcal{S}_1 \times \mathcal{S}_2$ and $\nabla_{T_{\mathbf{z}}}$ is the gradient operator within the tangent space $T_{\mathbf{z}} = T_{\mathbf{x}}(\mathcal{S}_1) \times T_{\mathbf{y}}(\mathcal{S}_2)$ (i.e., Riemannian connection; see Section 5.3 in [Absil et al. 2009](#)) so that $\nabla_{T_{\mathbf{z}}} f(\mathbf{z}) = \mathbf{grad} f(\mathbf{z})$, $\nabla_{T_{\mathbf{z}}}^2 f(\mathbf{z}) = \mathcal{H}f(\mathbf{z})$, and $\nabla_{T_{\mathbf{z}}}^3 f(\mathbf{z}) = \nabla_{T_{\mathbf{z}}} \mathcal{H}f(\mathbf{z})$.

The pointwise consistency results in Lemma 5 can be improved as the following uniform rates of convergence using the arguments in [Giné and Guillou \(2002\)](#); [Einmahl and Mason \(2005\)](#); [Chacón et al. \(2011\)](#); [Bai et al. \(1988\)](#); [Zhang and Chen \(2021b\)](#).

Lemma 6. *Assume conditions (A1-3). Then,*

$$\left\| \widehat{f}_{\mathbf{h}} - f \right\|_{\infty}^{(\ell)} = \sup_{\mathbf{z} \in \mathcal{S}_1 \times \mathcal{S}_2} \left\| \nabla_{T_{\mathbf{z}}}^{\ell} \widehat{f}_{\mathbf{h}}(\mathbf{z}) - \nabla_{T_{\mathbf{z}}}^{\ell} f(\mathbf{z}) \right\|_{\max} = O(h^2) + O_P \left(\sqrt{\frac{|\log h|}{nh^{D_1+D_2+2\ell}}} \right)$$

as $\max(\mathbf{h}) = \max\{h_1, h_2\} \lesssim h \rightarrow 0$ and $\frac{nh^{D_1+D_2+2\ell}}{|\log h|} \rightarrow \infty$ for any integer ℓ .

Notice that the pointwise and uniform consistency results for $\widehat{f}_{\mathbf{h}}$ only hold within the tangent space/bundle. The (uniform) consistency results are particularly useful for establishing the upcoming mode and ridge consistency theory. More importantly, they serve as a key building block for establishing the (linear) convergence of our proposed SCMS algorithm; see Section C.3.

B.2 Mode Consistency

Recall that $\mathcal{M} = \{\mathbf{z} \in \mathcal{S}_1 \times \mathcal{S}_2 : \mathbf{grad} f(\mathbf{z}) = \mathbf{0}, \lambda_1(\mathbf{z}) < 0\} \equiv \{\mathbf{m}_1, \dots, \mathbf{m}_N\}$ is the set of local modes of the true (density) function f on $\mathcal{S}_1 \times \mathcal{S}_2$, while

$$\widehat{\mathcal{M}} = \left\{ \mathbf{z} \in \mathcal{S}_1 \times \mathcal{S}_2 : \mathbf{grad} \widehat{f}_{\mathbf{h}}(\mathbf{z}) = \mathbf{0}, \widehat{\lambda}_1(\mathbf{z}) < 0 \right\} \equiv \{\widehat{\mathbf{m}}_1, \dots, \widehat{\mathbf{m}}_{\widehat{N}}\}$$

denotes the collection of estimated local modes obtained by KDE $\widehat{f}_{\mathbf{h}}$. Here, N refers to the number of true local modes, and \widehat{N} is number of estimated local modes. To quantify the difference between two sets of points \mathcal{M} and $\widehat{\mathcal{M}}$, we leverage the Hausdorff distance as:

$$\begin{aligned} \text{Haus}(\mathcal{M}, \widehat{\mathcal{M}}) &= \max \left\{ \sup_{\mathbf{m} \in \mathcal{M}} d(\mathbf{m}, \widehat{\mathcal{M}}), \sup_{\widehat{\mathbf{m}} \in \widehat{\mathcal{M}}} d(\widehat{\mathbf{m}}, \mathcal{M}) \right\} \\ &= \inf \left\{ \epsilon > 0 : \mathcal{M} \subset \widehat{\mathcal{M}} \oplus \epsilon, \widehat{\mathcal{M}} \subset \mathcal{M} \oplus \epsilon \right\}, \end{aligned} \quad (29)$$

where $d(\mathbf{m}, \widehat{\mathcal{M}}) = \inf \left\{ \|\mathbf{m} - \widehat{\mathbf{m}}\|_2 : \widehat{\mathbf{m}} \in \widehat{\mathcal{M}} \right\}$, $\mathcal{M} \oplus \epsilon = \{\mathbf{z} \in \mathcal{S}_1 \times \mathcal{S}_2 : d(\mathbf{z}, \mathcal{M}) \leq \epsilon\}$, and other quantities are defined similarly.

Theorem 7. *Assumes conditions (A1-3) and there exist constants $\lambda^*, \Theta^*, C^* > 0$ such that*

$$0 < \lambda^* \leq |\lambda_1(\mathbf{m})| \quad \text{for any } \mathbf{m} \in \mathcal{M} \quad (\text{strict definiteness condition})$$

as well as

$$\left\{ \mathbf{z} \in \mathcal{S}_1 \times \mathcal{S}_2 : \|\mathbf{grad} f(\mathbf{z})\|_2 \leq \Theta^*, \lambda_1(\mathbf{z}) \leq -\frac{\lambda^*}{2} < 0 \right\} \subset \mathcal{M} \oplus \frac{C^* \lambda^*}{\|f\|_{\infty}^{(3)}},$$

where we recall that $\lambda_1(\mathbf{z}) \geq \dots \geq \lambda_{D_1+D_2}(\mathbf{z})$ are the eigenvalues of the Riemannian Hessian $\mathcal{H}f(\mathbf{z})$ associated with the eigenvectors within the tangent space $T_{\mathbf{z}} = T_{\mathbf{x}}(\mathcal{S}_1) \times T_{\mathbf{y}}(\mathcal{S}_2)$. Then, when $\left\| \widehat{f}_{\mathbf{h}} - f \right\|_{\infty,2}^*$ is sufficiently small, there exist constant $A^*, B^* > 0$ such that

$$\mathbb{P}(\widehat{N} \neq N) \leq B^* e^{-A^* n h^{D_1+D_2+4}} \quad \text{and} \quad \text{Haus}(\mathcal{M}, \widehat{\mathcal{M}}) = O(h^2) + O_P\left(\sqrt{\frac{1}{nh^{D_1+D_2+2}}}\right)$$

with $\max(\mathbf{h}) = \max\{h_1, h_2\} \lesssim h$.

The extra assumptions imposed in Theorem 7 regularize the behavior of f around its local modes and ensure that the local modes are isolated. The proof is a direct adoption of the arguments in Theorem 1 of Chen et al. (2016) and Theorem 6 of Zhang and Chen (2021b), so we omit the details. The key ingredient of the proof is the Taylor's expansion of f on $\mathcal{S}_1 \times \mathcal{S}_2$ as (Penneec, 2006):

$$f(\text{Exp}_{\mathbf{z}}(\mathbf{v})) = f(\mathbf{z}) + \langle \text{grad } f(\mathbf{z}), \mathbf{v} \rangle + \frac{1}{2} \mathbf{v}^T \mathcal{H}f(\mathbf{z}) \mathbf{v} + O(\|\mathbf{v}\|_2^3) \quad (30)$$

for any $\mathbf{v} \in T_{\mathbf{z}}$, where $\text{Exp}_{\mathbf{z}} : T_{\mathbf{z}} \rightarrow \mathcal{S}_1 \times \mathcal{S}_2$ is the exponential map at $\mathbf{z} \in \mathcal{S}_1 \times \mathcal{S}_2$ such that the tangent vector $\mathbf{v} \in T_{\mathbf{z}}$ is mapped to the point $\mathbf{u} := \text{Exp}_{\mathbf{z}}(\mathbf{v}) \in \mathcal{S}_1 \times \mathcal{S}_2$ with $\alpha(0) = \mathbf{z}, \alpha(1) = \mathbf{u}$ and $\alpha'(0) = \mathbf{v}$. Here, $\alpha : [0, 1] \rightarrow \mathcal{S}_1 \times \mathcal{S}_2$ is a curve of minimum length between \mathbf{z} and \mathbf{u} (i.e., the so-called geodesic on $\mathcal{S}_1 \times \mathcal{S}_2$).

From (6), it is not difficult to see that $\left\| \widehat{f}_{\mathbf{h}} - f \right\|_{\infty,2}^*$ will be sufficiently small as $\max(\mathbf{h}) = \max\{h_1, h_2\} \lesssim h \rightarrow 0$ and $\frac{nh^{D_1+D_2+4}}{|\log h|} \rightarrow \infty$. It is also worth mentioning that the rate of convergence of $\text{Haus}(\mathcal{M}, \widehat{\mathcal{M}})$ is identical to the pointwise asymptotic rate of the (Riemannian) gradient estimator. Nevertheless, in order for such rate of convergence to be valid, the true (density) function f and its estimator $\widehat{f}_{\mathbf{h}}$ should be uniformly close up to their (Riemannian) Hessians.

B.3 Ridge Consistency

Recall that our definition of the order- d (density) ridge

$$\mathcal{R}_d = \{\mathbf{z} \in \mathcal{S}_1 \times \mathcal{S}_2 : V_d(\mathbf{z})V_d(\mathbf{z})^T \text{grad } f(\mathbf{z}) = \mathbf{0}, \lambda_{d+1}(\mathbf{z}) < 0\}$$

can be regarded as a generalized version of the set of local modes within the eigenspace spanned by the last $(D_1 + D_2 - d)$ eigenvector of the Riemannian Hessian $\mathcal{H}f(\mathbf{z})$ (i.e., the column of $V_d(\mathbf{z})$). Given a natural estimator $\widehat{\mathcal{R}}_d$ of the ridge provided by KDE $\widehat{f}_{\mathbf{h}}$, we modify the assumptions in Genovese et al. (2014); Zhang and Chen (2021c) to obtain its consistency under the Hausdorff distance.

Theorem 8. Assume conditions (A1-3) and there exist constants $r_*, \beta_* > 0$ such that

$$\lambda_{d+1}(\mathbf{z}) \leq -\beta^*, \quad \lambda_d(\mathbf{z}) - \lambda_{d+1}(\mathbf{z}) \geq \beta^* \quad (\text{eigengap condition})$$

as well as

$$(D_1+D_2+2)^{\frac{3}{2}} \left\| \left[\mathbf{I}_{D_1+1\{\mathcal{S}_1=\Omega_{D_1}\}+D_2+1\{\mathcal{S}_2=\Omega_{D_2}\}} - V_d(\mathbf{z})V_d(\mathbf{z})^T \right] \text{grad } f(\mathbf{z}) \right\|_2 \|\nabla^3 f(\mathbf{z})\|_{\max} \leq \frac{\beta_*^2}{4}$$

for any $\mathbf{z} \in \mathcal{R}_d \oplus r_*$. Then, when $\left\| \widehat{f}_{\mathbf{h}} - f \right\|_{\infty,3}^*$ is sufficiently small,

$$\text{Haus}(\widehat{\mathcal{R}}_d, \mathcal{R}_d) = O(h^2) + O_P \left(\sqrt{\frac{|\log h|}{nh^{D_1+D_2+4}}} \right)$$

with $\max(\mathbf{h}) = \max\{h_1, h_2\} \lesssim h$.

The eigengap condition in Theorem 8 is a natural generalization of the strict definiteness condition in Theorem 7. It requires f to be (locally) concave within the eigenspace spanned by the last $(D_1 + D_2 - d)$ eigenvector of the Riemannian Hessian $\mathcal{H}f(\mathbf{z})$, and the order- d ridge \mathcal{R}_d contains the lower order ridges but is isolated from higher order ridges. As our conditions in Theorem 8 imply the conditions in [Genovese et al. \(2014\)](#); [Zhang and Chen \(2021c\)](#), the proof follows from their arguments.

C. Linear Convergence of the Mean Shift and SCMS Algorithms on $\mathcal{S}_1 \times \mathcal{S}_2$

This section is dedicated to formulating the general (subspace constrained) gradient ascent framework on the product space/manifold $\mathcal{S}_1 \times \mathcal{S}_2$ and establishing the linear convergence of our proposed mean shift and SCMS algorithms (Theorems 2 and 4 in the main paper) under this framework. In particular, we argue that our rule of thumb for the step size η in the proposed SCMS algorithm is well-suited for the linear convergence of the algorithm when the bandwidth parameters are small. In contrast, we demonstrate via the subspace constrained gradient ascent framework and empirical examples that it is inappropriate to set a constant step size $\eta = 1$ in our proposed SCMS algorithm.

C.1 (Subspace Constrained) Gradient Ascent Framework on $\mathcal{S}_1 \times \mathcal{S}_2$

Whenever $\mathcal{S}_j = \Omega_{D_j}$ is a nonlinear manifold for $j = 1$ or 2 , the gradient ascent method with an objective function f on $\mathcal{S}_1 \times \mathcal{S}_2$ is defined through the exponential map $\text{Exp}_{\mathbf{z}} : T_{\mathbf{z}} = T_{\mathbf{x}}(\mathcal{S}_1) \times T_{\mathbf{y}}(\mathcal{S}_2) \rightarrow \mathcal{S}_1 \times \mathcal{S}_2$ as ([Absil et al., 2009](#); [Zhang and Sra, 2016](#)):

$$\mathbf{z}^{(t+1)} \leftarrow \text{Exp}_{\mathbf{z}^{(t)}} \left(\tilde{\eta}_t \cdot \text{grad } f(\mathbf{z}^{(t)}) \right) \quad (31)$$

for $t = 0, 1, \dots$, where we call $\tilde{\eta}_t$ the *intrinsic step size* of the gradient ascent method. While the exponential map on the entire product space $\mathcal{S}_1 \times \mathcal{S}_2$ may be difficult to work with, one may resort to the following lemma and express it in terms of the exponential maps on \mathcal{S}_1 and \mathcal{S}_2 .

Lemma 9. *Given the exponential maps $\text{Exp}_{\mathbf{x}} : T_{\mathbf{x}}(\mathcal{S}_1) \rightarrow \mathcal{S}_1$, $\text{Exp}_{\mathbf{y}} : T_{\mathbf{y}}(\mathcal{S}_2) \rightarrow \mathcal{S}_2$, and $\text{Exp}_{\mathbf{z}} : T_{\mathbf{x}}(\mathcal{S}_1) \times T_{\mathbf{y}}(\mathcal{S}_2) \rightarrow \mathcal{S}_1 \times \mathcal{S}_2$ with $\mathbf{z} = (\mathbf{x}, \mathbf{y}) \in \mathcal{S}_1 \times \mathcal{S}_2$, we have the following property:*

$$\text{Exp}_{\mathbf{z}}(\mathbf{v}) = \left(\text{Exp}_{\mathbf{x}}(\mathbf{v}_{\mathbf{x}}), \text{Exp}_{\mathbf{y}}(\mathbf{v}_{\mathbf{y}}) \right),$$

where $\mathbf{v} = (\mathbf{v}_{\mathbf{x}}, \mathbf{v}_{\mathbf{y}}) \in T_{\mathbf{x}}(\mathcal{S}_1) \times T_{\mathbf{y}}(\mathcal{S}_2)$.

Under the product metric, Lemma 9 follows easily from the definition of exponential maps. One can start by verifying that the Riemannian connection $\bar{\nabla}$ of $\mathcal{S}_1 \times \mathcal{S}_2$ is given by $\bar{\nabla}_{Y_1+Y_2}(X_1 + X_2) = \bar{\nabla}_{Y_1}^{(1)}(X_1) + \bar{\nabla}_{Y_2}^{(2)}(X_2)$ with $\bar{\nabla}^{(j)}$ being the Riemannian connection of \mathcal{S}_j respectively and X_j, Y_j as differentiable vector fields in \mathcal{S}_j for $j = 1, 2$; see Exercise 1 of Chapter 6 in Do Carmo (2013). Then, it is justifiable that $\gamma(t) = (\alpha_1(t), \alpha_2(t))$ is the unique geodesic on $\mathcal{S}_1 \times \mathcal{S}_2$ when $\alpha_j : [0, 1] \rightarrow \mathcal{S}_j, j = 1, 2$ are geodesics on \mathcal{S}_j ; see Chapter 3 of do Carmo (2016) and Chapter 5 of Lee (2006). We omit the detailed proof here.

Let $\Pi_j : \mathcal{S}_1 \times \mathcal{S}_2 \rightarrow \mathcal{S}_j$ for $j = 1, 2$ be the projection maps from $\mathcal{S}_1 \times \mathcal{S}_2$ to \mathcal{S}_1 and \mathcal{S}_2 , respectively. By Lemma 9, the above iterative equation (31) can be written in terms of the gradient ascent methods within \mathcal{S}_1 and \mathcal{S}_2 as:

$$\mathbf{z}^{(t+1)} \leftarrow \left(\text{Exp}_{\mathbf{x}^{(t)}} \left[\tilde{\eta}_t^{(1)} \cdot \Pi_1 \left(\text{grad } f(\mathbf{z}^{(t)}) \right) \right], \text{Exp}_{\mathbf{y}^{(t)}} \left[\tilde{\eta}_t^{(2)} \cdot \Pi_2 \left(\text{grad } f(\mathbf{z}^{(t)}) \right) \right] \right), \quad (32)$$

where $\tilde{\eta}_t^{(j)}, j = 1, 2$ are the corresponding intrinsic step sizes.

By replacing the Riemannian gradient $\text{grad } f(\mathbf{z})$ in (31) or (32) with the subspace constrained (Riemannian) gradient $V_d(\mathbf{z})V_d(\mathbf{z})^T \text{grad } f(\mathbf{z}) = V_d(\mathbf{z})V_d(\mathbf{z})^T \nabla f(\mathbf{z})$, we obtain the following iterative formula for the subspace constrained gradient ascent method on $\mathcal{S}_1 \times \mathcal{S}_2$ as:

$$\begin{aligned} \mathbf{z}^{(t+1)} &\leftarrow \text{Exp}_{\mathbf{z}^{(t)}} \left(\tilde{\eta}_t \cdot V_d(\mathbf{z})V_d(\mathbf{z})^T \nabla f(\mathbf{z}^{(t)}) \right) \\ &= \left(\text{Exp}_{\mathbf{x}^{(t)}} \left[\tilde{\eta}_t^{(1)} \cdot V_d^{(1)}(\mathbf{z}^{(t)})V_d(\mathbf{z}^{(t)})^T \nabla f(\mathbf{z}^{(t)}) \right], \text{Exp}_{\mathbf{y}^{(t)}} \left[\tilde{\eta}_t^{(2)} \cdot V_d^{(2)}(\mathbf{z}^{(t)})V_d(\mathbf{z}^{(t)})^T \nabla f(\mathbf{z}^{(t)}) \right] \right), \end{aligned} \quad (33)$$

where we write

$$V_d(\mathbf{z}) = (\mathbf{v}_{d+1}(\mathbf{z}), \dots, \mathbf{v}_{D_T}(\mathbf{z})) = \begin{pmatrix} V_d^{(1)}(\mathbf{z}) \\ V_d^{(2)}(\mathbf{z}) \end{pmatrix} \in \mathbb{R}^{D_F \times (D_F - d)} \quad (34)$$

with $D_F = D_1 + \mathbb{1}_{\{\mathcal{S}_1 = \Omega_{D_1}\}} + D_2 + \mathbb{1}_{\{\mathcal{S}_2 = \Omega_{D_2}\}}$, $\mathbf{v}_{d+1}(\mathbf{z}), \dots, \mathbf{v}_{D_T}(\mathbf{z})$ are the last $(D_1 + D_2 - d)$ eigenvectors of $\mathcal{H}f(\mathbf{z})$ within the tangent space $T_{\mathbf{z}}$, and $V_d^{(j)}(\mathbf{z}) \in \mathbb{R}^{D_{F_j} \times (D_{F_j} - d)}$ with $D_{F_j} = D_j + \mathbb{1}_{\{\mathcal{S}_j = \Omega_{D_j}\}}$ for $j = 1, 2$.

C.2 Intrinsic Step Size of the Proposed Mean Shift Algorithms Under the Gradient Ascent Framework on $\mathcal{S}_1 \times \mathcal{S}_2$

We first derive the intrinsic step size parameters $\tilde{\eta}_t^{(1)}, \tilde{\eta}_t^{(2)}$ of the simultaneous mean shift algorithm on $\mathcal{S}_1 \times \mathcal{S}_2$ (Version A) under the above gradient ascent framework. Recall from Section 3 in the main paper that the simultaneous mean shift algorithm on $\mathcal{S}_1 \times \mathcal{S}_2$ iterates

the following formula until convergence:

$$\begin{aligned}
 (\mathbf{z}^{(t+1)})^T &= (\mathbf{x}^{(t+1)}, \mathbf{y}^{(t+1)})^T \leftarrow (\mathbf{x}^{(t)}, \mathbf{y}^{(t)})^T + \Xi(\mathbf{x}^{(t)}, \mathbf{y}^{(t)}) \\
 &= \begin{pmatrix} \frac{\sum_{i=1}^n \mathbf{X}_i k'_1 \left(\left\| \frac{\mathbf{x}^{(t)} - \mathbf{X}_i}{h_1} \right\|_2^2 \right) K_2 \left(\frac{\mathbf{y}^{(t)} - \mathbf{Y}_i}{h_2} \right)}{\sum_{i=1}^n k'_1 \left(\left\| \frac{\mathbf{x}^{(t)} - \mathbf{X}_i}{h_1} \right\|_2^2 \right) K_2 \left(\frac{\mathbf{y}^{(t)} - \mathbf{Y}_i}{h_2} \right)} \\ \frac{\sum_{i=1}^n \mathbf{Y}_i K_1 \left(\frac{\mathbf{x}^{(t)} - \mathbf{X}_i}{h_1} \right) k'_2 \left(\left\| \frac{\mathbf{y}^{(t)} - \mathbf{Y}_i}{h_2} \right\|_2^2 \right)}{\sum_{i=1}^n K_1 \left(\frac{\mathbf{x}^{(t)} - \mathbf{X}_i}{h_1} \right) k'_2 \left(\left\| \frac{\mathbf{y}^{(t)} - \mathbf{Y}_i}{h_2} \right\|_2^2 \right)} \end{pmatrix} \quad (35)
 \end{aligned}$$

with some additional standardization whenever \mathcal{S}_1 and/or \mathcal{S}_2 are directional for $t = 0, 1, \dots$. Additionally, we remind the reader of the definition of KDE on $\mathcal{S}_1 \times \mathcal{S}_2$ as:

$$\begin{aligned}
 \widehat{f}_{\mathbf{h}}(\mathbf{z}) &= \widehat{f}_{\mathbf{h}}(\mathbf{x}, \mathbf{y}) = \frac{1}{n} \sum_{i=1}^n K_1 \left(\frac{\mathbf{x} - \mathbf{X}_i}{h_1} \right) K_2 \left(\frac{\mathbf{y} - \mathbf{Y}_i}{h_2} \right) \\
 &= \frac{\prod_{j=1}^2 C_{k_j, D_j}(h_j)}{n} \sum_{i=1}^n k_1 \left(\left\| \frac{\mathbf{x} - \mathbf{X}_i}{h_1} \right\|_2^2 \right) k_2 \left(\left\| \frac{\mathbf{y} - \mathbf{Y}_i}{h_2} \right\|_2^2 \right), \quad (36)
 \end{aligned}$$

whose (total) gradient is (c.f. Equation (13) in the main paper)

$$\begin{aligned}
 \nabla \widehat{f}_{\mathbf{h}}(\mathbf{z}) &= \begin{pmatrix} \nabla_{\mathbf{x}} \widehat{f}_{\mathbf{h}}(\mathbf{z}) \\ \nabla_{\mathbf{y}} \widehat{f}_{\mathbf{h}}(\mathbf{z}) \end{pmatrix} \\
 &= \frac{2 \prod_{j=1}^2 C_{k_j, D_j}(h_j)}{n} \begin{pmatrix} \frac{1}{h_1^2} \sum_{i=1}^n (\mathbf{x} - \mathbf{X}_i) \cdot k'_1 \left(\left\| \frac{\mathbf{x} - \mathbf{X}_i}{h_1} \right\|_2^2 \right) k_2 \left(\left\| \frac{\mathbf{y} - \mathbf{Y}_i}{h_2} \right\|_2^2 \right) \\ \frac{1}{h_2^2} \sum_{i=1}^n (\mathbf{y} - \mathbf{Y}_i) \cdot k_1 \left(\left\| \frac{\mathbf{x} - \mathbf{X}_i}{h_1} \right\|_2^2 \right) k'_2 \left(\left\| \frac{\mathbf{y} - \mathbf{Y}_i}{h_2} \right\|_2^2 \right) \end{pmatrix} \quad (37) \\
 &= \begin{pmatrix} G_{\mathbf{x}} \left[\frac{\sum_{i=1}^n \mathbf{X}_i \cdot k'_1 \left(\left\| \frac{\mathbf{x} - \mathbf{X}_i}{h_1} \right\|_2^2 \right) k_2 \left(\left\| \frac{\mathbf{y} - \mathbf{Y}_i}{h_2} \right\|_2^2 \right)}{\sum_{i=1}^n k'_1 \left(\left\| \frac{\mathbf{x} - \mathbf{X}_i}{h_1} \right\|_2^2 \right) k_2 \left(\left\| \frac{\mathbf{y} - \mathbf{Y}_i}{h_2} \right\|_2^2 \right)} - \mathbf{x} \right] \\ G_{\mathbf{y}} \left[\frac{\sum_{i=1}^n \mathbf{Y}_i \cdot k_1 \left(\left\| \frac{\mathbf{x} - \mathbf{X}_i}{h_1} \right\|_2^2 \right) k'_2 \left(\left\| \frac{\mathbf{y} - \mathbf{Y}_i}{h_2} \right\|_2^2 \right)}{\sum_{i=1}^n k_1 \left(\left\| \frac{\mathbf{x} - \mathbf{X}_i}{h_1} \right\|_2^2 \right) k'_2 \left(\left\| \frac{\mathbf{y} - \mathbf{Y}_i}{h_2} \right\|_2^2 \right)} - \mathbf{y} \right] \end{pmatrix}
 \end{aligned}$$

with

$$\begin{aligned}
 G_{\mathbf{x}} &= -\frac{2 \prod_{j=1}^2 C_{k_j, D_j}(h_j)}{n h_1^2} \sum_{i=1}^n k'_1 \left(\left\| \frac{\mathbf{x} - \mathbf{X}_i}{h_1} \right\|_2^2 \right) k_2 \left(\left\| \frac{\mathbf{y} - \mathbf{Y}_i}{h_2} \right\|_2^2 \right), \\
 G_{\mathbf{y}} &= -\frac{2 \prod_{j=1}^2 C_{k_j, D_j}(h_j)}{n h_2^2} \sum_{i=1}^n k_1 \left(\left\| \frac{\mathbf{x} - \mathbf{X}_i}{h_1} \right\|_2^2 \right) k'_2 \left(\left\| \frac{\mathbf{y} - \mathbf{Y}_i}{h_2} \right\|_2^2 \right).
 \end{aligned}$$

Thus, the mean shift vector $\Xi(\mathbf{z})$ can be written in terms of the (total) gradient estimator $\nabla \widehat{f}_{\mathbf{h}}(\mathbf{z})$ as:

$$\Xi(\mathbf{z}) = \begin{pmatrix} \nabla_{\mathbf{x}} \widehat{f}_{\mathbf{h}}(\mathbf{z}) / G_{\mathbf{x}} \\ \nabla_{\mathbf{y}} \widehat{f}_{\mathbf{h}}(\mathbf{z}) / G_{\mathbf{y}} \end{pmatrix}. \quad (38)$$

We consider the intrinsic step size under three different combinations of the product space.

• **Case 1:** $\mathcal{S}_1 \times \mathcal{S}_2 = \mathbb{R}^{D_1} \times \mathbb{R}^{D_2}$. Given (38), the simultaneous mean shift iterative formula can be written as

$$\mathbf{z}^{(t+1)} \leftarrow \mathbf{z}^{(t)} + \begin{pmatrix} \nabla_{\mathbf{x}} \widehat{f}_{\mathbf{h}}(\mathbf{z}^{(t)}) / G_{\mathbf{x}^{(t)}} \\ \nabla_{\mathbf{y}} \widehat{f}_{\mathbf{h}}(\mathbf{z}^{(t)}) / G_{\mathbf{y}^{(t)}} \end{pmatrix}.$$

Note that under linear kernel profiles, the normalizing constants $C_{k_1, D_1}, C_{k_2, D_2}$ are independent of the bandwidth parameters h_1, h_2 . Hence, it is natural to see that the intrinsic step size parameters $\widetilde{\eta}_t^{(1)}, \widetilde{\eta}_t^{(2)}$ are

$$\begin{aligned} \widetilde{\eta}_t^{(1)} &= \frac{1}{G_{\mathbf{x}^{(t)}}} = -\frac{h_1^2}{\frac{2 \prod_{j=1}^2 C_{k_j, D_j}}{n} \sum_{i=1}^n k_1' \left(\left\| \frac{\mathbf{x}^{(t)} - \mathbf{X}_i}{h_1} \right\|_2^2 \right) k_2 \left(\left\| \frac{\mathbf{y}^{(t)} - \mathbf{Y}_i}{h_2} \right\|_2^2 \right)}, \\ \widetilde{\eta}_t^{(2)} &= \frac{1}{G_{\mathbf{y}^{(t)}}} = -\frac{h_2^2}{\frac{2 \prod_{j=1}^2 C_{k_j, D_j}}{n} \sum_{i=1}^n k_1 \left(\left\| \frac{\mathbf{x}^{(t)} - \mathbf{X}_i}{h_1} \right\|_2^2 \right) k_2' \left(\left\| \frac{\mathbf{y}^{(t)} - \mathbf{Y}_i}{h_2} \right\|_2^2 \right)}. \end{aligned}$$

The following Lemma 10 elucidates the asymptotic rates of $\widetilde{\eta}_t^{(1)}, \widetilde{\eta}_t^{(2)}$ in terms of the bandwidth parameters.

Lemma 10. *Assume conditions (A1-2) and $\mathcal{S}_1 \times \mathcal{S}_2 = \mathbb{R}^{D_1} \times \mathbb{R}^{D_2}$. Then, when $h_1, h_2 \lesssim h \rightarrow 0$ and $nh^{D_1+D_2} \rightarrow \infty$, we have that*

$$\begin{aligned} h_1^2 \cdot G_{\mathbf{x}} &= -\frac{2 \prod_{j=1}^2 C_{k_j, D_j}}{n} \sum_{i=1}^n k_1' \left(\left\| \frac{\mathbf{x} - \mathbf{X}_i}{h_1} \right\|_2^2 \right) k_2 \left(\left\| \frac{\mathbf{y} - \mathbf{Y}_i}{h_2} \right\|_2^2 \right) \\ &= -2 \prod_{j=1}^2 C_{k_j, D_j} \cdot f(\mathbf{z}) \int_{\mathcal{S}_1 \times \mathcal{S}_2} k_1' \left(\|\mathbf{x}\|_2^2 \right) k_2 \left(\|\mathbf{y}\|_2^2 \right) d\mathbf{x} d\mathbf{y} + O(h^2) + O_P \left(\sqrt{\frac{1}{nh^{D_1+D_2}}} \right) \\ &= O(1) + O(h^2) + O_P \left(\sqrt{\frac{1}{nh^{D_1+D_2}}} \right), \end{aligned}$$

and similarly,

$$\begin{aligned} h_2^2 \cdot G_{\mathbf{y}} &= -\frac{2 \prod_{j=1}^2 C_{k_j, D_j}}{n} \sum_{i=1}^n k_1 \left(\left\| \frac{\mathbf{x} - \mathbf{X}_i}{h_1} \right\|_2^2 \right) k_2' \left(\left\| \frac{\mathbf{y} - \mathbf{Y}_i}{h_2} \right\|_2^2 \right) \\ &= -2 \prod_{j=1}^2 C_{k_j, D_j} \cdot f(\mathbf{z}) \int_{\mathcal{S}_1 \times \mathcal{S}_2} k_1 \left(\|\mathbf{x}\|_2^2 \right) k_2' \left(\|\mathbf{y}\|_2^2 \right) d\mathbf{x} d\mathbf{y} + O(h^2) + O_P \left(\sqrt{\frac{1}{nh^{D_1+D_2}}} \right) \\ &= O(1) + O(h^2) + O_P \left(\sqrt{\frac{1}{nh^{D_1+D_2}}} \right). \end{aligned}$$

The proof of Lemma 10 is similar to Theorem 1 in Cheng (1995) and Lemma 2 in Zhang and Chen (2021c), which is an application of Taylor's theorem; see the proof of

Proposition 3 in Section D for a sketch. It implies that $\tilde{\eta}_t^{(1)}, \tilde{\eta}_t^{(2)} = O(h^2)$ as the bandwidths $h_1, h_2 \lesssim h \rightarrow 0$ and $nh^{D_1+D_2} \rightarrow \infty$.

• **Case 2:** $\mathcal{S}_1 \times \mathcal{S}_2 = \Omega_{D_1} \times \mathbb{R}^{D_2}$. Apart from updating the sequence $\{\mathbf{z}^{(t)}\}_{t=0}^\infty = \{(\mathbf{x}^{(t)}, \mathbf{y}^{(t)})\}_{t=0}^\infty$ with (35), we need to standardize $\mathbf{x}^{(t+1)}$ as $\frac{\mathbf{x}^{(t+1)}}{\|\mathbf{x}^{(t+1)}\|_2}$. Hence, a complete mean shift iterative step reads

$$\begin{aligned} \mathbf{x}^{(t+1)} &\leftarrow -\frac{\sum_{i=1}^n \mathbf{X}_i \cdot k'_1 \left(\left\| \frac{\mathbf{x}^{(t)} - \mathbf{X}_i}{h_1} \right\|_2^2 \right) k_2 \left(\left\| \frac{\mathbf{y}^{(t)} - \mathbf{Y}_i}{h_2} \right\|_2^2 \right)}{\left\| \sum_{i=1}^n \mathbf{X}_i \cdot k'_1 \left(\left\| \frac{\mathbf{x}^{(t)} - \mathbf{X}_i}{h_1} \right\|_2^2 \right) k_2 \left(\left\| \frac{\mathbf{y}^{(t)} - \mathbf{Y}_i}{h_2} \right\|_2^2 \right) \right\|_2} \\ &= -\frac{\sum_{i=1}^n \mathbf{X}_i \cdot L' \left(\frac{1 - \mathbf{X}_i^T \mathbf{x}^{(t)}}{h_1^2} \right) k_2 \left(\left\| \frac{\mathbf{y}^{(t)} - \mathbf{Y}_i}{h_2} \right\|_2^2 \right)}{\left\| \sum_{i=1}^n \mathbf{X}_i \cdot L' \left(\frac{1 - \mathbf{X}_i^T \mathbf{x}^{(t)}}{h_1^2} \right) k_2 \left(\left\| \frac{\mathbf{y}^{(t)} - \mathbf{Y}_i}{h_2} \right\|_2^2 \right) \right\|_2}, \\ \mathbf{y}^{(t+1)} &\leftarrow \frac{\sum_{i=1}^n \mathbf{Y}_i \cdot k_1 \left(\left\| \frac{\mathbf{x}^{(t)} - \mathbf{X}_i}{h_1} \right\|_2^2 \right) k'_2 \left(\left\| \frac{\mathbf{y}^{(t)} - \mathbf{Y}_i}{h_2} \right\|_2^2 \right)}{\sum_{i=1}^n k_1 \left(\left\| \frac{\mathbf{x}^{(t)} - \mathbf{X}_i}{h_1} \right\|_2^2 \right) k'_2 \left(\left\| \frac{\mathbf{y}^{(t)} - \mathbf{Y}_i}{h_2} \right\|_2^2 \right)} = \mathbf{y}^{(t)} + \frac{1}{G_{\mathbf{y}^{(t)}}} \cdot \nabla_{\mathbf{y}} \widehat{f}_{\mathbf{h}}(\mathbf{z}^{(t)}) \end{aligned}$$

with the directional kernel profile $k_1 \left(\|\mathbf{u}\|_2^2 \right) = L \left(\frac{1}{2} \|\mathbf{u}\|_2^2 \right)$. Then, one can observe that when $h_1, h_2 \lesssim h$ are small,

$$\tilde{\eta}_t^{(2)} = \frac{1}{G_{\mathbf{y}^{(t)}}} = -\frac{h_2^2}{\frac{2C_{k_1, D_1}(h_1) \cdot C_{k_2, D_2}}{n} \sum_{i=1}^n k_1 \left(\left\| \frac{\mathbf{x}^{(t)} - \mathbf{X}_i}{h_1} \right\|_2^2 \right) k'_2 \left(\left\| \frac{\mathbf{y}^{(t)} - \mathbf{Y}_i}{h_2} \right\|_2^2 \right)} = O(h^2).$$

To derive $\tilde{\eta}_t^{(1)}$ and its asymptotic rate, we denote the angle between $\mathbf{x}^{(t+1)}$ and $\mathbf{x}^{(t)}$ by $\theta_t^{(1)}$. Under the gradient ascent framework (32) (projected to \mathcal{S}_1), we have the following equality for the geodesic distance $d_g(\mathbf{x}^{(t+1)}, \mathbf{x}^{(t)})$ on Ω_{D_1} as:

$$\begin{aligned} \arccos \left(\left(\mathbf{x}^{(t+1)} \right)^T \mathbf{x}^{(t)} \right) &= \theta_t^{(1)} = \tilde{\eta}_t^{(1)} \left\| \mathbf{grad} \widehat{f}_{\mathbf{h}}(\mathbf{z}^{(t)}) \right\|_2 \\ &= \tilde{\eta}_t^{(1)} \cdot \widetilde{\nabla}_{\mathbf{x}} \widehat{f}_{\mathbf{h}}(\mathbf{z}^{(t)}) \cdot \sin \theta_t^{(1)}, \end{aligned}$$

where

$$\widetilde{\nabla}_{\mathbf{x}} \widehat{f}_{\mathbf{h}}(\mathbf{z}) = -\frac{C_{k_1, D_1}(h_1) \cdot C_{k_2, D_2}}{n} \sum_{i=1}^n \mathbf{X}_i \cdot L' \left(\frac{1 - \mathbf{X}_i^T \mathbf{x}}{h_1^2} \right) k_2 \left(\left\| \frac{\mathbf{y} - \mathbf{Y}_i}{h_2} \right\|_2^2 \right).$$

See Figure 7 for a graphical illustration. Indeed, $\widetilde{\nabla}_{\mathbf{x}} \widehat{f}_{\mathbf{h}}(\mathbf{z})$ is also a total gradient of $\widehat{f}_{\mathbf{h}}(\mathbf{z})$ within \mathcal{S}_1 when $\mathcal{S}_1 \times \mathcal{S}_2 = \Omega_{D_1} \times \mathbb{R}^{D_2}$. Thus, the intrinsic step size on Ω_{D_1} is

$$\tilde{\eta}_t^{(1)} = \frac{\theta_t^{(1)}}{\widetilde{\nabla}_{\mathbf{x}} \widehat{f}_{\mathbf{h}}(\mathbf{z}^{(t)}) \cdot \sin \theta_t^{(1)}}.$$

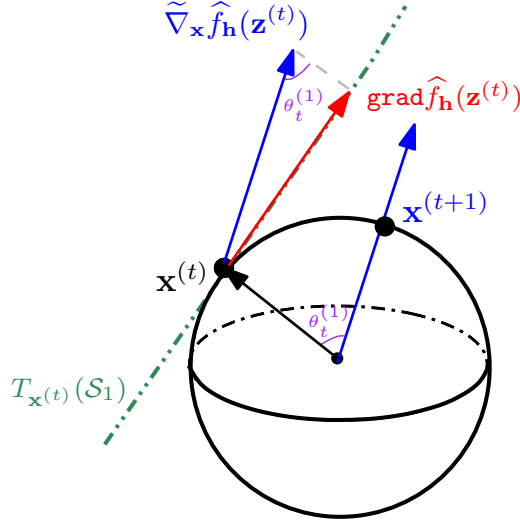


Figure 7: One-step iteration of the (simultaneous) mean shift algorithm on $\Omega_{D_1} \times \mathbb{R}^{D_2}$ projected onto Ω_{D_1} .

As $t \rightarrow \infty$ and the initial point $\mathbf{z}^{(0)}$ is near an estimated local mode $\widehat{\mathbf{m}} \in \widehat{\mathcal{M}}$, we know that $\theta_t^{(1)} \rightarrow 0$ and $\frac{\theta_t^{(1)}}{\sin \theta_t^{(1)}} \rightarrow 1$ will be upper bounded. Therefore, the intrinsic step size $\tilde{\eta}_t^{(1)}$ is essentially determined by $\tilde{\nabla}_x \hat{f}_{\hat{h}}(\mathbf{z}^{(t)})$. The following Lemma 11 sheds light on the asymptotic rate of the intrinsic step size $\tilde{\eta}_t^{(1)}$.

Lemma 11. *Assume conditions (A1-2). Then, for any fixed $\mathbf{z} = (\mathbf{x}, \mathbf{y}) \in \mathcal{S}_1 \times \mathcal{S}_2 = \Omega_{D_1} \times \mathbb{R}^{D_2}$, we have that*

$$h_1^2 \cdot \tilde{\nabla}_x \hat{f}_{\hat{h}}(\mathbf{z}) = \mathbf{x} f(\mathbf{z}) C_{L, D_1} + o(1) + O_P \left(\sqrt{\frac{1}{nh^{D_1+D_2}}} \right)$$

as $h_1, h_2 \lesssim h \rightarrow 0$ and $nh^{D_1+D_2} \rightarrow \infty$, where $C_{L, D_1} = -\frac{\int_0^\infty L'(r)r^{\frac{D_1}{2}-1} dr}{\int_0^\infty L(r)r^{\frac{D_1}{2}-1} dr} > 0$ is a constant depending exclusively on the directional kernel profile L and dimension D_1 of Ω_{D_1} .

The proof of Lemma 11 is almost identical to Lemma 10 in Zhang and Chen (2021b) and is thus omitted. It indicates that the limiting behavior of $\tilde{\nabla}_x \hat{f}_{\hat{h}}(\mathbf{z})$ will approach the radial direction \mathbf{x} on $\mathcal{S}_1 = \Omega_{D_1}$. More importantly, the result teaches us that $\tilde{\eta}_t^{(1)} = O(h^2)$ as the bandwidths $h_1, h_2 \lesssim h$ are small and the sample size n is large.

• **Case 3:** $\mathcal{S}_1 \times \mathcal{S}_2 = \Omega_{D_1} \times \Omega_{D_2}$. Given the mean shift iteration (35) and extra standardizations $\frac{\mathbf{x}^{(t+1)}}{\|\mathbf{x}^{(t+1)}\|_2}$ and $\frac{\mathbf{y}^{(t+1)}}{\|\mathbf{y}^{(t+1)}\|_2}$, an entire mean shift iterative step on $\Omega_{D_1} \times \Omega_{D_2}$

updates the sequence $\{\mathbf{z}^{(t)}\}_{t=0}^\infty = \{(\mathbf{x}^{(t)}, \mathbf{y}^{(t)})\}_{t=0}^\infty$ as:

$$\begin{aligned} \mathbf{x}^{(t+1)} &\leftarrow -\frac{\sum_{i=1}^n \mathbf{X}_i \cdot k'_1 \left(\left\| \frac{\mathbf{x}^{(t)} - \mathbf{X}_i}{h_1} \right\|_2^2 \right) k_2 \left(\left\| \frac{\mathbf{y}^{(t)} - \mathbf{Y}_i}{h_2} \right\|_2^2 \right)}{\left\| \sum_{i=1}^n \mathbf{X}_i \cdot k'_1 \left(\left\| \frac{\mathbf{x}^{(t)} - \mathbf{X}_i}{h_1} \right\|_2^2 \right) k_2 \left(\left\| \frac{\mathbf{y}^{(t)} - \mathbf{Y}_i}{h_2} \right\|_2^2 \right) \right\|_2} \\ &= -\frac{\sum_{i=1}^n \mathbf{X}_i \cdot L'_1 \left(\frac{1 - \mathbf{X}_i^T \mathbf{x}^{(t)}}{h_1^2} \right) L_2 \left(\frac{1 - \mathbf{Y}_i^T \mathbf{y}^{(t)}}{h_2^2} \right)}{\left\| \sum_{i=1}^n \mathbf{X}_i \cdot L'_1 \left(\frac{1 - \mathbf{X}_i^T \mathbf{x}^{(t)}}{h_1^2} \right) L_2 \left(\frac{1 - \mathbf{Y}_i^T \mathbf{y}^{(t)}}{h_2^2} \right) \right\|_2}, \\ \mathbf{y}^{(t+1)} &\leftarrow -\frac{\sum_{i=1}^n \mathbf{Y}_i \cdot k_1 \left(\left\| \frac{\mathbf{x}^{(t)} - \mathbf{X}_i}{h_1} \right\|_2^2 \right) k'_2 \left(\left\| \frac{\mathbf{y}^{(t)} - \mathbf{Y}_i}{h_2} \right\|_2^2 \right)}{\left\| \sum_{i=1}^n \mathbf{Y}_i \cdot k_1 \left(\left\| \frac{\mathbf{x}^{(t)} - \mathbf{X}_i}{h_1} \right\|_2^2 \right) k'_2 \left(\left\| \frac{\mathbf{y}^{(t)} - \mathbf{Y}_i}{h_2} \right\|_2^2 \right) \right\|_2} \\ &= -\frac{\sum_{i=1}^n \mathbf{Y}_i \cdot L_1 \left(\frac{1 - \mathbf{X}_i^T \mathbf{x}^{(t)}}{h_1^2} \right) L'_2 \left(\frac{1 - \mathbf{Y}_i^T \mathbf{y}^{(t)}}{h_2^2} \right)}{\left\| \sum_{i=1}^n \mathbf{Y}_i \cdot L_1 \left(\frac{1 - \mathbf{X}_i^T \mathbf{x}^{(t)}}{h_1^2} \right) L'_2 \left(\frac{1 - \mathbf{Y}_i^T \mathbf{y}^{(t)}}{h_2^2} \right) \right\|_2} \end{aligned}$$

with the directional kernel profile $k_j \left(\|\mathbf{u}\|_2^2 \right) = L_j \left(\frac{1}{2} \|\mathbf{u}\|_2^2 \right)$ for $j = 1, 2$. Let $\theta_t^{(1)}$ be the angle between $\mathbf{x}^{(t+1)}$ and $\mathbf{x}^{(t)}$ as well as $\theta_t^{(2)}$ be the angle between $\mathbf{y}^{(t+1)}$ and $\mathbf{y}^{(t)}$. If we denote

$$\begin{aligned} \tilde{\nabla}_{\mathbf{x}} \hat{f}_{\mathbf{h}}(\mathbf{z}) &= -\frac{\prod_{j=1}^2 C_{k_j, D_j}(h_j)}{n} \sum_{i=1}^n \mathbf{X}_i \cdot L'_1 \left(\frac{1 - \mathbf{X}_i^T \mathbf{x}^{(t)}}{h_1^2} \right) L_2 \left(\frac{1 - \mathbf{Y}_i^T \mathbf{y}^{(t)}}{h_2^2} \right), \\ \tilde{\nabla}_{\mathbf{y}} \hat{f}_{\mathbf{h}}(\mathbf{z}) &= -\frac{\prod_{j=1}^2 C_{k_j, D_j}(h_j)}{n} \sum_{i=1}^n \mathbf{Y}_i \cdot L_1 \left(\frac{1 - \mathbf{X}_i^T \mathbf{x}^{(t)}}{h_1^2} \right) L'_2 \left(\frac{1 - \mathbf{Y}_i^T \mathbf{y}^{(t)}}{h_2^2} \right), \end{aligned}$$

then the arguments in Case 2 can be adopted to show that the intrinsic step sizes are

$$\tilde{\eta}_t^{(1)} = \frac{\theta_t^{(1)}}{\tilde{\nabla}_{\mathbf{x}} \hat{f}_{\mathbf{h}}(\mathbf{z}^{(t)}) \cdot \sin \theta_t^{(1)}} \quad \text{and} \quad \tilde{\eta}_t^{(2)} = \frac{\theta_t^{(2)}}{\tilde{\nabla}_{\mathbf{y}} \hat{f}_{\mathbf{h}}(\mathbf{z}^{(t)}) \cdot \sin \theta_t^{(2)}}.$$

Therefore, by Lemma 11, $\tilde{\eta}_t^{(j)} = O(h^2)$ for $j = 1, 2$ when bandwidths $h_1, h_2 \lesssim h$ are small and the sample size n is large.

We have discussed the intrinsic step sizes of the simultaneous mean shift algorithm (Version A) under the gradient ascent framework (32). One can follow our preceding arguments to derive the intrinsic step sizes of the componentwise mean shift algorithm (Version B) as:

- **Case 1:** When $\mathcal{S}_1 \times \mathcal{S}_2 = \mathbb{R}^{D_1} \times \mathbb{R}^{D_2}$,

$$\tilde{\eta}_t^{(1)} = -\frac{nh_1^2}{2 \prod_{j=1}^2 C_{k_j, D_j} \sum_{i=1}^n k'_1 \left(\left\| \frac{\mathbf{x}^{(t)} - \mathbf{X}_i}{h_1} \right\|_2^2 \right) k_2 \left(\left\| \frac{\mathbf{y}^{(t)} - \mathbf{Y}_i}{h_2} \right\|_2^2 \right)}$$

$$\tilde{\eta}_t^{(2)} = - \frac{nh_2^2}{2 \prod_{j=1}^2 C_{k_j, D_j} \sum_{i=1}^n k_1 \left(\left\| \frac{\mathbf{x}^{(t+1)} - \mathbf{X}_i}{h_1} \right\|_2^2 \right) k'_2 \left(\left\| \frac{\mathbf{y}^{(t)} - \mathbf{Y}_i}{h_2} \right\|_2^2 \right)}.$$

- **Case 2:** When $\mathcal{S}_1 \times \mathcal{S}_2 = \Omega_{D_1} \times \mathbb{R}^{D_2}$,

$$\begin{aligned} \tilde{\eta}_t^{(1)} &= \frac{\theta_t^{(1)}}{\tilde{\nabla}_{\mathbf{x}} \hat{f}_{\mathbf{h}}(\mathbf{x}^{(t)}, \mathbf{y}^{(t)}) \cdot \sin \theta_t^{(1)}} \quad \text{and} \\ \tilde{\eta}_t^{(2)} &= - \frac{nh_2^2}{2 \prod_{j=1}^2 C_{k_j, D_j} \sum_{i=1}^n k_1 \left(\left\| \frac{\mathbf{x}^{(t+1)} - \mathbf{X}_i}{h_1} \right\|_2^2 \right) k'_2 \left(\left\| \frac{\mathbf{y}^{(t)} - \mathbf{Y}_i}{h_2} \right\|_2^2 \right)}. \end{aligned}$$

- **Case 3:** When $\mathcal{S}_1 \times \mathcal{S}_2 = \Omega_{D_1} \times \Omega_{D_2}$,

$$\tilde{\eta}_t^{(1)} = \frac{\theta_t^{(1)}}{\tilde{\nabla}_{\mathbf{x}} \hat{f}_{\mathbf{h}}(\mathbf{x}^{(t)}, \mathbf{y}^{(t)}) \cdot \sin \theta_t^{(1)}} \quad \text{and} \quad \tilde{\eta}_t^{(2)} = \frac{\theta_t^{(2)}}{\tilde{\nabla}_{\mathbf{y}} \hat{f}_{\mathbf{h}}(\mathbf{x}^{(t+1)}, \mathbf{y}^{(t)}) \cdot \sin \theta_t^{(2)}}.$$

Notice that each full iteration of the componentwise mean shift algorithm iterates the gradient ascent method (32) twice. Finally, analogous to the simultaneous mean shift algorithm, the intrinsic step sizes of the componentwise mean shift algorithm have their asymptotic rate $O(h^2)$ when the bandwidths $h_1, h_2 \lesssim h$ are small and the sample size n is large.

C.3 Intrinsic Step Size of the Proposed SCMS Algorithm Under the Subspace Constrained Gradient Ascent Framework on $\mathcal{S}_1 \times \mathcal{S}_2$

Recall from Section 4 in the main paper that our proposed SCMS algorithm on $\mathcal{S}_1 \times \mathcal{S}_2$ with Gaussian and/or von Mises kernels iterates the following equation:

$$\mathbf{z}^{(t+1)} \leftarrow \mathbf{z}^{(t)} + \eta \cdot \hat{V}_d(\mathbf{z}^{(t)}) \hat{V}_d(\mathbf{z}^{(t)})^T \mathbf{H}^{-1} \Xi(\mathbf{z}^{(t)})$$

with some additional standardization whenever \mathcal{S}_1 and/or \mathcal{S}_2 are directional for $t = 0, 1, \dots$, where $\eta > 0$ is the step size (i.e., a tuning parameter). We now derive the intrinsic step size parameter $\tilde{\eta}_t$ (or $\tilde{\eta}_t^{(1)}, \tilde{\eta}_t^{(2)}$) of the SCMS algorithm (23) as the subspace constrained gradient ascent method on $\mathcal{S}_1 \times \mathcal{S}_2$.

- **Case 1:** $\mathcal{S}_1 \times \mathcal{S}_2 = \mathbb{R}^{D_1} \times \mathbb{R}^{D_2}$. Some simple algebra show that

$$\mathbf{H}^{-1} \Xi(\mathbf{z}) = \frac{\nabla \hat{f}_{\mathbf{h}}(\mathbf{z})}{\hat{f}_{\mathbf{h}}(\mathbf{z})}$$

under Gaussian and/or von Mises kernels; see also [Chacón and Duong \(2013\)](#); [Chacón and Monfort \(2013\)](#). Thus, the iterative equation (23) becomes

$$\mathbf{z}^{(t+1)} \leftarrow \mathbf{z}^{(t)} + \eta \hat{V}_d(\mathbf{z}^{(t)}) \hat{V}_d(\mathbf{z}^{(t)})^T \cdot \frac{\nabla \hat{f}_{\mathbf{h}}(\mathbf{z}^{(t)})}{\hat{f}_{\mathbf{h}}(\mathbf{z}^{(t)})}, \quad (39)$$

so it is intuitive to see that the intrinsic step size is $\tilde{\eta}_t = \frac{\eta}{\hat{f}_{\mathbf{h}}(\mathbf{z}^{(t)})}$.

• **Case 2:** $\mathcal{S}_1 \times \mathcal{S}_2 = \Omega_{D_1} \times \mathbb{R}^{D_2}$. Besides updating the sequence $\{\mathbf{z}^{(t)}\}_{t=0}^\infty = \{(\mathbf{x}^{(t)}, \mathbf{y}^{(t)})\}_{t=0}^\infty$ with (39), we need to standardize $\mathbf{x}^{(t+1)}$ as $\frac{\mathbf{x}^{(t+1)}}{\|\mathbf{x}^{(t+1)}\|_2}$. Hence, a complete SCMS iterative step reads

$$\begin{aligned} \mathbf{x}^{(t+1)} &\leftarrow \frac{\widehat{f}_h(\mathbf{z}^{(t)})\mathbf{x}^{(t)} + \eta\widehat{V}_d^{(1)}(\mathbf{z}^{(t)})\widehat{V}_d(\mathbf{z}^{(t)})^T\nabla\widehat{f}_h(\mathbf{z}^{(t)})}{\left\|\widehat{f}_h(\mathbf{z}^{(t)})\mathbf{x}^{(t)} + \eta\widehat{V}_d^{(1)}(\mathbf{z}^{(t)})\widehat{V}_d(\mathbf{z}^{(t)})^T\nabla\widehat{f}_h(\mathbf{z}^{(t)})\right\|_2}, \\ \mathbf{y}^{(t+1)} &\leftarrow \mathbf{y}^{(t)} + \frac{\eta}{\widehat{f}_h(\mathbf{z}^{(t)})} \cdot \widehat{V}_d^{(2)}(\mathbf{z}^{(t)})\widehat{V}_d(\mathbf{z}^{(t)})^T\nabla\widehat{f}_h(\mathbf{z}^{(t)}), \end{aligned}$$

where we decompose $\widehat{V}_d(\mathbf{z})$ into two parts $\widehat{V}_d^{(j)}(\mathbf{z}), j = 1, 2$ within \mathcal{S}_1 and \mathcal{S}_2 respectively as in (34). Compared with (33), it is natural to obtain that $\widetilde{\eta}_t^{(2)} = \frac{\eta}{\widehat{f}_h(\mathbf{z}^{(t)})}$.

As for $\widetilde{\eta}_t^{(1)}$ within \mathcal{S}_1 , we first notice that \mathbf{x} are orthogonal to the columns of $\widehat{V}_d^{(1)}(\mathbf{z})$ for any $\mathbf{z} = (\mathbf{x}, \mathbf{y}) \in \mathcal{S}_1 \times \mathcal{S}_2$. This is because $(\mathbf{x}, \mathbf{0}) \in \mathcal{S}_1 \times \mathcal{S}_2$ is a unit eigenvector of the Riemannian Hessian $\mathcal{H}\widehat{f}_h(\mathbf{z})$ that is normal to the tangent space $T_{\mathbf{z}} = T_{\mathbf{x}}(\mathcal{S}_1) \times T_{\mathbf{y}}(\mathcal{S}_2)$. Given that the columns of $\widehat{V}_d(\mathbf{z})$ consist of the last $(D_1 + D_2 - d)$ eigenvectors of $\mathcal{H}\widehat{f}_h(\mathbf{z})$, it follows that $\mathbf{x}^T\widehat{V}_d^{(1)}(\mathbf{z}) = \mathbf{0} \in \mathbb{R}^{1 \times (D_1 + D_2 - d)}$; see Figure 8 for a graphical illustration.

If we denote the angle between $\mathbf{x}^{(t+1)}$ and $\mathbf{x}^{(t)}$ by $\theta_t^{(1)}$, then we have the following equality for the geodesic distance $d_g(\mathbf{x}^{(t)}, \mathbf{x}^{(t+1)})$ on Ω_{D_1} as:

$$\begin{aligned} \theta_t^{(1)} &= \widetilde{\eta}_t^{(1)} \left\| \widehat{V}_d^{(1)}(\mathbf{z}^{(t)})\widehat{V}_d(\mathbf{z}^{(t)})^T\nabla\widehat{f}_h(\mathbf{z}^{(t)}) \right\|_2 \\ &= \frac{\widetilde{\eta}_t^{(1)}}{\eta} \cdot \widehat{f}_h(\mathbf{z}^{(t)}) \tan \theta_t^{(1)}, \end{aligned}$$

where we leverage the orthogonality between $\mathbf{x}^{(t)}$ and the columns of $\widehat{V}_d^{(1)}(\mathbf{z}^{(t)})$ to obtain the second equality; see Figure 8. Thus, the intrinsic step on Ω_{D_1} is

$$\widetilde{\eta}_t^{(1)} = \frac{\eta}{\widehat{f}_h(\mathbf{z}^{(t)})} \cdot \frac{\theta_t^{(1)}}{\tan \theta_t^{(1)}}.$$

• **Case 3:** $\mathcal{S}_1 \times \mathcal{S}_2 = \Omega_{D_1} \times \Omega_{D_2}$. Under the iteration (39) and extra standardizations $\frac{\mathbf{x}^{(t+1)}}{\|\mathbf{x}^{(t+1)}\|_2}$ and $\frac{\mathbf{y}^{(t+1)}}{\|\mathbf{y}^{(t+1)}\|_2}$, a complete SCMS iteration on $\Omega_{D_1} \times \Omega_{D_2}$ updates the sequence $\{\mathbf{z}^{(t)}\}_{t=0}^\infty = \{(\mathbf{x}^{(t)}, \mathbf{y}^{(t)})\}_{t=0}^\infty$ as:

$$\begin{aligned} \mathbf{x}^{(t+1)} &\leftarrow \frac{\widehat{f}_h(\mathbf{z}^{(t)})\mathbf{x}^{(t)} + \eta\widehat{V}_d^{(1)}(\mathbf{z}^{(t)})\widehat{V}_d(\mathbf{z}^{(t)})^T\nabla\widehat{f}_h(\mathbf{z}^{(t)})}{\left\|\widehat{f}_h(\mathbf{z}^{(t)})\mathbf{x}^{(t)} + \eta\widehat{V}_d^{(1)}(\mathbf{z}^{(t)})\widehat{V}_d(\mathbf{z}^{(t)})^T\nabla\widehat{f}_h(\mathbf{z}^{(t)})\right\|_2}, \\ \mathbf{y}^{(t+1)} &\leftarrow \frac{\widehat{f}_h(\mathbf{z}^{(t)})\mathbf{y}^{(t)} + \eta\widehat{V}_d^{(2)}(\mathbf{z}^{(t)})\widehat{V}_d(\mathbf{z}^{(t)})^T\nabla\widehat{f}_h(\mathbf{z}^{(t)})}{\left\|\widehat{f}_h(\mathbf{z}^{(t)})\mathbf{y}^{(t)} + \eta\widehat{V}_d^{(2)}(\mathbf{z}^{(t)})\widehat{V}_d(\mathbf{z}^{(t)})^T\nabla\widehat{f}_h(\mathbf{z}^{(t)})\right\|_2}, \end{aligned}$$

where we again leverage the decomposition of $\widehat{V}_d(\mathbf{z})$ in (34). Moreover, since $(\mathbf{x}, \mathbf{0}), (\mathbf{0}, \mathbf{y}) \in \mathcal{S}_1 \times \mathcal{S}_2$ are unit eigenvectors of the Riemannian Hessian $\mathcal{H}\widehat{f}_h(\mathbf{x})$ that spanned the normal

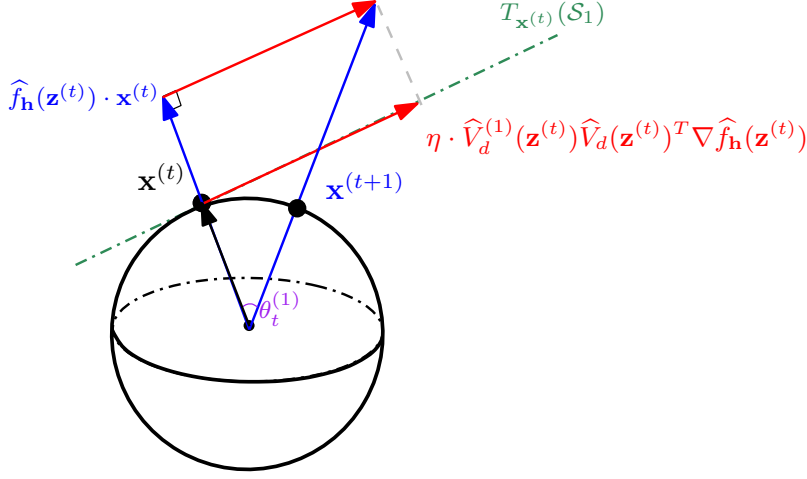


Figure 8: One-step iteration of the proposed SCMS algorithm on $\Omega_{D_1} \times \mathbb{R}^{D_2}$ projected onto Ω_{D_1} .

space of $\mathcal{S}_1 \times \mathcal{S}_2$, the same argument in **Case 2** implies that $\mathbf{x}^T \widehat{V}_d^{(1)}(\mathbf{z}) = \mathbf{y}^T \widehat{V}_d(\mathbf{z}) = \mathbf{0}$. Let $\theta_t^{(1)}$ be the angle between $\mathbf{x}^{(t)}$ and $\mathbf{x}^{(t+1)}$, and denote the angle between $\mathbf{y}^{(t)}$ and $\mathbf{y}^{(t+1)}$ by $\theta_t^{(2)}$. Thus, based on the arguments in **Case 2**, we know that the intrinsic steps on Ω_{D_1} and Ω_{D_2} are

$$\tilde{\eta}_t^{(1)} = \frac{\eta}{\widehat{f}_{\mathbf{h}}(\mathbf{z}^{(t)})} \cdot \frac{\theta_t^{(1)}}{\tan \theta_t^{(1)}} \quad \text{and} \quad \tilde{\eta}_t^{(2)} = \frac{\eta}{\widehat{f}_{\mathbf{h}}(\mathbf{z}^{(t)})} \cdot \frac{\theta_t^{(2)}}{\tan \theta_t^{(2)}}.$$

Our above derivations indicate that the intrinsic step sizes of our proposed SCMS algorithm (23) on $\mathcal{S}_1 \times \mathcal{S}_2$ under the subspace constrained gradient ascent framework (33) embrace the following bounds near $\widehat{\mathcal{R}}_d$:

$$\frac{\tilde{A}\eta}{\widehat{f}_{\mathbf{h}}(\mathbf{z}^{(t)})} \leq \tilde{\eta}_t \quad \text{or} \quad \tilde{\eta}_t^{(1)}, \tilde{\eta}_t^{(2)} \leq \frac{\eta}{\widehat{f}_{\mathbf{h}}(\mathbf{z}^{(t)})} \quad (40)$$

because $\frac{\theta_t^{(j)}}{\tan \theta_t^{(j)}} \leq 1$ but $\frac{\theta_t^{(j)}}{\tan \theta_t^{(j)}} \rightarrow 1$ as $\theta_t^{(j)} \rightarrow 0$ for $j = 1, 2$, where \tilde{A} is a constant that is independent of t and bandwidth $\mathbf{h} = (h_1, h_2)$. Therefore, if we set the tuning parameter $\eta = 1$ in our proposed SCMS algorithm as in the standard/naive SCMS iteration, the intrinsic step sizes have a lower bound around $\widehat{\mathcal{R}}_d$:

$$\tilde{\eta}_t \quad \text{or} \quad \tilde{\eta}_t^{(1)}, \tilde{\eta}_t^{(2)} \geq \frac{\tilde{A}}{\widehat{f}_{\mathbf{h}}(\mathbf{z}^{(t)})} \geq \frac{\tilde{A}}{\widehat{f}_{\mathbf{h}}(\widehat{\mathbf{m}})}$$

for some $\widehat{\mathbf{m}} \in \widehat{\mathcal{M}}$. Asymptotically, when the bandwidths $h_1, h_2 \lesssim h$ are small and the sample size n is large, we obtain by Lemma 5 of $\widehat{f}_{\mathbf{h}}$ that

$$\mathcal{P}_{\mathbf{z}} \mathbf{H}^{-1} \Xi(\mathbf{z}) = \frac{\mathbf{grad} \widehat{f}_{\mathbf{h}}(\mathbf{z})}{\widehat{f}_{\mathbf{h}}(\mathbf{z})} = \frac{\mathbf{grad} f(\mathbf{z}) + O(h^2) + O_P\left(\sqrt{\frac{1}{nh^{D_1+D_2+2}}}\right)}{f(\mathbf{z}) + O(h^2) + O_P\left(\sqrt{\frac{1}{nh^{D_1+D_2}}}\right)} \asymp \frac{\mathbf{grad} f(\mathbf{z})}{f(\mathbf{z})}$$

under Gaussian and/or von Mises kernels, where $\mathcal{P}_{\mathbf{z}}$ is the projection matrix onto the tangent space $T_{\mathbf{z}} = T_{\mathbf{x}}(\mathcal{S}_1) \times T_{\mathbf{y}}(\mathcal{S}_2)$ defined in (7) of the main paper and “ \asymp ” stands for the asymptotic equivalence. Therefore, the intrinsic adaptive step sizes have an asymptotic lower bound around \mathcal{R}_d :

$$\tilde{\eta}_t \text{ or } \tilde{\eta}_t^{(1)}, \tilde{\eta}_t^{(2)} \geq \frac{1}{f(\mathbf{z})} \geq \frac{1}{f(\mathbf{m})}$$

when h is sufficiently small and $nh^{D_1+D_2+2}$ is sufficiently large.

Here, we simulate two different datasets with true manifold structures under directional-linear and directional-directional data cases to empirically validate the undesired behaviors of our proposed SCMS algorithm with the step size $\eta = 1$.

Example 1 (Directional-Linear Data). *We sample 1000 points $t_i, i = 1, \dots, 1000$ uniformly from $[-\pi, \pi)$ to obtain the dataset*

$$\{(\cos(t_i + \epsilon_{i,1}), \sin(t_i + \epsilon_{i,1}), t_i/2 + \epsilon_{i,2})\}_{i=1}^{1000} \subset \Omega_1 \times \mathbb{R}$$

lying around an underlying directional-linear curve $(\cos t, \sin t, t/2)$ on the cylinder with radius 1, where $t \in [-\pi, \pi)$ and $\epsilon_{i,1}, \epsilon_{i,2} \sim \mathcal{N}(0, \sigma^2)$ are independent Gaussian noises with $\sigma = 0.3$; see Panel (a) of Figure 9. The first two coordinates of each simulated point come from the circular space Ω_1 , while the last coordinate lies on the Euclidean/linear space \mathbb{R} . We apply the SCMS algorithm (23) to this simulated dataset with different values of the step size η ; see Figure 9 for details. The bandwidth parameter h_1 for the directional component is selected via the rule of thumb 25. In this case, the directional dimension is $D_1 = 1$ and $h_1 \approx 0.886$. Further, the bandwidth parameter for the linear part is chosen through the normal reference rule (26) with $h_2 \approx 0.249$ under the linear dimension as $D_2 = 1$. The initial set of mesh points for the SCMS algorithm is chosen as the simulated dataset, and the tolerance level for terminating the algorithm is always set to $\epsilon = 10^{-7}$.

As shown in Figure 9, our proposed rule of thumb (24) in the main paper for the step size η strikes a balance between convergence speed and the precision of locating the (estimated) ridge line. When the step size is smaller than our proposed rule of thumb, the SCMS algorithm converges to the estimated ridge in a slow speed. When the step size is large compared to the bandwidth parameters, the SCMS algorithm overshoots our targeted (estimated) ridge and converges to some erroneous structures. The bias of recovering the underlying curve structure near its end point is due to the boundary bias of density estimation (Marron and Ruppert, 1994; Ruppert and Cline, 1994). As we observe from Panel (f) of Figure 9, the ridge line identified by our proposed SCMS algorithm is consistent with the contour plot of the estimated directional-linear density $\hat{f}_{\mathbf{h}}$, in which we unfold the cylinder along its linear direction in pursuit of a better visualization.

Example 2 (Directional-Directional Data). *We randomly sample 1000 points $\{(\theta_i, \phi_i)\}_{i=1}^{1000}$, in which*

$$\theta_i = \theta + \epsilon_{i,1} \text{ with } \theta = \begin{cases} 0 & \text{with probability } \frac{1}{2}, \\ \frac{3\pi}{4} & \text{with probability } \frac{1}{2}, \end{cases} \quad \text{and} \quad \phi_i = \phi + \epsilon_{i,2} \text{ with } \phi \sim \text{Unif}[-\pi, \pi).$$

Here, the two coordinates of each simulated point are independent and $\epsilon_{i,1}, \epsilon_{i,2} \sim \mathcal{N}(0, \sigma^2)$ are independent Gaussian noises with $\sigma = 0.3$; see Panel (a) of Figure 10. The hidden

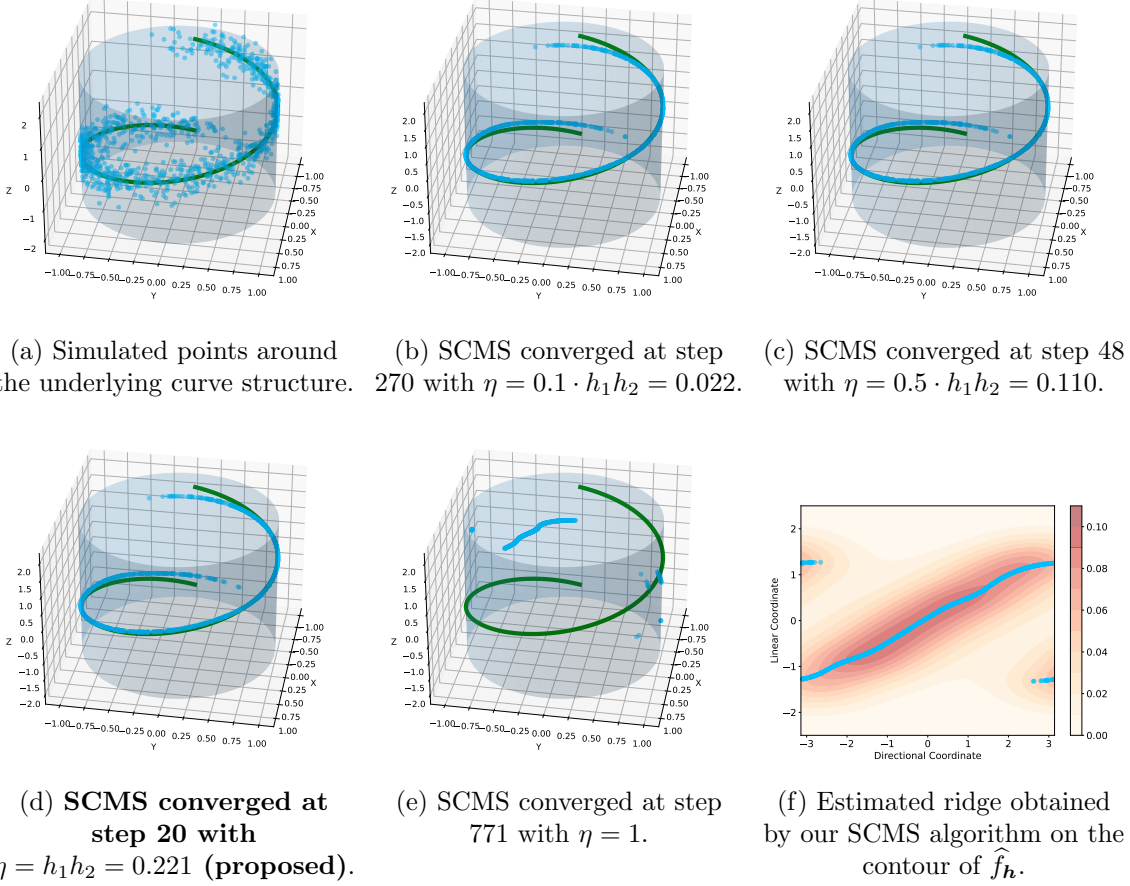


Figure 9: SCMS algorithm with different choices of the step size η on the simulated directional-linear dataset. In Panels (b-e), the blue points are the final convergent points of the SCMS algorithm under a certain step size η , while the green curve indicates the underlying curve structure.

manifold structures can be regarded as two curves in the toroidal direction on a torus. In Figure 10, we set the distance from the center of the tube to the center of the torus as 3 and the radius of the tube as 1 so that in the 3D Cartesian coordinate system, each directional-directional point (θ, ϕ) has its coordinate as:

$$\begin{cases} X &= (c + a \cos \theta) \cos \phi, \\ Y &= (c + a \cos \theta) \sin \phi, \\ Z &= a \sin \theta \end{cases}$$

The simulated angular-angular dataset has an alternative directional-directional representation as:

$$\{(\cos \theta_i, \sin \theta_i, \cos \phi_i, \sin \phi_i)\}_{i=1}^{1000} \subset \Omega_1 \times \Omega_1,$$

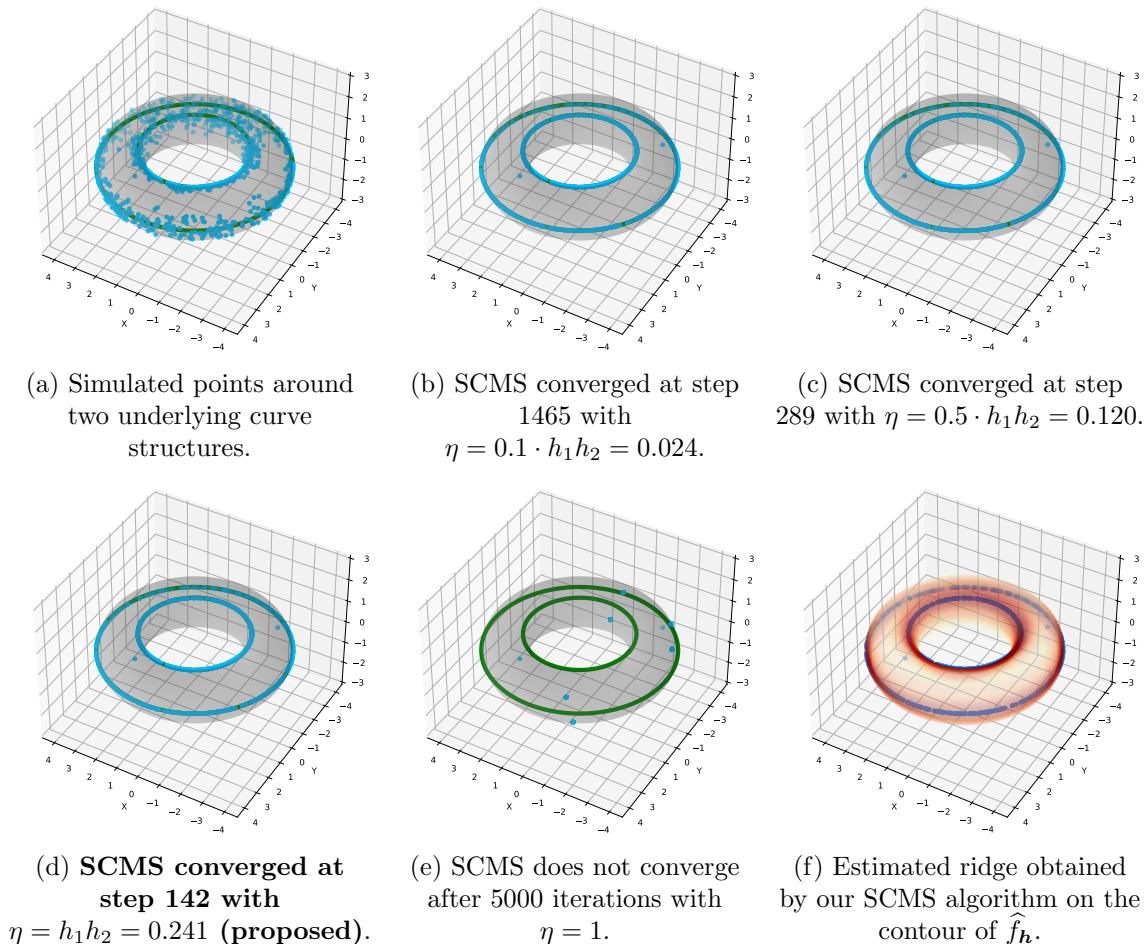


Figure 10: SCMS algorithm with different choices of the step size η on the simulated directional-directional dataset. In Panels (b-e), the blue points are the final convergent points of the SCMS algorithm under a certain step size η , while the green curve indicates the hidden manifold structure on a torus.

to which we apply the SCMS algorithm (23) with different values of the step size η . The bandwidth parameters h_1, h_2 are both selected using (25) so that $h_1 = 0.327$ and $h_2 = 0.736$. The initial set of mesh points is again chosen as the simulated dataset, and the tolerance level for terminating the algorithm is $\epsilon = 10^{-7}$.

On the one hand, similar to the results of simulation studies on the directional-linear data, Figure 10 suggests that our SCMS algorithm with the proposed step size is able to identify the ridge of the estimated density and approximate the hidden manifold structure. On the other hand, this example also illustrates that the step size $\eta = 1$ is not a desirable choice.

C.4 Linear Convergence of the Proposed Mean Shift and SCMS Algorithm on $\mathcal{S}_1 \times \mathcal{S}_2$

Our derivations in Section C.2 demonstrate that the intrinsic step sizes $\tilde{\eta}_t^{(1)}, \tilde{\eta}_t^{(2)}$ of our proposed mean shift algorithm on $\mathcal{S}_1 \times \mathcal{S}_2$ under the gradient ascent framework (32) have an asymptotic order $O(h^2)$ as the bandwidths $h_1, h_2 \lesssim h$ are small and the sample size n is large. Therefore, one can choose small bandwidths h_1, h_2 in order for the mean shift algorithm (either Version A or B) to converge linearly to an (estimated) local mode when the algorithm is initialized around the local mode; see the restated Theorem 2 in the main paper below.

Theorem 2. *Assume that the conditions of Theorem 7 hold. Given the sequence $\{\mathbf{z}^{(t)}\}_{t=0}^\infty$ defined by our mean shift algorithm (17) or (18), there exist constants $\tilde{r}_1 > 0, \Upsilon_1 \in (0, 1)$ such that*

$$d_g(\mathbf{z}^{(t)}, \widehat{\mathbf{m}}) \leq \Upsilon_1^t \cdot d_g(\mathbf{z}^{(0)}, \widehat{\mathbf{m}}),$$

and with probability at least $1 - \delta$ under any $\delta \in (0, 1)$,

$$d_g(\mathbf{z}^{(t)}, \mathbf{m}) \leq \Upsilon_1^t \cdot d_g(\mathbf{z}^{(0)}, \mathbf{m}) + O(h^2) + O_P\left(\sqrt{\frac{|\log h|}{nh^{D_1+D_2}}}\right)$$

when $\mathbf{z}^{(0)} \in \{\mathbf{z} \in \mathcal{S}_1 \times \mathcal{S}_2 : d_g(\mathbf{z}, \mathbf{m}) \leq \tilde{r}_1\}$ with $\mathbf{m} \in \mathcal{M}$ and $\max(\mathbf{h}) = \max\{h_1, h_2\} \lesssim h$ is sufficiently small, where $D_T = D_1 + D_2$ is the intrinsic dimension and $d_g(\cdot, \cdot)$ is the geodesic distance on $\mathcal{S}_1 \times \mathcal{S}_2$.

Thanks to our formulation of the proposed mean shift algorithm as the gradient ascent method on $\mathcal{S}_1 \times \mathcal{S}_2$, one can leverage the arguments in Theorem 12 from Zhang and Chen (2021b) to establish the above theorem. We do not repeat their proof here.

As for the linear convergence of our proposed SCMS algorithm on $\mathcal{S}_1 \times \mathcal{S}_2$, given the bounds (40) and Lemma 5, the intrinsic step size of the algorithm with our proposed rule of thumb for the step size $\eta = \min\{\max(\mathbf{h}) \cdot \min(\mathbf{h}), 1\} = \min\{h_1 h_2, 1\}$ under the subspace constrained gradient ascent framework (33) has an asymptotic rate $O(h^2)$ when the bandwidths $h_1, h_2 \lesssim h$ are small and the sample size n is large. The shrinking property of the intrinsic step size with respect to the bandwidths $h_1, h_2 \lesssim h$ infers that our SCMS algorithm on $\mathcal{S}_1 \times \mathcal{S}_2$ converges linearly to the estimated ridge $\widehat{\mathcal{R}}_d$ (and true ridge \mathcal{R}_d) when the bandwidths are small; see the restated Theorem 4 in the main paper below.

Theorem 3. *Assume that all the assumptions in Theorem 8 hold. Under the constant $\beta_* > 0$ in Theorem 8, we also assume that there exists a constant $\gamma_* \in (0, \beta_*)$ such that*

- (A4) $d \cdot (D_1 + D_2 + 2) \|\nabla f(\mathbf{z})\|_2 \|\nabla^3 f(\mathbf{z})\|_{\max} \leq \beta_*(\beta_* - \gamma_*)$ for all $\mathbf{z} \in \mathcal{R}_d$.

Given the sequence $\{\mathbf{z}^{(t)}\}_{t=0}^\infty$ defined by our SCMS algorithm (23) with step size η dominated by $\max(\mathbf{h})$, there exist constants $\tilde{A}, \tilde{r}_2 > 0$ and $\Upsilon_2 \in (0, 1)$ such that with probability at least $1 - \delta$ for any $\delta \in (0, 1)$,

$$\max\left\{d_g(\mathbf{z}^{(t)}, \widehat{\mathcal{R}}_d), d_g(\mathbf{z}^{(t)}, \mathcal{R}_d)\right\} \leq \tilde{A} \cdot \Upsilon_2^t$$

when $\mathbf{z}^{(0)} \in \mathcal{R}_d \oplus \tilde{r}_2 = \{\mathbf{z} \in \mathcal{S}_1 \times \mathcal{S}_2 : d_g(\mathbf{z}, \mathcal{R}_d) \leq \tilde{r}_2\}$ and $\max(\mathbf{h})$ is sufficiently small, where $d_g(\cdot, \cdot)$ is the geodesic distance on $\mathcal{S}_1 \times \mathcal{S}_2$.

The assumption (A4) is the regularity condition on the third-order derivative proposed by [Chen et al. \(2015\)](#) in order for a well-defined local normal coordinate along the ridge \mathcal{R}_d . As we have cast our SCMS algorithm into the subspace constrained gradient ascent framework in Section C.3 and our imposed conditions imply the assumptions in Theorem 10 in [Zhang and Chen \(2021c\)](#), their arguments can be adopted to prove Theorem 4 here. We omit the details.

D. Proofs of Theorem 1 and Proposition 3

Theorem 1. Denote the sequence defined by the mean shift algorithm by $\{\mathbf{z}^{(t)}\}_{t=0}^{\infty} = \{(\mathbf{x}^{(t)}, \mathbf{y}^{(t)})\} \subset \mathcal{S}_1 \times \mathcal{S}_2$. Assume that

- **(C1)** The kernel profiles k_1, k_2 (either linear k or directional L) are strictly decreasing and differentiable on $[0, \infty)$ with $k_1(0), k_2(0) < \infty$.

- **(Weak Condition)** Both k_1 and k_2 are convex.

- **(Strong Condition)** The entire product kernel profile $K(r, s) = k_1(r) \cdot k_2(s)$ is convex.

(a) Under **(C1)** and **Weak Condition**, the sequence of density estimates $\{\hat{f}_{\mathbf{h}}(\mathbf{z}^{(t)})\}_{t=0}^{\infty}$ yielded by Version B is non-decreasing and thus converges.

(b) Under **(C1)** and **Strong Condition**, the sequence of density estimates $\{\hat{f}_{\mathbf{h}}(\mathbf{z}^{(t)})\}_{t=0}^{\infty}$ yielded by either Version A or B is non-decreasing and thus converges.

(c) Under the assumptions in (a) or (b), we have that $\lim_{t \rightarrow \infty} \|\mathbf{z}^{(t+1)} - \mathbf{z}^{(t)}\|_2 = 0$.

(d) Assume the conditions in (a) or (b). If the local modes of $\hat{f}_{\mathbf{h}}$ are isolated, $\{\mathbf{z}^{(t)}\}_{t=0}^{\infty}$ converges to a local mode of $\hat{f}_{\mathbf{h}}$ when it is initialized within its small neighborhood.

Proof We only present the proof for the most complex scenario, where one of the kernel profiles k_1, k_2 is directional L and the other is linear k . One can slightly modify our argument to the linear-linear and directional-directional cases. Without the loss of generality, we assume that $k_1(r) = L(r)$ is directional and $k_2(s) = k(s)$ is linear.

(a) Our condition (C1) guarantees that the sequence $\{\hat{f}_{\mathbf{h}}(\mathbf{x}^{(t)}, \mathbf{y}^{(t)})\}_{t=0}^{\infty}$ is bounded. Hence, it suffices to prove that it is non-decreasing. The convexity and differentiability of L and k imply that

$$L(x_2) - L(x_1) \geq L'(x_1) \cdot (x_2 - x_1) \quad \text{and} \quad k(x_2) - k(x_1) \geq k'(x_1) \cdot (x_2 - x_1) \quad (41)$$

for any $x_1, x_2 \in [0, \infty)$. Notice that $\|\mathbf{x}^{(t)}\|_2 = \|\mathbf{X}_i\|_2 = 1$ for all $t = 0, 1, \dots$ and $i = 1, \dots, n$. Given the inequalities in (41), we calculate that

$$\begin{aligned} & \hat{f}_{\mathbf{h}}(\mathbf{x}^{(t+1)}, \mathbf{y}^{(t+1)}) - \hat{f}_{\mathbf{h}}(\mathbf{x}^{(t)}, \mathbf{y}^{(t)}) \\ &= \frac{C_{L, D_1}(h_1) \cdot C_{k, D_2}}{nh_2^{D_2}} \sum_{i=1}^n \left[L \left(\frac{1 - \mathbf{X}_i^T \mathbf{x}^{(t+1)}}{h_1^2} \right) k \left(\left\| \frac{\mathbf{y}^{(t+1)} - \mathbf{Y}_i}{h_2} \right\|_2^2 \right) \right. \\ & \quad \left. - L \left(\frac{1 - \mathbf{X}_i^T \mathbf{x}^{(t)}}{h_1^2} \right) k \left(\left\| \frac{\mathbf{y}^{(t)} - \mathbf{Y}_i}{h_2} \right\|_2^2 \right) \right] \end{aligned}$$

$$\begin{aligned}
 &= \frac{C_{L,D_1}(h_1) \cdot C_{k,D_2}}{nh_2^{D_2}} \sum_{i=1}^n \left[L \left(\frac{1 - \mathbf{X}_i^T \mathbf{x}^{(t+1)}}{h_1^2} \right) k \left(\left\| \frac{\mathbf{y}^{(t+1)} - \mathbf{Y}_i}{h_2} \right\|_2^2 \right) \right. \\
 &\quad - L \left(\frac{1 - \mathbf{X}_i^T \mathbf{x}^{(t+1)}}{h_1^2} \right) k \left(\left\| \frac{\mathbf{y}^{(t)} - \mathbf{Y}_i}{h_2} \right\|_2^2 \right) + L \left(\frac{1 - \mathbf{X}_i^T \mathbf{x}^{(t+1)}}{h_1^2} \right) k \left(\left\| \frac{\mathbf{y}^{(t)} - \mathbf{Y}_i}{h_2} \right\|_2^2 \right) \\
 &\quad \left. - L \left(\frac{1 - \mathbf{X}_i^T \mathbf{x}^{(t)}}{h_1^2} \right) k \left(\left\| \frac{\mathbf{y}^{(t)} - \mathbf{Y}_i}{h_2} \right\|_2^2 \right) \right] \\
 &\stackrel{(i)}{=} \frac{C_{L,D_1}(h_1) \cdot C_{k,D_2}}{nh_2^{D_2+2}} \sum_{i=1}^n L \left(\frac{1 - \mathbf{X}_i^T \mathbf{x}^{(t+1)}}{h_1^2} \right) k' \left(\left\| \frac{\mathbf{y}^{(t)} - \mathbf{Y}_i}{h_2} \right\|_2^2 \right) \left[\left\| \mathbf{y}^{(t+1)} - \mathbf{Y}_i \right\|_2^2 - \left\| \mathbf{y}^{(t)} - \mathbf{Y}_i \right\|_2^2 \right] \\
 &\quad + \frac{C_{L,D_1}(h_1) \cdot C_{k,D_2}}{nh_1^2 h_2^{D_2}} \sum_{i=1}^n L' \left(\frac{1 - \mathbf{X}_i^T \mathbf{x}^{(t)}}{h_1^2} \right) k \left(\left\| \frac{\mathbf{y}^{(t)} - \mathbf{Y}_i}{h_2} \right\|_2^2 \right) \mathbf{X}_i^T (\mathbf{x}^{(t)} - \mathbf{x}^{(t+1)}) \\
 &\stackrel{(ii)}{=} \frac{C_{L,D_1}(h_1) \cdot C_{k,D_2}}{nh_2^{D_2+2}} \sum_{i=1}^n L \left(\frac{1 - \mathbf{X}_i^T \mathbf{x}^{(t+1)}}{h_1^2} \right) k' \left(\left\| \frac{\mathbf{y}^{(t)} - \mathbf{Y}_i}{h_2} \right\|_2^2 \right) \\
 &\quad \times \left[\left\| \mathbf{y}^{(t+1)} \right\|_2^2 - 2\mathbf{Y}_i^T \mathbf{y}^{(t+1)} - \left\| \mathbf{y}^{(t)} \right\|_2^2 + 2\mathbf{Y}_i^T \mathbf{y}^{(t)} \right] \\
 &\quad + \frac{C_{L,D_1}(h_1) \cdot C_{k,D_2}}{nh_1^2 h_2^{D_2}} (\mathbf{x}^{(t+1)})^T (\mathbf{x}^{(t+1)} - \mathbf{x}^{(t)}) \cdot \left\| \sum_{i=1}^n \mathbf{X}_i \cdot L' \left(\frac{1 - \mathbf{X}_i^T \mathbf{x}^{(t)}}{h_1^2} \right) k \left(\left\| \frac{\mathbf{y}^{(t)} - \mathbf{Y}_i}{h_2} \right\|_2^2 \right) \right\|_2 \\
 &\stackrel{(iii)}{=} \frac{C_{L,D_1}(h_1) \cdot C_{k,D_2}}{nh_2^{D_2+2}} \sum_{i=1}^n L \left(\frac{1 - \mathbf{X}_i^T \mathbf{x}^{(t+1)}}{h_1^2} \right) k' \left(\left\| \frac{\mathbf{y}^{(t)} - \mathbf{Y}_i}{h_2} \right\|_2^2 \right) \\
 &\quad \times \left[\left\| \mathbf{y}^{(t+1)} \right\|_2^2 - 2 \left\| \mathbf{y}^{(t+1)} \right\|_2^2 - \left\| \mathbf{y}^{(t)} \right\|_2^2 + 2 (\mathbf{y}^{(t+1)})^T \mathbf{y}^{(t)} \right] \\
 &\quad + \frac{C_{L,D_1}(h_1) \cdot C_{k,D_2}}{2nh_1^2 h_2^{D_2}} \left\| \mathbf{x}^{(t+1)} - \mathbf{x}^{(t)} \right\|_2^2 \cdot \left\| \sum_{i=1}^n \mathbf{X}_i \cdot L' \left(\frac{1 - \mathbf{X}_i^T \mathbf{x}^{(t)}}{h_1^2} \right) k \left(\left\| \frac{\mathbf{y}^{(t)} - \mathbf{Y}_i}{h_2} \right\|_2^2 \right) \right\|_2 \\
 &= - \frac{C_{L,D_1}(h_1) \cdot C_{k,D_2}}{nh_2^{D_2+2}} \sum_{i=1}^n L \left(\frac{1 - \mathbf{X}_i^T \mathbf{x}^{(t+1)}}{h_1^2} \right) k' \left(\left\| \frac{\mathbf{y}^{(t)} - \mathbf{Y}_i}{h_2} \right\|_2^2 \right) \left\| \mathbf{y}^{(t)} - \mathbf{y}^{(t+1)} \right\|_2^2 \\
 &\quad + \frac{C_{L,D_1}(h_1) \cdot C_{k,D_2}}{nh_1^2 h_2^{D_2}} \left\| \mathbf{x}^{(t+1)} - \mathbf{x}^{(t)} \right\|_2^2 \cdot \left\| \sum_{i=1}^n \mathbf{X}_i \cdot L' \left(\frac{1 - \mathbf{X}_i^T \mathbf{x}^{(t)}}{h_1^2} \right) k \left(\left\| \frac{\mathbf{y}^{(t)} - \mathbf{Y}_i}{h_2} \right\|_2^2 \right) \right\|_2 \\
 &\geq 0,
 \end{aligned}$$

where we leverage the inequalities (41) in (i), plug in the first-step iterative equation derived from (18) of **Version B** in the main paper as:

$$\mathbf{x}^{(t+1)} = - \frac{\sum_{i=1}^n \mathbf{X}_i \cdot L' \left(\frac{1 - \mathbf{X}_i^T \mathbf{x}^{(t)}}{h_1^2} \right) k \left(\left\| \frac{\mathbf{y}^{(t)} - \mathbf{Y}_i}{h_2} \right\|_2^2 \right)}{\left\| \sum_{i=1}^n \mathbf{X}_i \cdot L' \left(\frac{1 - \mathbf{X}_i^T \mathbf{x}^{(t)}}{h_1^2} \right) k \left(\left\| \frac{\mathbf{y}^{(t)} - \mathbf{Y}_i}{h_2} \right\|_2^2 \right) \right\|_2}$$

to obtain (ii), as well as plug in the second-step iterative equation derived from (18) of **Version B** in the main paper as:

$$\mathbf{y}^{(t+1)} = \frac{\sum_{i=1}^n \mathbf{Y}_i \cdot L \left(\frac{1 - \mathbf{X}_i^T \mathbf{x}^{(t+1)}}{h_1^2} \right) k' \left(\left\| \frac{\mathbf{y}^{(t)} - \mathbf{Y}_i}{h_2} \right\|_2^2 \right)}{\sum_{i=1}^n L \left(\frac{1 - \mathbf{X}_i^T \mathbf{x}^{(t+1)}}{h_1^2} \right) k' \left(\left\| \frac{\mathbf{y}^{(t)} - \mathbf{Y}_i}{h_2} \right\|_2^2 \right)}$$

and use the fact that $(\mathbf{x}^{(t+1)})^T (\mathbf{x}^{(t+1)} - \mathbf{x}^{(t)}) = \frac{1}{2} \|\mathbf{x}^{(t+1)} - \mathbf{x}^{(t)}\|_2^2$ in (iii). Finally, we utilize the non-increasing property of k to argue that $-k'(s) \geq 0$ for all $s \in [0, \infty)$ and the final summands are non-negative. The result follows.

(b) By holding r constant in $K(r, s) = L(r) \cdot k(s)$, it is easy to verify by definition that k is convex given that the entire directional-linear kernel profile $K(r, s)$ is jointly convex. Similarly, we can demonstrate that L is convex. By (a), the sequence $\left\{ \widehat{f}_h(\mathbf{x}^{(t)}, \mathbf{y}^{(t)}) \right\}_{t=0}^{\infty}$ of density estimates defined by **Version B** in (18) of the main paper is non-decreasing and thus converges.

Now, we show that the sequence $\left\{ \widehat{f}_h(\mathbf{x}^{(t)}, \mathbf{y}^{(t)}) \right\}_{t=0}^{\infty}$ defined by **Version A** is also non-decreasing and thus converges. Notice that by the joint convexity and differentiability of $K(r, s)$,

$$\begin{aligned} K(r_2, s_2) - K(r_1, s_1) &\geq [(r_2, s_2) - (r_1, s_1)] \nabla K(r_1, s_1) \\ &= (r_2 - r_1) \cdot \frac{\partial}{\partial r} K(r_1, s_1) + (s_2 - s_1) \cdot \frac{\partial}{\partial s} K(r_1, s_1). \end{aligned} \quad (42)$$

Given this inequality and the fact that $\|\mathbf{x}^{(t)}\|_2 = \|\mathbf{X}_i\|_2 = 1$ for all $t = 0, 1, \dots$ and $i = 1, \dots, n$, we compute that

$$\begin{aligned} &\widehat{f}_h(\mathbf{x}^{(t+1)}, \mathbf{y}^{(t+1)}) - \widehat{f}_h(\mathbf{x}^{(t)}, \mathbf{y}^{(t)}) \\ &= \frac{C_{L, D_1}(h_1) \cdot C_{k, D_2}}{n h_2^{D_2}} \sum_{i=1}^n \left[L \left(\frac{1 - \mathbf{X}_i^T \mathbf{x}^{(t+1)}}{h_1^2} \right) k \left(\left\| \frac{\mathbf{y}^{(t+1)} - \mathbf{Y}_i}{h_2} \right\|_2^2 \right) \right. \\ &\quad \left. - L \left(\frac{1 - \mathbf{X}_i^T \mathbf{x}^{(t)}}{h_1^2} \right) k \left(\left\| \frac{\mathbf{y}^{(t)} - \mathbf{Y}_i}{h_2} \right\|_2^2 \right) \right] \\ &\stackrel{(i)}{=} \frac{C_{L, D_1}(h_1) \cdot C_{k, D_2}}{n h_2^{D_2}} \sum_{i=1}^n \left(\frac{1 - \mathbf{X}_i^T \mathbf{x}^{(t+1)}}{h_1^2} - \frac{1 - \mathbf{X}_i^T \mathbf{x}^{(t)}}{h_1^2}, \left\| \frac{\mathbf{y}^{(t+1)} - \mathbf{Y}_i}{h_2} \right\|_2^2 - \left\| \frac{\mathbf{y}^{(t)} - \mathbf{Y}_i}{h_2} \right\|_2^2 \right) \end{aligned}$$

$$\begin{aligned}
 & \times \left(L' \left(\frac{1 - \mathbf{X}_i^T \mathbf{x}^{(t)}}{h_1^2} \right) k \left(\left\| \frac{\mathbf{y}^{(t)} - \mathbf{Y}_i}{h_2} \right\|_2^2 \right) \right. \\
 & \left. L \left(\frac{1 - \mathbf{X}_i^T \mathbf{x}^{(t)}}{h_1^2} \right) k' \left(\left\| \frac{\mathbf{y}^{(t)} - \mathbf{Y}_i}{h_2} \right\|_2^2 \right) \right) \\
 = & \frac{C_{L,D_1}(h_1) \cdot C_{k,D_2}}{nh_1^2 h_2^{D_2}} \sum_{i=1}^n \mathbf{X}_i^T \left(\mathbf{x}^{(t)} - \mathbf{x}^{(t+1)} \right) L' \left(\frac{1 - \mathbf{X}_i^T \mathbf{x}^{(t)}}{h_1^2} \right) k \left(\left\| \frac{\mathbf{y}^{(t)} - \mathbf{Y}_i}{h_2} \right\|_2^2 \right) \\
 & + \frac{C_{L,D_1}(h_1) \cdot C_{k,D_2}}{nh_2^{D_2+2}} \sum_{i=1}^n L \left(\frac{1 - \mathbf{X}_i^T \mathbf{x}^{(t)}}{h_1^2} \right) k' \left(\left\| \frac{\mathbf{y}^{(t)} - \mathbf{Y}_i}{h_2} \right\|_2^2 \right) \\
 & \quad \times \left[\left\| \mathbf{y}^{(t+1)} \right\|_2^2 - 2\mathbf{Y}_i^T \mathbf{y}^{(t+1)} - \left\| \mathbf{y}^{(t)} \right\|_2^2 + 2\mathbf{Y}_i^T \mathbf{y}^{(t)} \right] \\
 \stackrel{\text{(ii)}}{=} & \frac{C_{L,D_1}(h_1) \cdot C_{k,D_2}}{nh_1^2 h_2^{D_2}} \left(\mathbf{x}^{(t+1)} \right)^T \left(\mathbf{x}^{(t+1)} - \mathbf{x}^{(t)} \right) \left\| \sum_{i=1}^n \mathbf{X}_i \cdot L' \left(\frac{1 - \mathbf{X}_i^T \mathbf{x}^{(t)}}{h_1^2} \right) k \left(\left\| \frac{\mathbf{y}^{(t)} - \mathbf{Y}_i}{h_2} \right\|_2^2 \right) \right\|_2 \\
 & + \frac{C_{L,D_1}(h_1) \cdot C_{k,D_2}}{nh_2^{D_2+2}} \sum_{i=1}^n L \left(\frac{1 - \mathbf{X}_i^T \mathbf{x}^{(t)}}{h_1^2} \right) k' \left(\left\| \frac{\mathbf{y}^{(t)} - \mathbf{Y}_i}{h_2} \right\|_2^2 \right) \\
 & \quad \times \left[\left\| \mathbf{y}^{(t+1)} \right\|_2^2 - 2 \left\| \mathbf{y}^{(t+1)} \right\|_2^2 - \left\| \mathbf{y}^{(t)} \right\|_2^2 + 2 \left(\mathbf{y}^{(t+1)} \right)^T \mathbf{y}^{(t)} \right] \\
 = & \frac{C_{L,D_1}(h_1) \cdot C_{k,D_2}}{2nh_1^2 h_2^{D_2}} \left\| \mathbf{x}^{(t+1)} - \mathbf{x}^{(t)} \right\|_2^2 \cdot \left\| \sum_{i=1}^n \mathbf{X}_i \cdot L' \left(\frac{1 - \mathbf{X}_i^T \mathbf{x}^{(t)}}{h_1^2} \right) k \left(\left\| \frac{\mathbf{y}^{(t)} - \mathbf{Y}_i}{h_2} \right\|_2^2 \right) \right\|_2 \\
 & - \frac{C_{L,D_1}(h_1) \cdot C_{k,D_2}}{nh_2^{D_2+2}} \left\| \mathbf{y}^{(t+1)} - \mathbf{y}^{(t)} \right\|_2^2 \cdot \sum_{i=1}^n L \left(\frac{1 - \mathbf{X}_i^T \mathbf{x}^{(t)}}{h_1^2} \right) k' \left(\left\| \frac{\mathbf{y}^{(t)} - \mathbf{Y}_i}{h_2} \right\|_2^2 \right) \\
 \geq & 0,
 \end{aligned}$$

where we apply the inequality (42) in (i), plug in the updating equation derived from (17) of **Version A** as:

$$\begin{aligned}
 \mathbf{x}^{(t+1)} &= - \frac{\sum_{i=1}^n \mathbf{X}_i \cdot L' \left(\frac{1 - \mathbf{X}_i^T \mathbf{x}^{(t)}}{h_1^2} \right) k \left(\left\| \frac{\mathbf{y}^{(t)} - \mathbf{Y}_i}{h_2} \right\|_2^2 \right)}{\left\| \sum_{i=1}^n \mathbf{X}_i \cdot L' \left(\frac{1 - \mathbf{X}_i^T \mathbf{x}^{(t)}}{h_1^2} \right) k \left(\left\| \frac{\mathbf{y}^{(t)} - \mathbf{Y}_i}{h_2} \right\|_2^2 \right) \right\|_2}, \\
 \mathbf{y}^{(t+1)} &= \frac{\sum_{i=1}^n \mathbf{Y}_i \cdot L \left(\frac{1 - \mathbf{X}_i^T \mathbf{x}^{(t)}}{h_1^2} \right) k' \left(\left\| \frac{\mathbf{y}^{(t)} - \mathbf{Y}_i}{h_2} \right\|_2^2 \right)}{\sum_{i=1}^n L \left(\frac{1 - \mathbf{X}_i^T \mathbf{x}^{(t)}}{h_1^2} \right) k' \left(\left\| \frac{\mathbf{y}^{(t)} - \mathbf{Y}_i}{h_2} \right\|_2^2 \right)}
 \end{aligned}$$

in (ii), and leverage the non-increasing property of k to argue the last inequality. The results thus follow.

(c) Our previous calculations in (a) and (b) suggest that

$$\begin{aligned}
 & \widehat{f}_{\mathbf{h}}(\mathbf{x}^{(t+1)}, \mathbf{y}^{(t+1)}) - \widehat{f}_{\mathbf{h}}(\mathbf{x}^{(t)}, \mathbf{y}^{(t)}) \\
 &= \frac{C_{L,D_1}(h_1) \cdot C_{k,D_2}}{2nh_1^2 h_2^{D_2}} \left\| \mathbf{x}^{(t+1)} - \mathbf{x}^{(t)} \right\|_2^2 \cdot \left\| \sum_{i=1}^n \mathbf{X}_i \cdot L' \left(\frac{1 - \mathbf{X}_i^T \mathbf{x}^{(t)}}{h_1^2} \right) k \left(\left\| \frac{\mathbf{y}^{(t)} - \mathbf{Y}_i}{h_2} \right\|_2^2 \right) \right\|_2 \\
 &= \begin{cases} \frac{C_{L,D_1}(h_1) \cdot C_{k,D_2}}{nh_2^{D_2+2}} \left\| \mathbf{y}^{(t+1)} - \mathbf{y}^{(t)} \right\|_2^2 \cdot \sum_{i=1}^n L \left(\frac{1 - \mathbf{X}_i^T \mathbf{x}^{(t)}}{h_1^2} \right) k' \left(\left\| \frac{\mathbf{y}^{(t)} - \mathbf{Y}_i}{h_2} \right\|_2^2 \right) & \text{for Version A,} \\ \frac{C_{L,D_1}(h_1) \cdot C_{k,D_2}}{nh_2^{D_2+2}} \left\| \mathbf{y}^{(t)} - \mathbf{y}^{(t+1)} \right\|_2^2 \cdot \sum_{i=1}^n L \left(\frac{1 - \mathbf{X}_i^T \mathbf{x}^{(t+1)}}{h_1^2} \right) k' \left(\left\| \frac{\mathbf{y}^{(t)} - \mathbf{Y}_i}{h_2} \right\|_2^2 \right) & \text{for Version B.} \end{cases} \tag{43}
 \end{aligned}$$

Under the conditions that k and L are strictly decreasing on $[0, \infty)$ and the data-generating density f has a compact support on $\mathcal{S}_1 \times \mathcal{S}_2$, all the factors in front of $\left\| \mathbf{x}^{(t+1)} - \mathbf{x}^{(t)} \right\|_2^2$ and $\left\| \mathbf{y}^{(t+1)} - \mathbf{y}^{(t)} \right\|_2^2$ in (43) are strictly positive. Because we have shown that

$$\widehat{f}_{\mathbf{h}}(\mathbf{x}^{(t+1)}, \mathbf{y}^{(t+1)}) - \widehat{f}_{\mathbf{h}}(\mathbf{x}^{(t)}, \mathbf{y}^{(t)}) \rightarrow 0$$

as $t \rightarrow \infty$ in (a) and (b), it implies that $\left\| (\mathbf{x}^{(t+1)}, \mathbf{y}^{(t+1)}) - (\mathbf{x}^{(t)}, \mathbf{y}^{(t)}) \right\|_2 = \left\| \mathbf{z}^{(t+1)} - \mathbf{z}^{(t)} \right\|_2 \rightarrow 0$ as $t \rightarrow \infty$.

(d) The proof of (d) follows from (c) together with the arguments of Theorem 2 in Li et al. (2007), Theorem 1 in Aliyari Ghassabeh (2015), and Theorem 11 in Zhang and Chen (2021b). We only outline the key steps. First, given the isolation of local modes of $\widehat{f}_{\mathbf{h}}$, one can derive that

$$\text{grad } \widehat{f}_{\mathbf{h}}(\mathbf{z}) > 0 \quad \text{for any } \mathbf{z} \in B(\widehat{\mathbf{m}}, \rho) \setminus \{\widehat{\mathbf{m}}\},$$

where $\widehat{\mathbf{m}} \in \widehat{\mathcal{M}}$ is a local mode of $\widehat{f}_{\mathbf{h}}$ and $B(\widehat{\mathbf{m}}, \rho)$ is the ρ -neighborhood of $\widehat{\mathbf{m}}$ in $\mathcal{S}_1 \times \mathcal{S}_2$. Then, as $\left\| \mathbf{z}^{(t+1)} - \mathbf{z}^{(t)} \right\|_2 \rightarrow 0$ when $t \rightarrow \infty$, one can argue that

$$\text{grad } \widehat{f}_{\mathbf{h}}(\mathbf{z}^{(t)}) \rightarrow 0 \quad \text{and} \quad \mathbf{z}^{(t)} \in B(\widehat{\mathbf{m}}, \rho) \quad \text{as } t \rightarrow \infty.$$

Lastly, as $\widehat{\mathbf{m}}$ is the only point satisfying $\text{grad } \widehat{f}_{\mathbf{h}}(\widehat{\mathbf{m}}) = 0$ within $B(\widehat{\mathbf{m}}, \rho)$, it follows that $\mathbf{z}^{(t)} \rightarrow \widehat{\mathbf{m}}$ as $t \rightarrow \infty$. \blacksquare

We restate the full version of Proposition 3 here.

Proposition 3. *Assume conditions (A1-2). For any fixed $\mathbf{z} \in \mathcal{S}_1 \times \mathcal{S}_2$, we have that*

$$\mathcal{P}_{\mathbf{z}} \mathbf{H}^{-1} \widetilde{D}(\mathbf{z})^{-1} \nabla \widehat{f}_{\mathbf{h}}(\mathbf{z}) = \widetilde{D}(\mathbf{z})^{-1} \mathbf{H}^{-1} \text{grad } \widehat{f}_{\mathbf{h}}(\mathbf{z})$$

under any given h_1, h_2, n and

$$\left[\mathbf{H} \widetilde{D}(\mathbf{z}) \right]^{-1} \text{grad } \widehat{f}_{\mathbf{h}}(\mathbf{z}) - \widetilde{F}(\mathbf{z})^{-1} \text{grad } f(\mathbf{z}) = O(h^2) + O_P \left(\sqrt{\frac{1}{nh^{D_1+D_2+2}}} \right)$$

as $h_1, h_2 \lesssim h \rightarrow 0$ and $nh^{D_1+D_2+2} \rightarrow \infty$, where

$$\tilde{F}(\mathbf{z}) = \begin{pmatrix} \tilde{F}_1 \cdot \mathbf{I}_{D_1+1_{\{S_1=\Omega_{D_1}\}}} & \mathbf{0} \\ \mathbf{0} & \tilde{F}_2 \cdot \mathbf{I}_{D_2+1_{\{S_2=\Omega_{D_2}\}}} \end{pmatrix}$$

$$\text{with } \tilde{F}_1 = \begin{cases} -C_{k,D_1} \int_{\mathbb{R}^{D_1}} k' \left(\frac{\|\mathbf{x}\|_2^2}{2} \right) d\mathbf{x} \cdot f(\mathbf{z}) & \text{if } S_1 = \mathbb{R}^{D_1}, \\ -\frac{\int_0^\infty L(r)r^{\frac{D_1}{2}-1} dr}{\int_0^\infty L'(r)r^{\frac{D_1}{2}-1} dr} \cdot f(\mathbf{z}) & \text{if } S_1 = \Omega_{D_1}, \end{cases}$$

$$\text{and } \tilde{F}_2 = \begin{cases} -C_{k,D_2} \int_{\mathbb{R}^{D_2}} k' \left(\frac{\|\mathbf{y}\|_2^2}{2} \right) d\mathbf{y} \cdot f(\mathbf{z}) & \text{if } S_2 = \mathbb{R}^{D_2}, \\ -\frac{\int_0^\infty L(r)r^{\frac{D_2}{2}-1} dr}{\int_0^\infty L'(r)r^{\frac{D_2}{2}-1} dr} \cdot f(\mathbf{z}) & \text{if } S_2 = \Omega_{D_2}. \end{cases}$$

Proof Based on the definitions of the projection matrix \mathcal{P}_z in (7), bandwidth matrix \mathbf{H} in (4), and $\tilde{D}(\mathbf{z})$ in (16) in the main paper, we know that $\mathbf{H}, \tilde{D}(\mathbf{z})$ are diagonal and \mathcal{P}_z is block diagonal. It is intuitive that $\mathcal{P}_z, \mathbf{H}^{-1}, \tilde{D}(\mathbf{z})^{-1}$ are mutually commutative. Hence, for any given h_1, h_2, n ,

$$\mathcal{P}_z \mathbf{H}^{-1} \tilde{D}(\mathbf{z})^{-1} \nabla \hat{f}_h(\mathbf{z}) = \tilde{D}(\mathbf{z})^{-1} \mathbf{H}^{-1} \text{grad } \hat{f}_h(\mathbf{z}).$$

As for the pointwise convergence of $\tilde{D}(\mathbf{z})^{-1} \mathbf{H}^{-1} \text{grad } \hat{f}_h(\mathbf{z})$, we know from Lemma 5 that for any fixed $\mathbf{z} \in S_1 \times S_2$,

$$\text{grad } \hat{f}_h(\mathbf{z}) - \text{grad } f(\mathbf{z}) = O(h^2) + O_P \left(\sqrt{\frac{1}{nh^{D_1+D_2+2}}} \right) \quad (44)$$

as $h_1, h_2 \lesssim h \rightarrow 0$ and $nh^{D_1+D_2+2} \rightarrow 0$. It remains to derive the pointwise convergence rate of $\tilde{D}(\mathbf{z})^{-1} \mathbf{H}^{-1} = [\mathbf{H} \tilde{D}(\mathbf{z})]^{-1}$. Recall that

$$\mathbf{H} \tilde{D}(\mathbf{z}) = \text{Diag} \left(h_1^2 G_{\mathbf{x}} \mathbf{I}_{D_1+1_{\{S_1=\Omega_{D_1}\}}}, h_2^2 G_{\mathbf{y}} \mathbf{I}_{D_2+1_{\{S_2=\Omega_{D_2}\}}} \right),$$

where

$$\begin{aligned} h_1^2 G_{\mathbf{x}} &= -\frac{2C(\mathbf{h})}{n} \sum_{i=1}^n k_1' \left(\left\| \frac{\mathbf{x} - \mathbf{X}_i}{h_1} \right\|_2^2 \right) K_2 \left(\frac{\mathbf{y} - \mathbf{Y}_i}{h_2} \right) \\ &= -\frac{2 \prod_{j=1}^2 C_{k_j, D_j}(h_j)}{n} \sum_{i=1}^n k_1' \left(\left\| \frac{\mathbf{x} - \mathbf{X}_i}{h_1} \right\|_2^2 \right) k_2 \left(\left\| \frac{\mathbf{y} - \mathbf{Y}_i}{h_2} \right\|_2^2 \right), \\ h_2^2 G_{\mathbf{y}} &= -\frac{2C(\mathbf{h})}{n} \sum_{i=1}^n K_1 \left(\frac{\mathbf{x} - \mathbf{X}_i}{h_1} \right) k_2' \left(\left\| \frac{\mathbf{y} - \mathbf{Y}_i}{h_2} \right\|_2^2 \right) \\ &= -\frac{2 \prod_{j=1}^2 C_{k_j, D_j}(h_j)}{n} \sum_{i=1}^n k_1 \left(\left\| \frac{\mathbf{x} - \mathbf{X}_i}{h_1} \right\|_2^2 \right) k_2' \left(\left\| \frac{\mathbf{y} - \mathbf{Y}_i}{h_2} \right\|_2^2 \right). \end{aligned}$$

It suggests that $h_1^2 G_{\mathbf{x}}, h_2^2 G_{\mathbf{y}}$ can be viewed as ‘‘KDEs’’ with kernel profiles $-k_1'(\cdot)k_2(\cdot)$ and $-k_1(\cdot)k_2'(\cdot)$, respectively. With regards to the pointwise convergence rate of $h_1^2 G_{\mathbf{x}}$, we consider the following two cases of the kernel profile k_1 .

- **Case 1:** k_1 is a linear kernel profile. In this case, $\mathcal{S}_1 = \mathbb{R}^{D_1}$ and

$$C_{k_1, D_1}(h_1) \cdot k_1 \left(\|\mathbf{u}\|_2^2 \right) = \frac{C_{k, D_1}}{h_1^{D_1}} \cdot k \left(\frac{\|\mathbf{u}\|_2^2}{2} \right).$$

Then,

$$h_1^2 G_{\mathbf{x}} = -\frac{C_{k, D_1} \cdot C_{k_2, D_2}(h_2)}{nh_1^{D_1}} \sum_{i=1}^n k' \left(\frac{1}{2} \left\| \frac{\mathbf{x} - \mathbf{X}_i}{h_1} \right\|_2^2 \right) k_2 \left(\left\| \frac{\mathbf{y} - \mathbf{Y}_i}{h_2} \right\|_2^2 \right).$$

One can follow the arguments in Theorems 1 and 2 of [Chacón et al. \(2011\)](#) or Lemma 2 of [Zhang and Chen \(2021c\)](#) to show that

$$h_1^2 G_{\mathbf{x}} - \left(-C_{k, D_1} \int_{\mathbb{R}^{D_1}} k' \left(\|\mathbf{x}\|_2^2 / 2 \right) d\mathbf{x} \cdot f(\mathbf{z}) \right) = O(h^2) + O_P \left(\sqrt{\frac{1}{nh^{D_1+D_2}}} \right) \quad (45)$$

as $h_1, h_2 \lesssim h \rightarrow 0$ and $nh^{D_1+D_2} \rightarrow \infty$.

- **Case 2:** k_1 is a directional kernel profile. In this case, $\mathcal{S}_1 = \Omega_{D_1}$ and

$$C_{k_1, D_1}(h_1) \cdot k_1 \left(\|\mathbf{u}\|_2^2 \right) = C_{L, D_1}(h_1) \cdot L \left(\frac{\|\mathbf{u}\|_2^2}{2} \right).$$

Then, using the fact that $\|\mathbf{x}\|_2 = \|\mathbf{X}_i\|_2 = 1$ for any $i = 1, \dots, n$,

$$h_1^2 G_{\mathbf{x}} = -\frac{C_{L, D_1}(h_1) \cdot C_{k_2, D_2}(h_2)}{n} \sum_{i=1}^n L' \left(\frac{1 - \mathbf{x}^T \mathbf{X}_i}{h_1^2} \right) k_2 \left(\left\| \frac{\mathbf{y} - \mathbf{Y}_i}{h_2} \right\|_2^2 \right).$$

One can follow the arguments in Proposition 1 of [García-Portugués et al. \(2013\)](#) and Theorem 2 of [Zhang and Chen \(2021b\)](#) to show that

$$h_1^2 G_{\mathbf{x}} - \left(-\frac{\int_0^\infty L(r) r^{\frac{D_1}{2}-1} dr}{\int_0^\infty L'(r) r^{\frac{D_1}{2}-1} dr} \cdot f(\mathbf{z}) \right) = O(h^2) + O_P \left(\sqrt{\frac{1}{nh^{D_1+D_2}}} \right) \quad (46)$$

as $h_1, h_2 \lesssim h \rightarrow 0$ and $nh^{D_1+D_2} \rightarrow \infty$.

Combining (44), (45), and (46), we obtain by Taylor's theorem that

$$\frac{\mathbf{grad} \hat{f}_{\mathbf{h}}(\mathbf{z})}{h_1^2 G_{\mathbf{x}}} - \frac{\mathbf{grad} f(\mathbf{z})}{\tilde{F}_1} = O(h^2) + O_P \left(\sqrt{\frac{1}{nh^{D_1+D_2+2}}} \right)$$

as $h_1, h_2 \lesssim h \rightarrow 0$ and $nh^{D_1+D_2+2} \rightarrow \infty$. A similar argument demonstrates that

$$\frac{\mathbf{grad} \hat{f}_{\mathbf{h}}(\mathbf{z})}{h_2^2 G_{\mathbf{y}}} - \frac{\mathbf{grad} f(\mathbf{z})}{\tilde{F}_2} = O(h^2) + O_P \left(\sqrt{\frac{1}{nh^{D_1+D_2+2}}} \right)$$

as $h_1, h_2 \lesssim h \rightarrow 0$ and $nh^{D_1+D_2+2} \rightarrow \infty$. The results thus follow. \blacksquare

Under an extra condition (A3), one can easily extend the result in Proposition 3 to an uniform convergence rate. Such stronger result will not provide more insights into the inconsistency of the naive SCMS algorithm, so we omit its presentation.